Studies on the Novel Nonwoven Separators for High power and Large-scale Lithium-ion Battery

Tanaka, Masanao

(Degree)
博士（学術）

(Date of Degree)
2012-03-25

(Date of Publication)
2014-12-09

(Resource Type)
doctoral thesis

(Report Number)
甲5465

(URL)
https://hdl.handle.net/20.500.14094/D1005465

博　士　論　文

Studies on the Novel Nonwoven Separators for High power and Large-scale Lithium-ion Battery

(高出力大型リチウムイオン電池用新規不織布セパレータに関する研究)

平成 24 年 1 月

神戸大学大学院工学研究科

田中　政尚

博　士　論　文

Studies on the Novel Nonwoven Separators for High power and Large-scale Lithium-ion Battery

(高出力大型リチウムイオン電池用新規不織布セパレータに関する研究)

January, 2012

Department of Chemical Science and Engineering

Graduate School of Engineering

Kobe University

Masanao TANAKA

Contents

Chapter 1

Introduction

1.1 General introduction

After the first petroleum crash in 1973, human beings were aware of the importance of energy storage. Development of science and technology is greatly making our life convenient and causes serious problems in our ecosystem by increase in heating of our environment and releasing CO_2 gas as a result of rapid increase in fuel consumption. Batteries play an important role not only in assisting our new information technology (IT), but also suppressing the damage of the ecosystem by improving energy efficiency. In fact, from 1998, the Treaty of Kyoto signed by most developed countries urges to improve the production and storage of clean energy. An important issue in the new era is to reduce the consumption of fossil fuels promptly. Otherwise, the warming of our global atmosphere will drastically change the climate of the ecosystem, which is critical for human beings.

In present time, outstanding growth in electronics industry requires huge amount of electric energy. A large portion of the energy is generated by fossil fuels, which emit greenhouse gases resulting global warming. Here, we can image the energy systems in near future. The electric power will produce by environment-friendly wind, solar and ocean thermal energy and the produced electric power can be stored using batteries which are friendly and not harmful to environmental. From the point of view, secondary batteries will play a critical role in reducing the environmental hazard and enable the effective construction of green energy society.

In 1958, an American Ph. D student published a thesis mainly based on the study of propylene carbonate and its electrolyte solution. This investigation may be considered as the first milestone marking the road of an entirely new research trend on batteries. Since Li element is light and possesses a relatively lower potential, many research groups tried to apply this element to high power density battery material [1].

Obviously, lithium, an anode material, can give higher energy density than other anode materials. However, metallic lithium easily reacts with water and emits hydrogen gas. Therefore the aqueous electrolyte cannot be used for metallic lithium anode. The researches of lithium battery were activated since it was reported that the metallic lithium can be stable in some electrolyte such as molten salt, liquid SO_2 and organic electrolyte like PC (propylene carbonate) / $LiClO_4$. The primary lithium battery had been developed in 1970's [2].

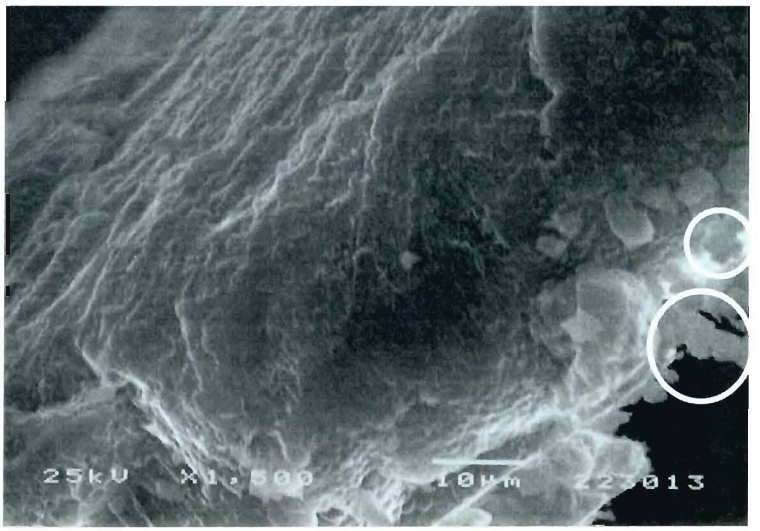

Figure 1.1 The growth of lithium dendrites on the surface of Cu foil. The dendrite is shown in the circles.

Attempt to develop rechargeable lithium batteries have been carried out from the beginning of 1970's, and extensive researches allow the commercialization of the lithium secondary batteries. However, the lithium secondary battery has a severe problem such as dendrite formation of lithium metal during charge process as shown in Fig. 1.1. As a matter of fact, several cellular phones, which are mounted lithium secondary batteries as power sources, were recalled at the end of 1980's with respect to several undesirable accidents, such as firing or explosion during use. In the early stage of 1980's, a new concept, "Rocking chair", was proposed [3] and demonstrated by some

research groups [4-6]. However, cathode material should have high redox potential in order to compensate the decrease in cell voltage.

In 1990's, lithium ion battery have commercialized by Sony Energytech based on a carbon (non-graphitic) as an anode and $LiCoO_2$ as a cathode. The name of "lithium ion battery" was given by T. Nagaura and K. Tozawa [7], and the concept of "lithium ion battery" was firstly introduced by Asahi Kasei Co. Ltd and they obtained patents around the world [8]. Sony has made several interactive improvements on the performance of their particular rocking chair battery (RCB) system.

The battery industry has seen enormous growth over the past few years in portable, rechargeable battery packs. The majority of this surge can be attributed to the wide-spread use of cell phones, personal digital assistants (PDAs), laptop computers and other wireless electronics. Batteries remained the mainstream of power source for systems ranging from mobile phones and PDAs to electric and hybrid electric vehicles. The world market for batteries was approximately $41 billion in 2000. This includes $16 billion primary and $24.9 billion secondary cells [9].

A recent market survey shows that the lithium battery is becoming an almighty rechargeable battery and in 2006 the demand is around 2 billion cells with more than 10 % annual growth [10]. There is a steady increase in the demand for lithium batteries for notebook PCs and cellular phones and in addition the demand for another important application, namely power tools is also more than expected even though the nickel-cadmium (Ni-Cd) battery demand for power tools is still increasing. Lithium battery-powered Uninterruptible Power Supply (UPS) is already commercialized and there is no doubt that lithium ion battery hybrid electric vehicle, plug-in hybrid electric vehicle and electric vehicle will be a major breakthrough in 2011 and beyond.

1.2 General concept of lithium battery

1.2.1 Lithium metal battery

The discharge process of this battery involves three main steps in the metallic lithium anode; i) dissolution of lithium ion from lithium metal anode, ii) the migration of lithium ions across the electrolyte and separator and iii) insertion of lithium ions into the host structure of the cathode. Common cathode materials for lithium metal battery are inorganic compounds, such as transition metal dechalcogenides and oxides. They are characterized by layered or tunneled structure, which can provide channels in order to transfer lithium ions reversibly and faster in the host matrix. In fact, it is well known that Li/V_6O_{13} [11], Li/TiS_2 [12] and Li/MoS_2 [13] cells have been proved to have a reversible behavior. The Li/MoS_2 cell was commercialized by Moli Energy.

In the view point of reversibility, it can be believed that the lithium secondary battery with lithium metal anode is capable of very long cycle life and supplies a fairly stable operation voltage and capacity. However, practical cycle stability of the battery is limited due to the dendritic growth of lithium metal, which causes short circuit of cell, followed a drastic increase in volume of the anode [14,15]. The abrupt changes in the anode would bring about safety hazard or explosion by thermal abuse.

1.2.2 Lithium ion battery

Lithium ion battery (LIB) has emerged from lithium metal battery to eliminate its un-safety. The principle of the Li-ion battery is explained in the Fig. 1.2. The inorganic compound, $LiCoO_2$, is used as the cathode material. This material has a rhombohedral structure where Li and Co cations fill alternating layers of edge-sharing octahedral sites in a close packed oxygen array. During charging, lithium is extracted from the layers, then transported and doped into the carbonaceous anode. In the discharge process, the

lithium ions are un-doped from the anode and return again to the space between layers in the cathode. Thus, this battery is sometimes called as the "Rocking Chair Battery" or the "Swing Battery" in the view point of lithium transfer. The reaction scheme of the lithium ion battery is expressed in Fig. 1.2, where $LiCoO_2$ is used as cathode material. When a cell is assembled, lithium ions are not doped into carbon. Therefore, the battery has low voltage near 0 V.

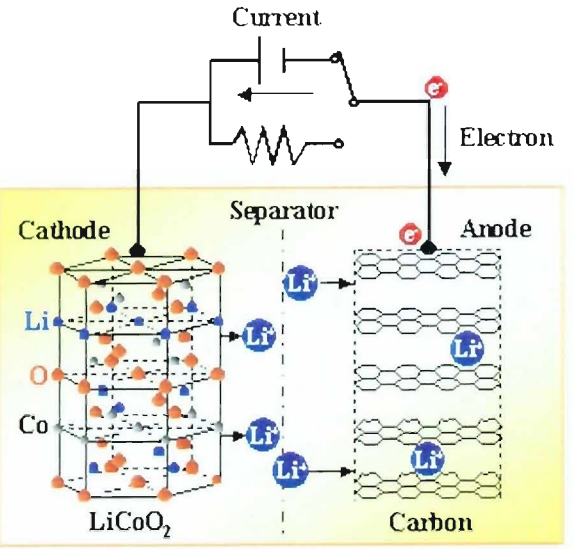

(+, Positive electrode):

$$LiCoO_2 \underset{\text{discharge}}{\overset{\text{charge}}{\rightleftharpoons}} Li_{1-x}CoO_2 + xLi^+ + xe^-$$

(-, Negative electrode):

$$C + xLi^+ + xe^- \underset{\text{discharge}}{\overset{\text{charge}}{\rightleftharpoons}} Li_xC$$

Figure 1.2 Basic structure of electroactive material and its redox reaction in lithium ion battery.

1.3 Components for lithium ion battery

1.3.1 Requisites for electrode materials [16]

High specific energy density (related to both average working voltage and reversible capacity) and long cyclic life (related to the stability of structure and

electrode-electrolyte interface) are simultaneously required for a high performance Li-ion battery. Therefore, some aspects should be considered in the design of new electrode materials for lithium rechargeable batteries. In general, structure, chemical stability and the available redox couple of electroactive materials are the primary points. Ideally, it should simultaneously match following conditions:

a) An open structure to permit reversible lithium migration

In brief, the working principle of lithium rechargeable battery is the reversible migration of lithium between cathode and anode accompanied by a redox process, that reversibility is prerequisite to Li secondary battery. Thus, the structure of the compound should be open for lithium insertion in its lattice.

b) Stability of electrode and electrolyte

This is the requirement for a long cycle life. The insertion/extraction reaction has a topotactic character and both insertion and extraction of guest lithium ions into and from host compound should ideally not modify the host structure. On the other hand, the oxidation of electrolyte should be avoided for oxidation and reduction.

c) A higher specific energy density

The specific energy density (per weight or per volume) is related to both the working voltage and the reversible capacity. The former depends on the potential of the redox process and the latter is restricted by the reversible amount of lithium intercalation. The available redox pair should locate in a suitable energy and the structure of material should be stable in wide composition range in order to obtain a high specific energy density.

d) Higher electrode conductivities

The lithium insertion/extraction involves both lithium ions diffusion in the lattice and charge transfer process on the particle surface. Thus, electrode's conductivity

includes both bulk lithium ion conductivity in active material and electronic conductivity of electrode. Higher electronic conductivity is helpful to keep the inner resistance low and gives an excellent rate capability. Beside this, lower interfacial resistance for electrochemical reaction is desirable for lower the polarization of electrode.

e) A low cost and environment benign.

The cost and environmental impact should be always kept in mind for new battery design. It is one of the future challenges to develop cheaper and hazardless electrode materials with excellent battery performances.

Figure 1.3 shows the working potential and capacity of the various electrode materials [17]. Compounds with a working potential of above 3 V can be used as cathode materials in lithium ion battery. They include lithium containing transition metal oxides, such as $LiCoO_2$, $LiMn_2O_4$, $LiNiO_2$, $LiMnO_2$ and their derivatives, and polyanionic compounds, for example, $LiFePO_4$ and Li_2MSiO_4 (M = Fe, Mn) compound.

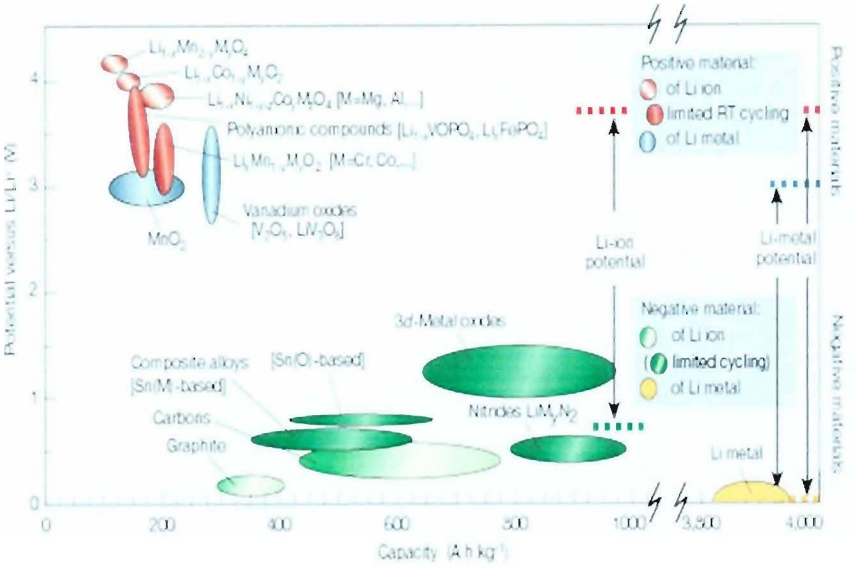

Figure 1.3 Voltage vs. capacity of some electrode materials.

1.3.2 Cathode materials for lithium ion battery

The layered metal oxides with a general formula of $LiMeO_2$ (Me = Transition metal elements such as Co, Ni and Mn), in which the Li ion and Me ion occupy the alternate (111) planes of the rock salt structure. The structure has an oxygen stacking sequence of ···ABCABC··· along the c axis of hexagonal setting and the Li and Me ions occupy the octahedral sites. There are three MeO_2 sheet per unit cell. This structure can be described as a layered structure with a space group of *R3m*, and the unit cell parameters are conveniently defined in terms of the hexagonal setting [18]. A schematic layered structure is presented in the Fig. 1.4. The structure with MeO_2 layers allows a reversible extraction/insertion of lithium ions from/into the lithium planes.

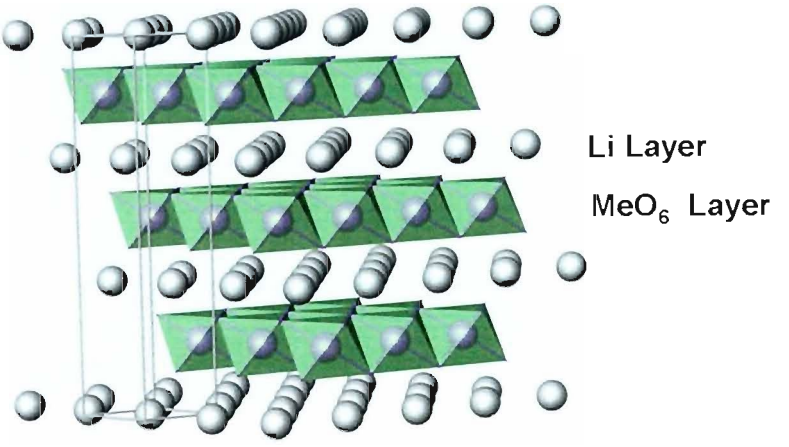

Figure 1.4 Schematic model of an ideal $LiMeO_2$ structure with *R3m*.

A spinel compound, $LiMe_xMn_{1-x}O_4$ (Me = Metal element), is an attractive cathode material for replacing Co or Ni based layered cathode materials in the next generation of Li-ion batteries. Especially, it has been extensively studied as positive electrode materials of large-size lithium ion batteries for power sources of hybrid electric vehicles (HEV) [19,20] because they have several advantages such as lower cost, high-rate

capability and higher thermal stability compared to those of Co or Ni based layered materials (e.g. $LiCoO_2$ or $LiNiO_2$).

As shown in the Fig. 1.5, the $LiMn_2O_4$ crystallizes in space group, $Fd\bar{3}m$, with Li and Mn present in 8a tetrahedral sites and 16d octahedral sites in the cubic close-packed oxygen array, respectively. All other sites, such as tetrahedral 8b and 48f sites and octahedral 16c sites, are empty [21]. MnO_6 octahedra share edges to build a rigid three-dimensional framework. Li ions diffuse through 8a-16c-8a path [22].

From the spinel cathode, about 1 mole of lithium can be reversibly extracted in two steps, at 4.05 V and 4.15 V, leading to the delithiated λ-MnO_2 [23]. On the other hand, the spinel $LiMn_2O_4$ is changed to tetragonal $Li_2Mn_2O_4$ when more lithium ions are inserted into the 16c site at 2.8 V.

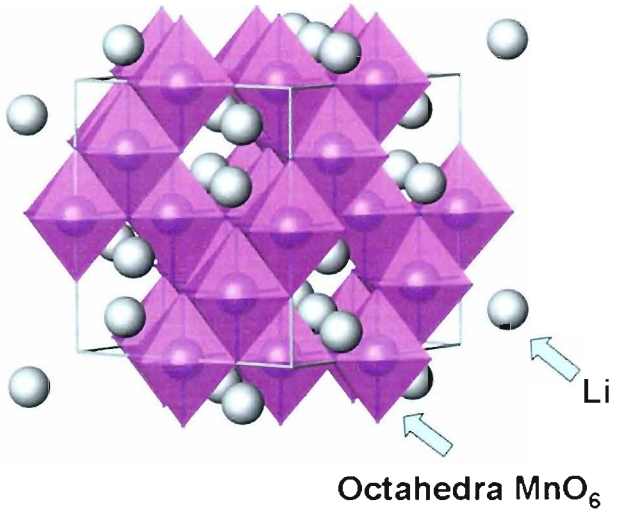

Figure 1.5 Structure of cubic spinel $LiMn_2O_4$.

$LiMnO_2$ compound shows higher theoretical capacity of 285 mAh g^{-1} than spinel $LiMn_2O_4$ 148 mAh g^{-1}, $LiMnO_2$ as cathode materials is of interest. $LiMnO_2$ is

polymorphous, mainly orthorhombic (zigzag layered structure, *Pmmn*) and monoclinic (layered structure, *C2/m*) structure as shown in Fig. 1.6 (a) and (b), respectively.

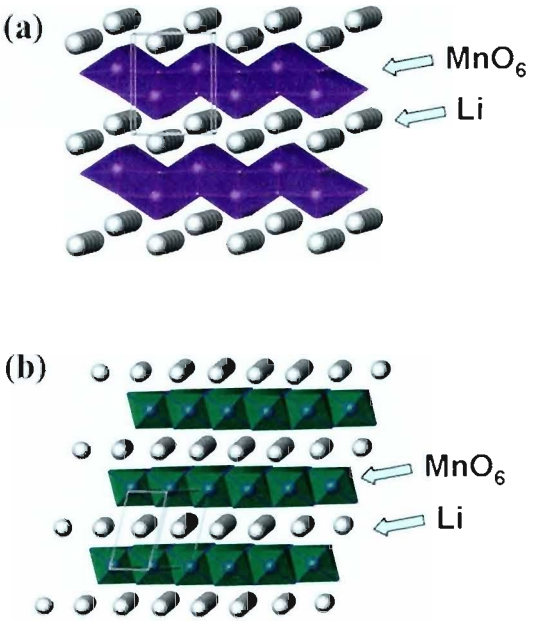

Figure 1.6 The structure of (a) orthorhombic and (b) monoclinic $LiMnO_2$.

Orthorhombic $LiMnO_2$ crystallizes in the space group *Pmnm* where Mn (y = 5/8) and Li (y = 1/8) occupies in octahedral 2a sites in the distorted cubic close packed oxygen array, respectively [24,25]. Generally, this cathode material is prepared by solid state reaction method by using manganese oxide and lithium hydroxide at various temperatures under inert atmosphere. When the material is synthesized at low temperature, this compound can deliver higher capacity about 200 mAh g^{-1}. On the other hand, the sample synthesized at higher temperature displays lower capacity with better cycle stability than low temperature product [26-31]. The cathode material undergoes irreversible phase transformation to spinel-like structure during cycling in the voltage range between 2 and 4.3 V.

Monoclinic $LiMnO_2$ has iso-structural with layered $LiCoO_2$. It is not thermodynamically stable, thus it can be prepared by ion exchange from α-$NaFeO_2$. It also undergoes phase transformation to spinel as orthorhombic $LiMnO_2$.

An olivine type $LiMPO_4$ (M = transition metal) is one of polyanionic compounds, such as NASICON $Li_3Fe_2(PO_4)_3$ [32] and monoclinic (or rhombohedral) $Fe_2(SO_4)_3$ [33]. The polyanionic compounds can be viewed as replacement of O^{2-} anions by larger size $(XO_4)^{m-}$ polyanions such as PO_4^{3-}, SO_4^{2-}, MoO_4^{2-}, WO_4^{2-} and so forth. Olivine type $LiFePO_4$ (orthorhombic structure, *Pnma*) allows two-dimensional Li^+ diffusion pathway as shown in Fig. 1.7. Padhi et.al demonstrated firstly that orthorhombic $LiFePO_4$ could be used as a cathode for rechargeable lithium battery [34]. It has a theoretical capacity of 170 mAh g^{-1} and is environmentally benign and inexpensive. Further it shows excellent cycle stability due to structural similarity between charged/discharged states. Especially, this material exhibits very good thermal stability [35,36]. These properties make it an attractive candidate for large scale batteries, such as power source for an electric vehicle.

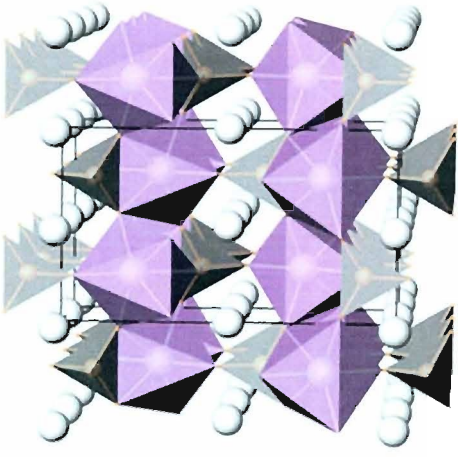

Figure. 1.7 Structure of $LiFePO_4$.

1.3.3 Anode materials for lithium ion battery

Lithium metal is the most attractive material for use as an anode in rechargeable batteries because of its low potential (-3.04 V *vs.* SHE) and high capacity (3863 mAh g^{-1}). However, it caused dendrite formation by prolonged cycling, which brings about serious safety and cycleability problems [37]. The safety problems with dendrite formation urgently demanded a replacement by carbonaceous material which can be intercalated and deinterclated into their host structure.

The types of carbonaceous materials used in lithium ion battery are roughly divided into three: graphite, soft carbon and hard carbon. The structure of graphite is quite regular, namely constructed from regular stacking of graphene sheet. Lithium ions are doped into the layers to form the substance of graphite intercalation compound (GIC) during the charge. The composition of fully lithiated Li-GIC is expressed as LiC_6, so the theoretical discharge capacity is calculated to be 372 mAh g^{-1}. It is well known that it cannot be used in PC (propylene carbonate) based electrolyte for the sake of predominant decomposition of PC on graphite surface. Moreover, EC (ethylene carbonate) based electrolyte also gradually decompose. Therefore, only hard carbon was used along PC and EC based solvent before 1997. With invention of electrolyte additive, which suppress decomposition of EC based solvent, graphite can be used as anode. As shown in Fig. 1.8, soft carbons have fairly developed layered structures, but crystal growth is poor comparing to graphite. The soft carbon can be used in EC based electrolyte. This also shows 372 mAh g^{-1} as theoretical discharge capacity.

On the other hand, hard carbon is quite different from above two. The anode particle is an aggregate of small crystallites randomly oriented, in which there are small irregular spaces. Each crystallite has a layer structure like a broken piece of graphite. It

is smoothly capable of storing and releasing lithium ion. This material may show more than 372 mAh g^{-1} of discharge capacity.

Figure 1.8 Three types of carbon used in lithium ion battery.

1.3.4 Separator for lithium ion battery

The separator used in lithium ion battery has two important functions: one is to avoid the direct contact between the anode and cathode, while it allows a free mass transfer of the electrolyte, and the other is a shutter action to stop the mass transfer in the case of accidental heat generation, which cause it melt down, resulting in shut down of a cell. The material should be sufficiently stable for a long time while it is kept in contact with the electrolyte. The development of tough, thin, micro porous separators made practical the use of resistive, organic electrolytes in high-rate cells while maximizing the volumetric energy density of batteries. The advent of rechargeable lithium batteries for consumer electronics placed another requirement on battery separator: high temperature integrity. If a battery overheats due to overcharging or a short circuit, the rise in temperature causes thermal shrinkages of a separator resulting thermal runaway of battery such as firing or explosion.

Traditionally, lithium-ion battery separators were made from polyethylene (PE), polypropylene (PP), or some combination of the two, because these polyolefins provide

excellent mechanical properties and chemical stability at a reasonable cost. Recently, ceramic materials and aramid polymers have been introduced as a means to improve the thermal stability of separators to temperatures of 200 °C and above.

The processes for manufacturing micro porous membranes can be broadly divided into wet processes and dry processes. Both processes usually employ one or more orientation steps to impart porosity and/or increase tensile strength.

Wet processes involve mixing a hydrocarbon liquid or some other low molecular-weight substance with a polyolefin resin, heating and melting the mixture, extruding the melt into a sheet, orientating the sheet either in the machine direction or biaxially, and then extracting the liquid with a volatile solvent [38-40]. A drawback of the biaxial orientation is that the separator tends to shrink in both machine and transverse directions on heating.

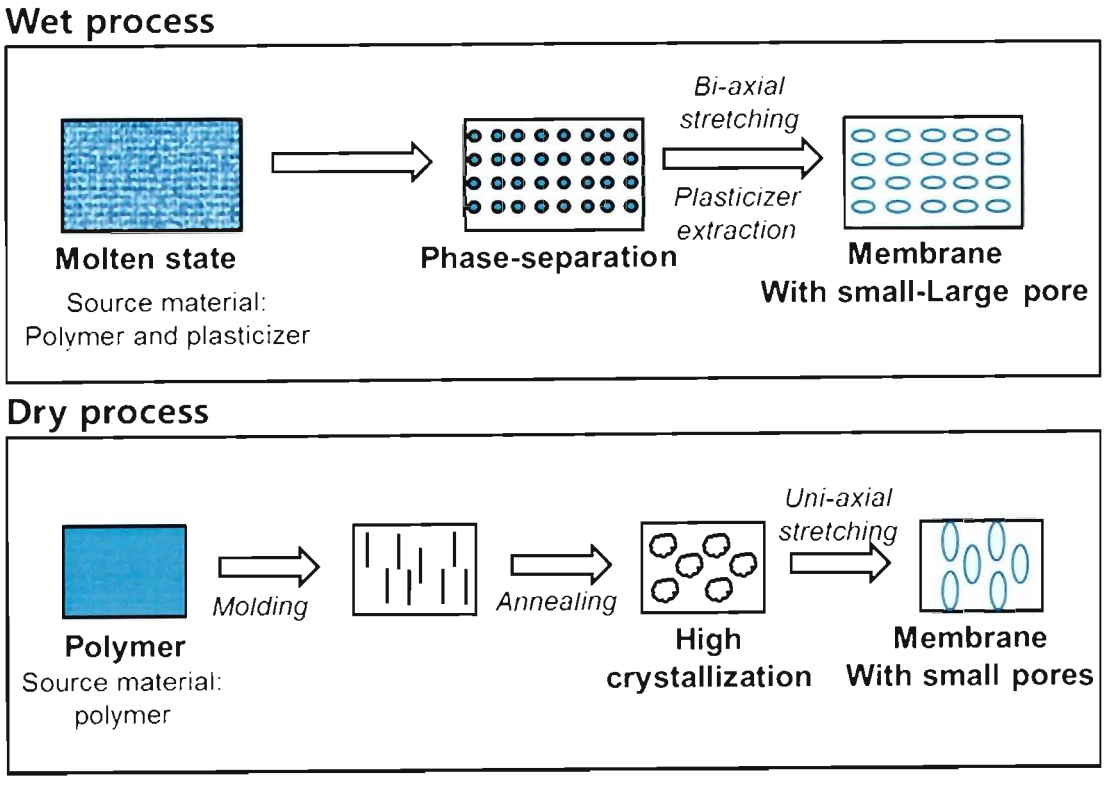

Figure 1.9 Production processes for wet and dry separators.

Dry processes involve melting a polyolefin resin, extruding it into a film, thermal annealing, orientation at a low temperature to form micro-pore initiators, and then uniaxial orientation at a high temperature to form micro-pores [41,42]. The dry process involves only virgin polyolefin resins and so presents little possibility of battery contamination. However, the dry process is typically a batch process, so can be more prone to variability. Currently, the dry process can only be applied to PPs and PEs, so the membrane properties are limited by these materials. Fig. 1.9 shows schematically the processes used to make wet and dry separators, and Fig. 1.10 shows scanning electron micrographs of surfaces of separators made by the dry and wet processes.

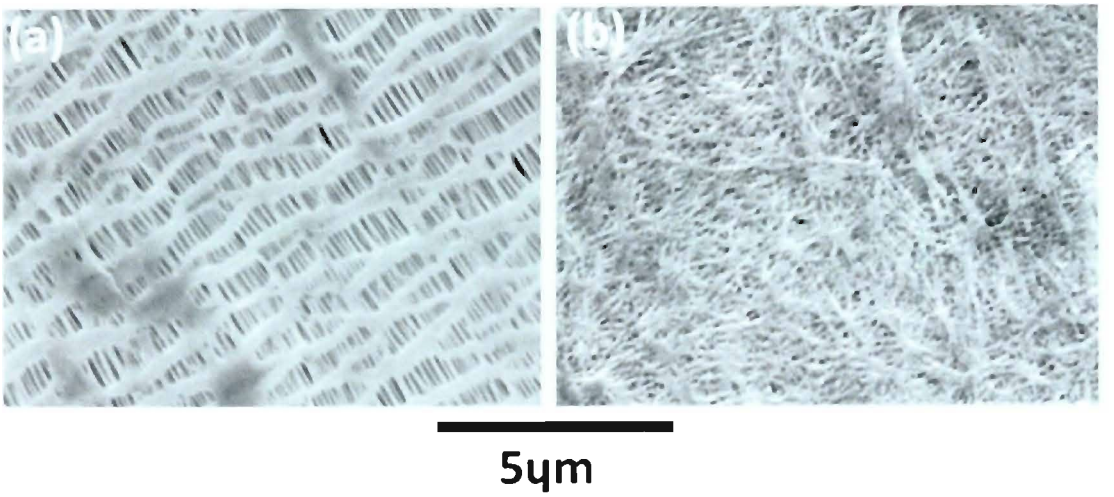

Figure 1.10 Scanning electron micrographs of (a) a separator produced by dry process and (b) a separator produced by wet process.

1.3.4.1 Separator Requirements [43]

In lithium-ion batteries, the essential function of the battery separator is to prevent electronic contact, while enabling ionic transport between the positive and negative electrodes. The most commonly used separators for lithium-ion batteries are micro

porous polyethylene and laminates of polypropylene and polyethylene membranes. These materials are chemically and electrochemically stable in secondary lithium batteries. The general requirements for the separators for lithium-ion battery are given below.

a) Thickness

The lithium-ion battery used in consumer applications use thin micro porous separators below 25μm. The separator being developed for EV/HEV applications will require thicker (~40 μm) separator. The thicker separator can give strong tensile and puncture strength, but the smaller the amount of active materials. On the other hand, the thinner separator takes less space and permits the use of longer electrode. It also can reduce internal resistance of battery.

b) Permeability

The separators should not limit the electrical performance of the battery under normal condition. Typically, the presence of a separator increases the effective resistivity of the electrolyte by a factor of 6-7. The ratio of the resistivity of the separator filled with an electrolyte divided by the resistivity of the electrolyte alone is called the McMullin number. The McMullin number as high as 10 – 12 has been used in consumer cells.

c) The Gurley (Air permeability)

Air permeability is proportional to electrical resistivity for a given separator morphology. It can be used in place of electrical resistance measurements once the relationship between the Gurley value and electrical resistance is established. The separator should have low the Gurley values for good electrical performance.

d) Porosity

A porosity control of the separators is very important for battery separators because it directly related to uptake amount of an electrolyte. The large amount of the electrolyte between a positive and a negative electrode could increase conductivity of lithium ion during charge-discharge process.

e) Wettability

The wettability of the separator is directly related to production speed and charge-discharge performance of battery. The separator should wet out quickly and completely in electrolyte.

f) Electrolyte Absorption and Retention

A separator should be able to absorb and retain electrolyte. Electrolyte absorption is needed for ion transport. The micro porous membranes usually do not swell on electrolyte absorption.

g) Chemical stability

The separators should be stable in battery for a long period of time. It should be inert to both strong reducing and oxidizing conditions and should not degrade or lose mechanical strength or produce impurities, which can interfere with the function of the battery. The separator must be able to withstand the strong oxidizing positive electrode and the corrosive nature of the electrolyte at temperatures as high as 75 °C. The greater the oxidation resistance, the longer the separator will survive in a cell.

h) Puncture strength

The separators used in wound cells require high puncture strength to avoid penetration of electrode material through the separator. If particulate material from the electrodes penetrates the separator, an electrical short will result and the battery will be failed. The separators used in lithium-ion battery require more strength than the one used in lithium-primary batteries.

i) Thermal stability

Lithium-ion batteries can be poisoned by water and so materials going into the battery are typically dried at 80 °C under vacuum. Under these conditions, the separator must not shrink significantly and definitely must not wrinkle. The requirement of thermal shrinkage of separator is less than 5% or original size after drying at 90 °C for 60 min.

1.4 Target of this research

The lithium-ion battery market has grown tremendously over the last decade to keep pace with consumer electronics. In the last-few years, high-power lithium-ion batteries have penetrated into the power tool market, and now, large-scale lithium-ion batteries are finding use in stationary and transportation applications [44-46]. These applications require battery to have long cycle life and high safety than traditional one.

A separator can retain electrolyte, prevent shortage between the two electrodes while maintaining high ion permeation, and to perform safe deactivation of the cell under overcharge, abnormal heating or mechanical rupture conditions [43,47]. Thus, the structural and physiochemical properties of the separator material strongly influence the overall cell performance, although the separator does not "actively" participate in the battery operation.

As mentioned in the preceding section, Polyolefin microporous membranes have been used as major separator for the lithium-ion battery. Obviously, the conventional separators have quite suitable properties, i.e., chemical resistance, suitable thickness, and mechanical strength. However, low porosity of about 40% [48] and the large difference of the polarity between the nonpolar polyolefin separator and the highly polar liquid electrolyte, which leads low pore wettability, [49,50] leading an increase in cell

resistance. This nature of polyolefin separators could restrict performance of the lithium-ion battery [51]. But, very little work (relative to research of electrode materials and electrolyte) is directed toward characterizing and developing new separators. Similarly, not much attention has been given to separators in publications reviewing batteries [52-61].

One of candidates for new separator is nonwoven fabrics. Polyolefin-, polyamide-, and nylon-based nonwoven separators are commonly used as separators for primary and secondary batteries such as Ni–Cd and Ni–MH batteries. The nonwoven separator can give several advantages, i.e., ease of controlling microstructures (pore size and porosity), lower cost, and ease in preparation of composite matrix using various materials. Nonetheless, it has not yet been used as a separator for lithium-ion batteries due to its large pore size and/or thicker nature. The large pore size and thicker nature can lead to internal short circuits and a decrease in energy density of the battery, respectively. To decrease pore size and thickness of the nonwoven separator, i.e., densification of nonwoven separator, preparation of a thinner fiber is necessary because the nonwoven fabric is formed by stacking or bonding of fibers together. However, up to now, the minimum diameter of polyolefin fiber is around 1 μm. Thus preparation of a nonwoven separator having close pore size and thickness to a microporous membrane separator is very difficult. For this reason, little research has been reported for the nonwoven fabrics as a separator for lithium-ion batteries [50,62,63].

For preparing nonwoven fabric having similar thickness and pore-size to conventional polyolefin membrane separator, fabrication of finer fiber (under 0.5 μm) is key parameter. ***In Chapter 2***, I have applied an electrospinning technique to obtain polyacrylonitrile (PAN) and polyvinylalcohol (PVA) based nano-fiber nonwoven

fabrics and investigated potential of the nonwovens as separators for high power lithium-ion battery.

As mentioned above, large pore size and inhomogeneous pore-size distribution of nonwoven fabric prevent the nonwoven fabric from practical application as a lithium-ion battery separator. ***In Chapter 3,*** in order to reduce mean pore size and increase thermal integrity of nonwoven fabric, I have tried to develop ceramic composite nonwoven fabric consist of nano-size silica powder and fine polyolefin fiber (2 μm in diameter) using new preparation technique named air-laid method. And I have investigated thermal stability and battery performance of the ceramic composite nonwoven separator.

Cells with the nano-fiber nonwoven separators (studied in the Chapter 2) showed outstanding rate capabilities and stable cycling performances. However, it suffers from low tensile strength and thermal stability above 150 °C in an electrolyte. And, cells with the ceramic composite nonwoven separators (studied in the Chapter 3) showed stable battery performances and better thermal stabilities than a cell with a conventional micro porous membrane separator. However, it also has some drawbacks for instance dropping out of ceramic particles and low air permeability due to the large amount of ceramic powder inside of the separator. Therefore, ***in Chapter 4,*** I have developed a new concept separator in order to overcome the drawbacks (mentioned above) of nonwoven separator by combining nano-fiber nonwoven and ceramic containing nonwoven. I have investigated thermal and physical properties as well as battery performance of the separators.

References

[1]. J. M. Tararascon, in "Rencet Advances in Rechargeable Li Batteries", *special Issue of Solid State Ionics,* eds. M. S. Whittingham, **69,** No. 3-4 (1994).

[2]. H. Ikeda, T. Saito, and H. Tamura, in *Proc. Manganese Dioxide Symp.* **Vol.1,** eds. A. Kozawa and R. H. Brodd (IC sample Office, Cleveland. OH.1975).

[3]. M. Armand, *"Materials for Advanced Batteries"*, eds. D. W. Murphy, J. Broadhead and B. C. H. Steele (Plenum press, New York, **1980**) P. 145.

[4]. B. di Pietro, M. Patriarca, and B. Scrosati, *J Power Sources*, **8** (1982) 289.

[5]. M. Lazzari, and B. Scrosati, *J. Electrochem. Soc.*, **127** (1980) 773.

[6]. S. Morzilli, B. Scrosati, and F. Sgarlata, *Electrochim. Acta*, **30** (1985) 1271.

[7]. T. Nagaura, and K. Tozawa, *Prog. Batt. Solar cells*, **9** (1990) 209.

[8]. A. Yoshino, K. Sanechika, and T. Nakashima, Japan Kokai Shou 62-90863 (1987).

[9]. R. J. Brodd, K. R. Bullock, R. A. Leising, R. L. Middaugh, J. R. Miller, and E. Takeuchi, *J. Electrochem. Soc.*, **151** (2004) K1

[10]. H. Takeshita, The 23rd International Battery Seminar & Exhibit, Fort Lauderdale, FL, Florida Educational Seminars, Inc., March **13**, 2004

[11]. A. Hooper, and B. C. Tofield, *J. Power Sources,* **11** (1984) 33.

[12]. F. Croce, S. Passerini, and B. Scrosati, *J. Power Sources*, **43** (1993) 481.

[13]. R. R. Haering, J. A. R. Stile, and K. Brandt, US Patent (1982) No. 4,281,048.

[14]. Y. Toyoguchi, T. Matsui, T. Yamaura, and T. Iijima, *3rd International Meeting on Lithium Batteries*, **1986**, 117.

[15]. J. J. Auborn, and Y. L. Barberio, *J. Electrochem. Soc.*, **134** (1987) 638.

[16]. J. B. Goodenough, and V. Manivannan, *DENKI KAGAKU*, **66** (1998) 1173.

[17]. J. M. Tarascon, and M. Armand, *Nature*, **414** (2001) 359.

[18]. K. Mizushima, P. C. Jones, P. J. Wiseman, and J. B. Goodenough, *Mater. Res. Bull.*, **17** (1980) 783.

[19]. T. Kai, H. Ando, Y. Muranaka, T. Horiba, and K. Hironaka, Shin-Kobe Tech. Rep., **11** (2001) 9.

[20]. T. Horiba, K. Hironaka, T. Matsumura, T. Kai, M. Kosek, and Y. Muranaka, *J. Power Soreces*, **119-121** (2003) 893.

[21]. S. Megahed, and B. Scrosati, *J. Power Sources*, **51** (1994) 79.

[22]. M. M. Thackeray, P. J. Johnson, L. A. de Picciotto, P. G. Bruce, and J. B. Goodenough, *Mater. Res. Bull.*, **19** (1984) 179.

[23]. J. C. Hunter, *J. Solid State Chem.*, **39** (1981) 142.

[24]. R. Hoppe, G. Brachtel, M. Jansen, and Z. Anorg, *Allg. Chem.*, **417** (1975) 1.

[25]. A. R. Armstrong, and P. G. Bruce, *Nature*, **381** (1996) 499.

[26]. Y.-I, Jang, B. Huang, Y.-M. Chiang, and D. R. Sadoway, *Electrochem. Solid-State Lett.*, **1** (1998) 13.

[27]. Y.-I. Jang, B. Huang, H. Wang, D. R. Sadoway, and Y.-M. Chiang, *J. Electrochem. Soc.*, **146** (1999) 3217.

[28]. Y.-M. Chiang, D. R. Sadoway, Y.-I. Jang, B. Huang, and H. Wang, *Electrochem. Solid-State Lett.*, **2** (1999) 107.

[29]. Y.-I. Jang, and Y.-M. Chiang, *Solid State Ionics*, **130** (2000) 53.

[30]. H. Wang, Y.-I. Jang, and Y.-M. Chiang, *Electrochem. Solid-State Lett.*, **2** (1999) 490.

[31]. Y.-M. Chiang, H. Wang, and Y.-I. Jang, *Chem. Mater.*, **13** (2001) 53.

[32]. A. K. Padhi, K. S. Nanjundaswamy, C. Masquelier, and J. B. Goodenough, *J. Electrochem. Soc.*, **144** (1997) 2581.

[33]. A. Manthiram, and J. B. Goodenough, *J. Power Sources*, **26** (1989) 403.

[34]. A. K. Pahdi, K. S. Najundaswamy, and J. B. Goodenough, *J. Electrochem. Soc.*, **144** (1997) 1188.

[35]. D. D. MacNeil, Z. Lu, Z. Chen, and J. R. Dahn, *J. Power Sources,* **108** (2002) 8.

[36]. M. Takahashi, S. Tobishima, K. Takei, and Y. Sakurai, *Solid State Ionics,* **148** (2002) 283.

[37]. D. Fauteux, and R. Koksbang, *J. appl. Electrochem.*, **23**, (1993) 1.

[38]. K. Takita, K. Kono, T. Takesima, and K. Okamoto, US Patent (1991) No. 5,051,183.

[39]. T. Fujii, K. Handa, K. Watanabe, H. Nakanishi, Y. Usami, and K. Sugiura, European Patent Application (1994) No. 0603500A1.

[40]. K. Yagi, A. Hashimoto, and H. Mantoku, European Patent Application (1995) No. 0683196A2.

[41]. R. B. Isaacson, and H. S. Bierenbaum, US Patent (1971) No. 3,558,764.

[42]. E. Kamei, and Y. Shimomura, US Patent (1986) No. 4,563,317.

[43]. P. Arora, and Z. Zhang, *Chemical Review*, **104** (2004) 4419.

[44]. J. M. Tarascon, M. Armand, *Nature*, **414** (2001) 359.

[45]. K. Kang, Y. Meng, J. Breger, C. Grey, G. Ceder, *Science*, *311* (2006) 977.

[46]. D. Lindley, Nature, **463** (2010) 7277.

[47]. S.S. Zhang, *J. Power Sources*, **164** (2007) 351.

[48]. F. G. B. Ooms, E. M. Kelder, J. Schoonman, N. Gerrits, J. Smedinga, and G. Callis, *J. Power Sources*, **97–98** (2001) 598.

[49]. J. Saunier, F. Alloin, J. Y. Sanchez, and G. Caillon, *J. Power Sources*, **119–121** (2003) 451.

[50]. Y. M. Lee, J. W. Kim, N. S. Choi, J. A. Lee, W. H. Seol, and J. K. Park, *J.*

Power Sources, **139** (2005) 235.

[51]. K. M. Abraham, and M. Alamgir, *J. Electrochem. Soc.*, **142** (1995) 683.

[52]. D. Linden, and T. B. Reddy, *Handbook of batteries*, 3rd ed., McGraw Hill: New York, (2002)

[53]. J. O. Besenhard Editor, *Handbook of Battery Materials*, Wiley: Weimheim, (1999).

[54]. D. Berndt, *Maintenance Free Batteries*, 3rd ed., Research Studies Press Ltd.: Taunton, Somerset, England, (2003).

[55]. H. Bode, *Lead-Acid Batteries*, Wiley: Now York, (1977).

[56]. S. U. Falk, and A. J. Salkind, *Alkaline Storage batteries*, Wiley: New York, (1977).

[57]. A. Fleischer, and J. J. Lander, *Zinc-Silver Oxide Batteries*, Wiley: Now York, (1971).

[58]. R. J. Brodd, H. M. Friend, and J. C. Nardi Editors, *Lithium Ion Battery Technology*, ITE-JEC: Brunswick, OH, (1995).

[59]. M. Wakihara, O. Yamamoto Editors, *Lithium Ion Batteries, Fundamentals and Performance*, Wiley: New York, (1998).

[60]. A. Yoshino, *Chem. Ind.*, **146** (1995) 870.

[61]. W. A. V. Schalkwijk Editor, *Advances in Lithium Ion Batteries*, Kluwer: New York, (2002).

[62]. Y. M. Lee, N. S. Choi, J. A. Lee, K. Y. Cho, H. Y. Jung, J. W. Kim, and J. K. Park, *J. Power Sources*, **146** (2005) 431.

[63]. K. Gao, X. Hu, C. Dai, and T. Yi, *Mater. Sci. Eng., B*, **131**, (2006) 100.

Chapter 2

Development of Nano-fiber based Nonwoven Separators for Lithium-ion Battery and their Battery Performance

2.1 Development and Characterization of PAN based Nano-fiber Nonwoven Separator

2.1.1 Introduction

Because higher energy density of batteries can be translated into longer operating times for portable electronic products, lithium-ion batteries with the highest energy density among commercial batteries, are rapidly replacing other battery systems. Recently, lithium-ion batteries have been extensively studied as a promising power source for hybrid electric vehicles (HEVs). In the lithium-ion battery system, a separator could be an ionic resistor because lithium ions pass through a separator during charge discharge processes. Thus, electrochemical performance of the lithium-ion battery is closely related to structure of separator, i.e., thickness, porosity, and permeability [1].

A separator is totally necessary in order to separate positive and negative electrode and maintaining liquid electrolyte between both of the electrodes. However, the existence of the separator increases cell resistance by a factor of 6-7 [1] and reduces volumetric energy density of the battery. Polyolefin micro porous membranes have been used as major separator for the lithium ion battery. But, the rate capabilities of the separators are not enough for high power application, such as electric vehicles, hybrid electric vehicles and robots. The micro porous membrane separators have some disadvantages to be improved, e.g. low wettability [2,3] and low porosity of about 40 % [4]. On the contrary, nonwoven separators have higher porosity (60 - 90 %) and higher air permeability than the polyolefin one, which would increase the rate capability of the lithium ion battery. However, the nonwoven separators have some disadvantages, such as large pore size and thicker nature. Therefore, it is very worth developing a new nonwoven separator with small pore size, small volume, high porosity and high air permeability for high power lithium ion battery.

I have developed several series of PAN nano-fiber based nonwoven separators using different PAN nano-fibers (250 and 380 nm in diameters) with close thickness and similar pore size to the conventional micro porous membrane one and similar porosity and air permeability to the conventional nonwoven one. In this section, I have studied the physical, thermal and electrochemical properties of the PAN nonwovens as separator for lithium ion battery.

2.1.2 Experimental

PAN nanofiber-based nonwoven separators were prepared by electrospinning technique. To obtain PAN nonwoven separator, we prepared 10.5 wt % solution by dissolving polyacrylonitrile using *N*,*N*-dimethylformamide (DMF) then ejected through a voltage applied (14 kV) nozzle to the grounded target plate with a feeding rate of 1.2 mL h^{-1}. The distance between capillary and target plate was 8 cm. The thickness of the obtained fabric was controlled by rollpressing after drying process. Fig. 2.1.1 shows schematic depiction of equipment for electrospinning.

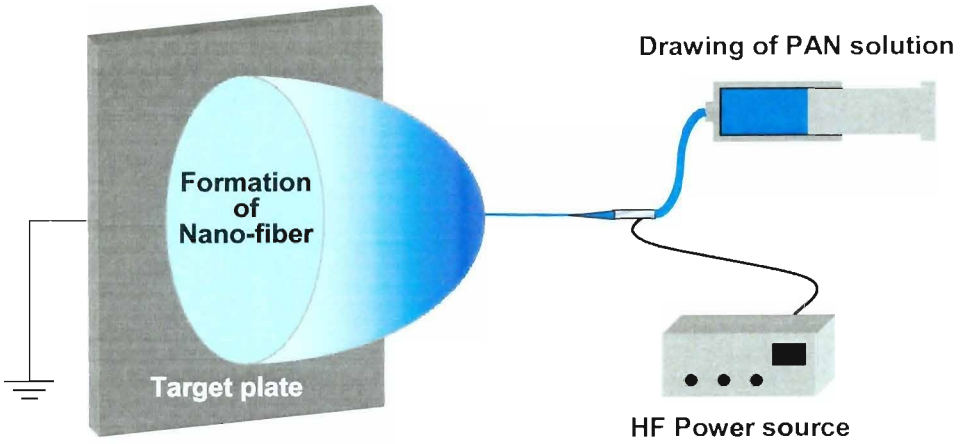

Figure 2.1.1 Schematic depiction of equipment for electrospinning.

The morphologies of the electrospun PAN nano-fibers at fresh and after tests, e.g. charge-discharge test and hot oven test, were observed by Scanning Electron Microscope (SEM). For the observation after tests, the separators were washed by using dimethyl carbonate (DMC).

The average pore sizes of the PAN-based nonwoven separators were obtained by bubble point method. The pore size and distribution was decided by follow equation.

$$D=\frac{4\gamma\times\cos\theta}{P} \tag{1}$$

where D is the diameter of the pores, P is the bubble-point pressure, γ is the surface tension of the liquid, and θ is the liquid-solid contact angle.

Differential scanning calorimetry (DSC) measurements were carried out for PE, PP membrane separators, and PAN nonwoven separator in the temperature range of 40 – 300 °C at a scan rate of 5 °C min^{-1} using Rigaku Thermo plus DSC 8230 instrument.

The wettabilities of the PAN nonwoven and a conventional polyolefin micro porous membrane were estimated by monitoring the variation of contact angle between liquid electrolyte and the membranes at every 0.01 second by use of a DAT1100 (Fibro system ab, Sweden).

Electrochemical characterizations were carried out using the 2032-type coin cell. A cathode was prepared according to the following. The lithium cobalt oxide (Nippon Chemical industrial Co. Ltd.), ketjen black, and polyvinylidene fluoride (90:5:5 in wt %) were blended in *N*-methylpyrrolidinone. The blended slurry was coated on an aluminum foil. The electrode sheet was role-pressed then punched 12 mm in diam. The coin type cell was composed of the cathode, graphite electrode (Hohsen Co. Ltd.) as an

anode and 1 M $LiPF_6$-EC/DEC (1:1 in volume) as an electrolyte. The electrochemical cycling tests were carried out in the voltage range of 3.0 - 4.2 V at 30 °C. In order to form a stable solid electrolyte interface (SEI) on the surface of the graphite anode, the first cycles for all of the test cells were charged under constant current-constant voltage (CC-CV) mode at the 0.2 C-rate, and then discharged under constant current mode at the 0.2 C-rate. In the following cycles, charge-discharge tests were carried out under constant current mode at the 0.5 C-rate. In order to investigate the discharge rate capability for the cells with various separators, the cells were charged up to 4.2 V at the 0.2 C-rate, and then discharged to 3.0 V at the C-rates of 0.2, 0.5, 1, 2, 4 and 8 C. Cyclic voltammetry (CV) study was conducted at a scan speed of 0.1 mV s^{-1} between 3.0 and 4.5 V vs Li using a two-electrode coin type cell. The coin type cell was composed of $LiCoO_2$ as a working electrode, 1 M $LiPF_6$-EC/DEC (1:1 in volume) as an electrolyte and lithium foil as counter electrode and reference.

The ionic conductivities of the electrolyte with and without separators were measured by an ac impedance spectroscopy using HS cell (Hohsen, Japan). The cells were formed by sandwiching the electrolyte soaked separator between two stainless steel electrodes. The ac impedance measurements were carried out using the Solatron SI1280B frequency response analyzer (FRA). The impedances of the coin type cells were estimated at the fresh state and at the end of charge-discharge tests using the FRA over the frequency range of 20 kHz to 0.1 Hz with 10 mV of the AC amplitude.

2.1.3 Results and discussion

In order to manufacture micro porous nonwoven with small pore size and complex pore structure enough to prevent the internal short circuit during charge-discharge test, it is very important to use fine fibers with homogeneous diameter. The

diameter and morphology of the electrospun nano-fiber are greatly influenced by electrospinning parameters, such as the polymer concentration, applied voltage, feeding speed of the polymer solution and capillary-screen distance [5]. I have prepared successfully fine PAN fibers with homogeneous diameters of around 250 and 380 nm by controlling these parameters. Fig. 2.1.2 shows SEM photographs of the nano-fibers. The fibers exhibited homogeneous diameters and any observable beads did not exist on the fibers.

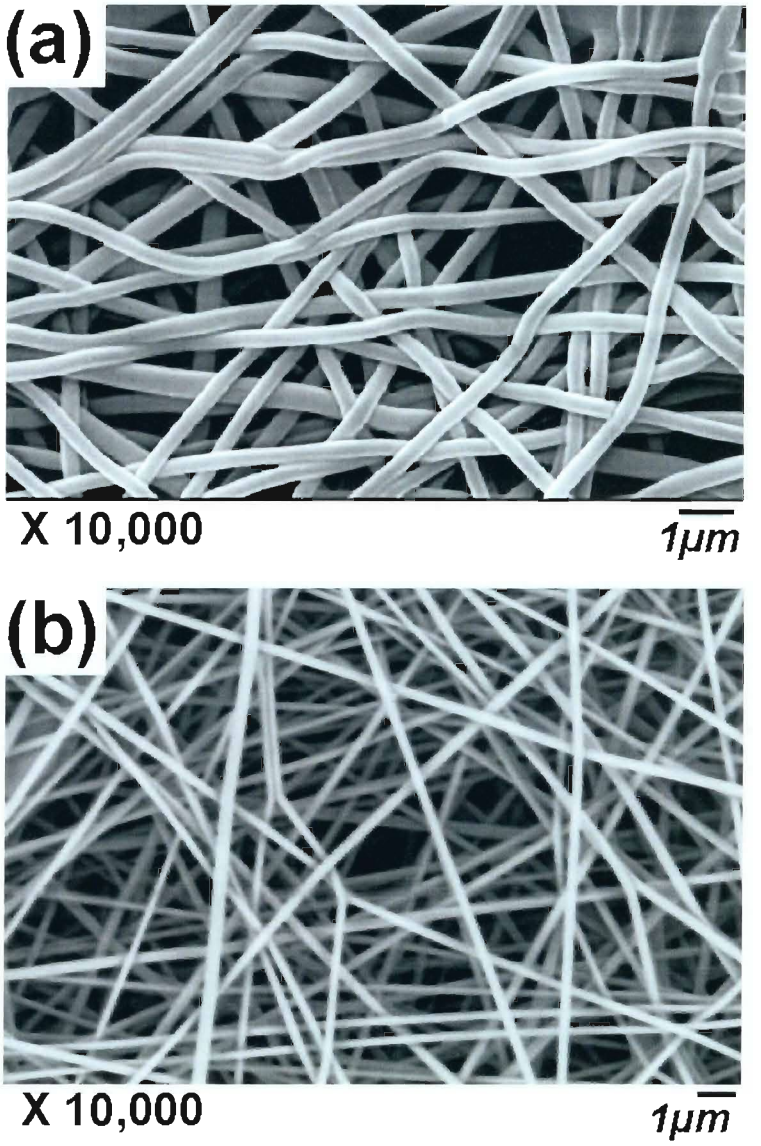

Figure 2.1.2 SEM photographs of the electrospun PAN nano-fiber with diameter of (a) 380 and (b) 250 nm.

Table 2.1.1 shows brief physical properties of the PAN nonwovens, compared with that of the conventional polypropylene membrane (Celgard® 2400). Hereinafter I refer the four PAN wonwovens as PAN *No.1* to *No.4*. The PAN *No.1* and *No.2*, which were made of 380 nm fibers, showed mean pore size of 0.28 and 0.38 μm, respectively. The mean pore sizes of the PAN nonwovens were reduced to 0.18 (PAN *No.3*) and 0.17 μm (PAN *No.4*) by using finer PAN fibers (250 nm) without remarkable decrease in the porosities. The measured thicknesses of the PAN nonwovens were in the range of 25 - 35 μm, of which values are similar to that of the Celgard membrane. In spite of similar thickness, the PAN nonwovens showed roughly two times higher porosities than that of the Celgard one. Besides, The PAN nonwovens showed enormously low gurley values compared with the Celgard one.

Table 2.1.1 Brief physical properties of separators

Property	Celgard® 2400	PAN *No.1*	PAN *No.2*	PAN *No.3*	PAN *No.4*
Composition	PP	PAN	PAN	PAN	PAN
Thickness (μm)	25	33	35	25	30
Pore size (μm)	0.1 × 0.04	0.28	0.38	0.18	0.17
Porosity* (%)	37	64	76	64	56
Gurley (Sec./100cc)	730	7	3	9.5	11
Fiber Diameter (nm)	–	380	380	250	250

In order to confirm the electrochemical stability of the PAN nonwoven separator, cycle voltametry was conducted using 2032 coin type cell with PAN #1 then result is presented in Fig. 2.1.3. The cyclic voltammogram shows only typical redox peak of the

$LiCoO_2$ in the sweep voltage range. This result indicates that the newly developed PAN nonwoven separator can be stables in the voltage range 3.0 – 4.5 V vs. Li.

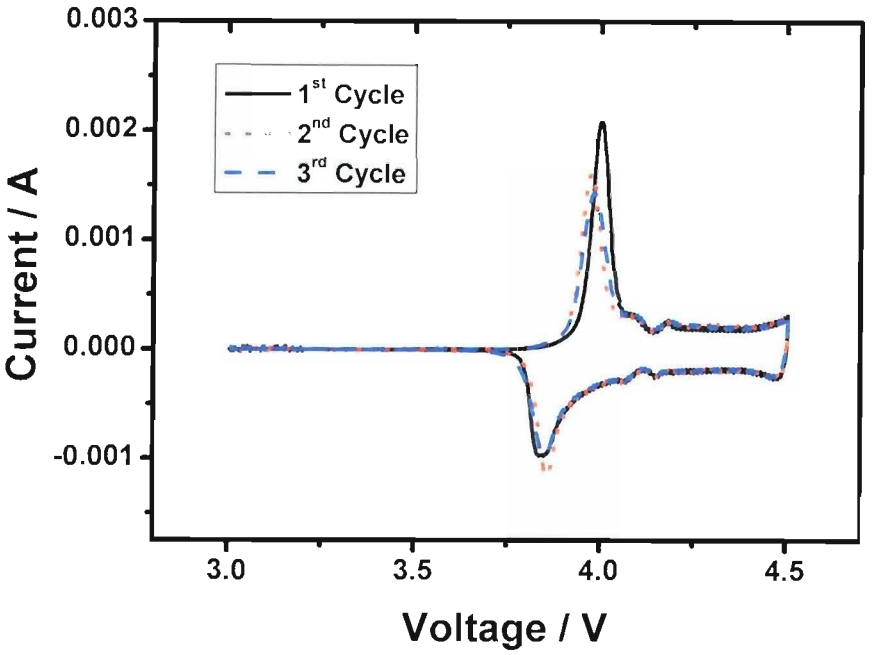

Figure 2.1.3 Cyclic voltammogram of the cell with PAN nano-fiber based separator in the voltage range 3.0 – 4.5V vs. Li.

The wettability of the separator in non-aqueous electrolyte is important parameter because the separator with good wettability can retain the electrolyte effectively and facilitates an electrolyte to diffuse smoothly into the cell assembly [6]. The variations of the contact angles of the PAN nonwoven and the polyolefin membrane *vs.* time are presented in Fig. 2.1.4. The contact angle of the PAN nonwoven decreased more rapidly than that of the polyolefin one. It means that the PAN nonwoven has better wettability than the polyolefin one. The better wettability of the PAN nonwoven could be ascribed to hydrophilicity of the PAN polymer.

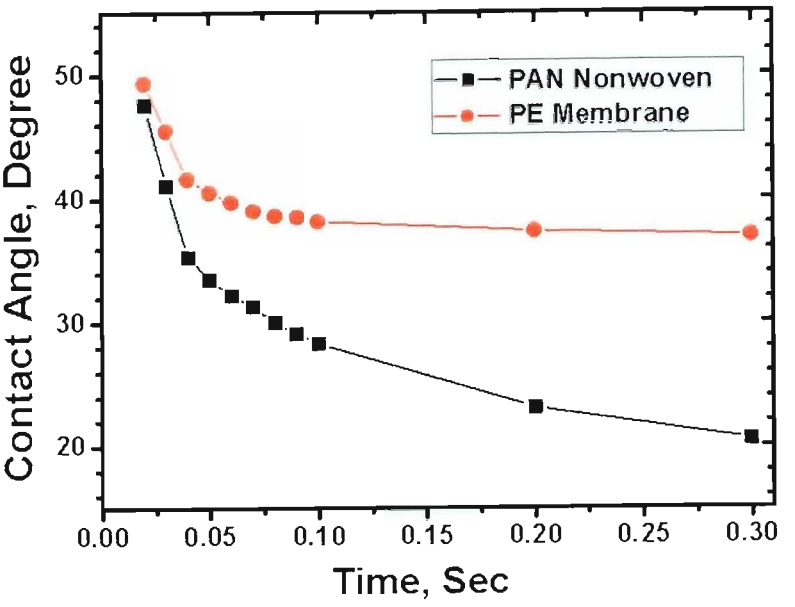

Figure 2.1.4 Variation of contact angles between separators and electrolyte depending on time.

The existence of a separator between positive and negative electrodes causes the decrease in mobility of conductive ions during the charge-discharge process. The MacMullin number (N_M), which is defined as the ratio of the conductivity of separator containing electrolyte to that of the pure electrolyte, could be used in order to evaluate the influence of the separator on the high rate capability [1,7], i.e. lower N_M value of separator would be preferred for the high power application. The porosities, ionic conductivities and the N_M value of the separators are summarized in Table 2.1.2. The N_M value was calculated by following equation [8]:

$$N_M = \frac{\sigma_0}{\sigma_{eff}} \tag{2}$$

where σ_0 and σ_{eff} are the conductivities of electrolyte and separator containing electrolyte, respectively. The PAN nonwovens made of the 250 nm fibers showed

slightly higher N_M value than the PAN nonwovens made of the 380 nm fibers. The higher N_M values of the PAN *No.3* and *No.4* could be ascribed to their high Gurley values, low porosities and smaller pore size. The N_M values of the PAN *No.1* to *No.4* were 3.96, 3.54, 4.62 and 4.39, respectively. It is clear that the PAN nonwovens possessed less than half of the N_M value of the Celgard membrane because of higher porosities and lower Gurley values.

Table 2.1.2 The values of porosity, conductivities (σ_{eff}) and MacMullin number (N_M) obtained from conductivity measurement of separators

Separator	Porosity, %	σ_{eff}, $mS\,cm^{-1}$	N_M
Celgard® 2400	37	0.8	11.3
PAN *No.1*	64	2.2	4.3
PAN *No.2*	76	2.6	3.6
PAN *No.3*	64	1.5	6.5
PAN *No.4*	58	2.1	4.6

$\sigma_0 = 9.64$ mS cm^{-1} at 30 °C

Figure 2.1.5 (a) shows a comparison of the initial charge-discharge curves at the 0.5 C-rate for the test cells using the Celgard membrane and the PAN nonwovens. The cells showed stable charge-discharge curves with discharge capacities of about 120 - 125 mAh g^{-1} based on the weight of $LiCoO_2$. In a preliminary charge-discharge test, a cell using a polyolefin nonwoven (35 μm in thickness) made of polyolefin fibers with about 2 μm in diameter showed unstable voltage profile above 4.0 V at charge process probably due to the micro short circuit by formation of lithium dendrite. It is noticeable that any unstable voltage profile was not observed for the cells with the PAN nonwovens with almost the same or less thickness to the previous polyolefin nonwoven.

The stable voltage profiles would be ascribed to the small pore size of the PAN nonwovens. Fig. 2.1.5 (b) shows cycle stabilities of the test cells. The cells using the PAN nonwovens showed better cycling performances than that of the Celgard one. The obtained discharge capacities and capacity retention ratios of the cells after 250 cycles are summarized in Table 2.1.3.

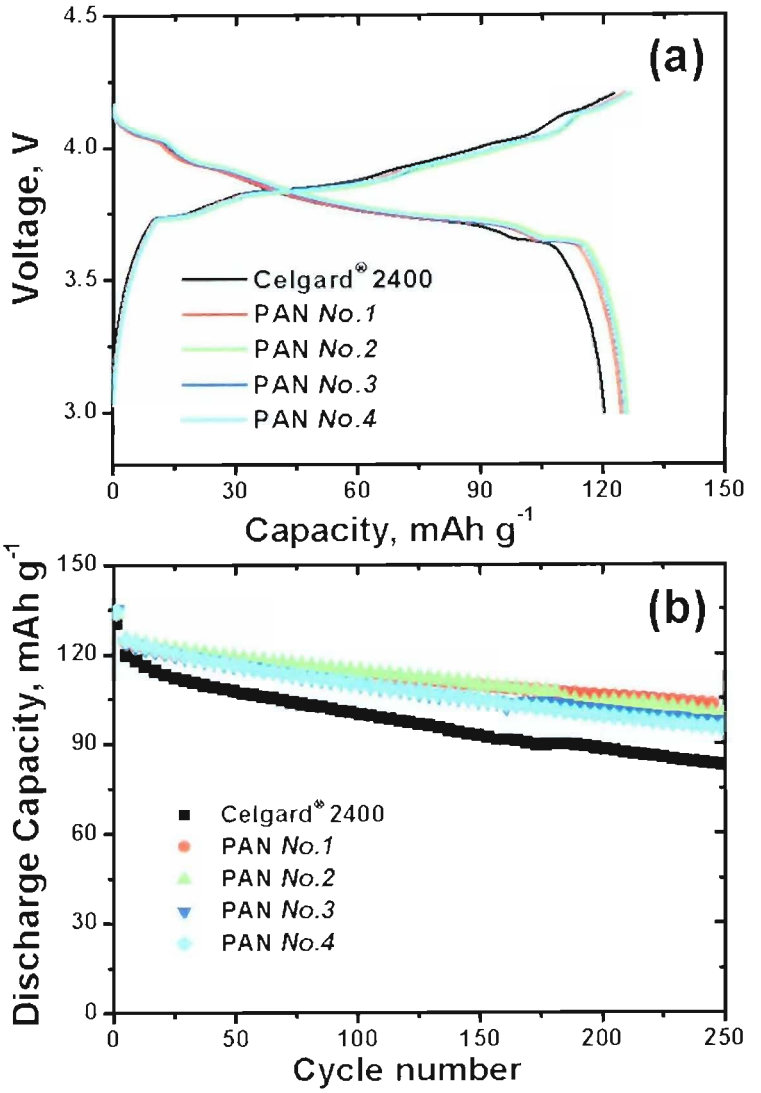

Figure 2.1.5 (a) Initial charge-discharge curves for the cells with the Celgard membrane and the PAN nonwoven membranes. (b) Discharge capacities vs. cycle mumbers of the test cells at the 0.5 C-rate.

Table 2.1.3 Summarized data of charge-discharge performances and charge transfer resistances estimated by EIS measurements for the cells.

Separators	Capacity			Resistance, Ω		
	Initial, mAh g^{-1}	At 250 cycle, mAh g^{-1}	Capacity retention ratio after 250 cycles, %	$R_{CT\,(Ini.)}$	$R_{CT\,(250)}$	ΔR_{CT}
Celgard® 2400	120.4	82.7	68.7	8.0	20.0	12.0
PAN *No.1*	124.5	102.7	82.5	7.2	14.2	7.0
PAN *No.2*	125.9	99.8	79.3	7.2	12.5	5.3
PAN *No.3*	125.3	97.1	77.5	5.5	14.2	8.7
PAN *No.4*	125.4	95.4	76.1	6.7	12.1	5.3

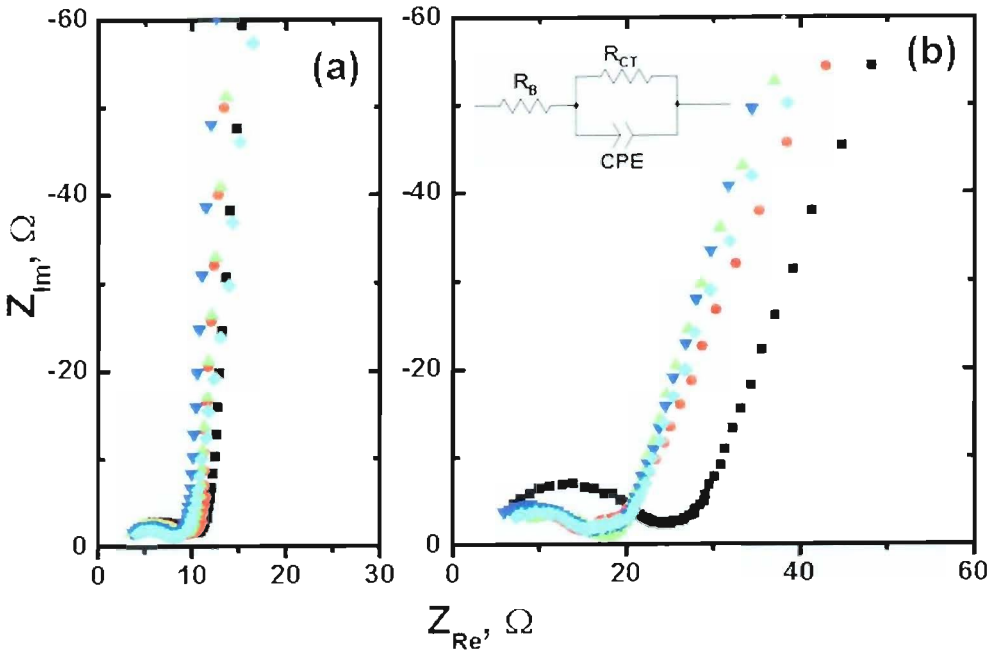

Figure 2.1.6 Nyquist plots for the cells with the Celgard membrane (■), PAN *No.1* (●), PAN *No.2* (▲), PAN *No.3* (▼) and PAN *No.4* (♦) measured at (a) the fresh state and (b) the end of the cycle test.

In order to investigate the variation of cell impedances during cycle test, the electrochemical impedance spectroscopy measurement was carried out for the cells at the fresh state and the end of the charge-discharge test. Fig 2.1.6 (a) and (b) show Nyquist plots of the cells measured at the fresh state and the end of the cycle test, respectively. The spectra consist of a semicircle in the high-middle frequency region and a straight line in the low frequency region. The semicircle corresponds to the charge-transfer process, accompanied with migration of the lithium ion at the electrode/electrolyte interface. The straight line in the low frequency region corresponds to the diffusion process of lithium ion in the electrode. The charge-transfer resistances for the spectra were estimated by fitting the semicircle in the spectra based on an equivalent circuit (the inset of the Fig. 2.1.6 (b)). The components in the equivalent circuit, such as R_B, R_{CT} and CPE represent a bulk resistance including the resistance of

the electrolyte and electrode, a charge-transfer one and a capacitative constant-phase element, respectively. The estimated charge-transfer resistances of the cells are summarized in the Table 2.1.3. The charge-transfer resistances of the cells at the fresh state were almost the same. However, a clear difference on them was observed after the end of cycle test. The charge-transfer resistances of the PAN nonwovens were in the range of 12 – 14 Ω, whereas that of the Celgard membrane showed 20 Ω. The different increasing ratio (ΔR_{CT}) of the charge-transfer resistance between the PAN nonwovens and the Celgard membrane would be ascribed to the difference in the retainability of the liquid electrolyte in the separator. The higher porosities and better wettabilities of the PAN nonwovens than that of the Celgard one would help to retain large amount of electrolyte in the separator, facilitating the migration of lithium ion at the electrode/electrolyte boundary and then suppressing the increase in charge-transfer resistance during cycle test. The better cycleability for the cells with PAN nonwovens than that with the Celgard membrane would be understood in terms of lower increasing ratio of the charge-transfer resistances.

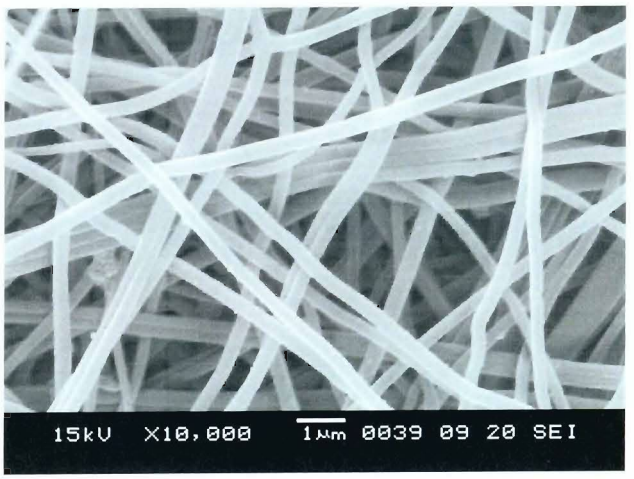

Figure 2.1.7 SEM photograph of the PAN *No.1* after the charge-discharge test.

Figure 2.1.7 shows SEM photograph of the PAN *No.1* after 250th cycle. The PAN nonwoven kept its highly porous structure.

Figure 2.1.8 shows rate capabilities of the cells with the separators. The cell with the Celgard membrane showed capacity retention ratio of about 90 % at the 1 C-rate, and then decreased rapidly with increasing the C-rate up to 8 C-rate. The obtained ratio at the 2, 4, 8 C-rate were 81, 42 and 7 %, respectively. The cells with the PAN nonwovens showed outstanding rate capabilities. Up to the 4 C-rate, the cells retained more than 90 % of the capacities obtained at the 0.2 C-rate. The ratios were higher more than 2 times that for the Celgard one at the same C-rate. A clear difference on the capacity retention ratio of the cells with the PAN nonwovens was observed at the 8 C-rate. The ratios of the PAN No.1 to No.4 at the 8 C-rate were 53, 62, 37 and 45 %, respectively. There is a tendency that the separator with lower N_M value exhibits higher rate capability.

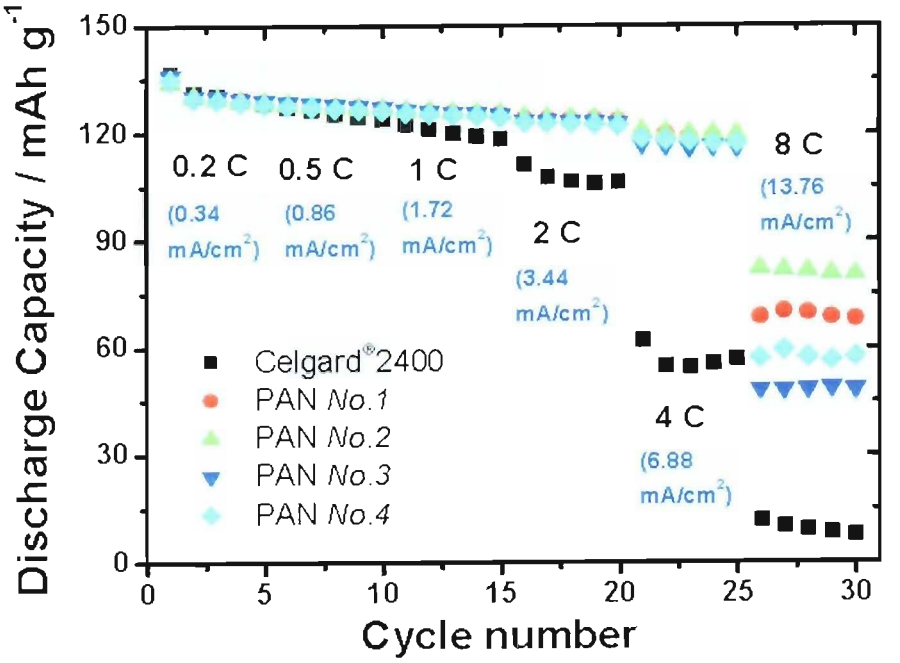

Figure 2.1.8 Results of rate capability tests for the cells with the Celgard membrane and the PAN nonwovens.

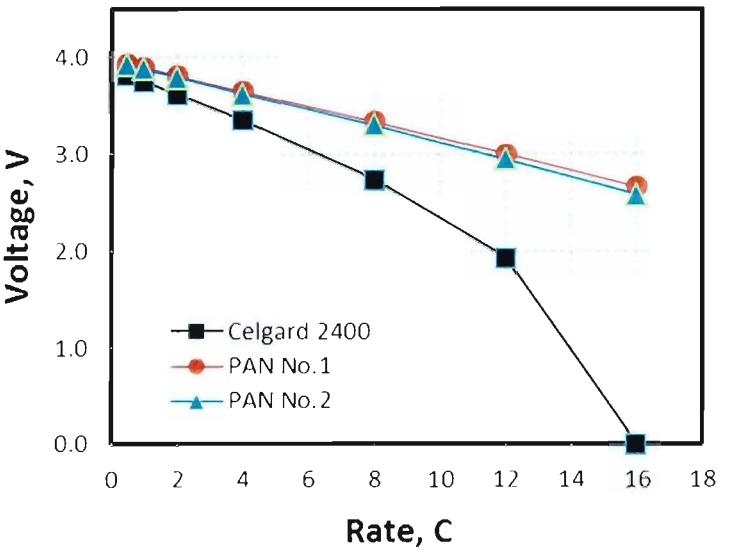

Figure 2.1.9 Relationship between discharge rates and voltages of cells after discharge for 17 seconds at 20 % of DOD.

In order to evaluate the effect of separator on the instantaneous discharge characteristic of the cell, the pulse discharging tests were conducted at various C rates. For the experiment, the cells using four types of separators, i.e., PP, PAN No.1 and PAN No.2, were preliminarily cycled for two cycles at 0.2 C rate in order to activate the cells then discharged for 17 seconds at 20 % of DOD (depth of discharge) state with various C rate of 0.5, 1, 2, 4, 8, 12 and 16 C. The obtained voltages after discharging for 17 seconds at each C rate are summarized in Fig. 2.1.9. Both of the PAN based separators showed linear voltage drop with increase in C rates. On the other hand, the voltages for the cell with PP separator dropped linearly up to 8 C then dropped nonlinearly above 12 C. In general, voltage drop at low rate discharging is mainly due to the ohmic loss generated from substrate or consisting materials. Thus the cell voltage decreases linearly with increase in current. However, in the high rate discharging, voltage drop can be influenced by not only ohmic resistance but diffusion resistance of lithium ion by separator. Accordingly, cell voltage drops rapidly deviated from linear

voltage drop by increasing of current. Based on the above discussion, therefore, it can be concluded that the PAN based separators show smaller ionic resistance at high C-rate than that of PP separator and the separators are very suitable for high power battery application.

In order to investigate thermal stability of the separators, I have conducted differential scanning calorimetry (DSC) measurement for the PE, PP and PAN based separators and results are shown in Fig. 2.1.10. The PE and PP separators show endothermic peaks at 133 and 163 °C, respectively. These peak temperatures are typical melting temperature of PE and PP polymer, respectively. On the other hand, endo- or exothermic peak was not observed up to 250 °C for the PAN based separator. The separator exhibited two exothermic peaks during heating up to 300 °C. The first exothermic reaction was occurred at 253 °C and then following exothermic reaction was observed at 283 °C. The exothermic peaks are due to oxidation of PAN. Based on the DSC analysis, it is reasonable to consider that the PAN separator has better thermal stability than that of polyolefin one.

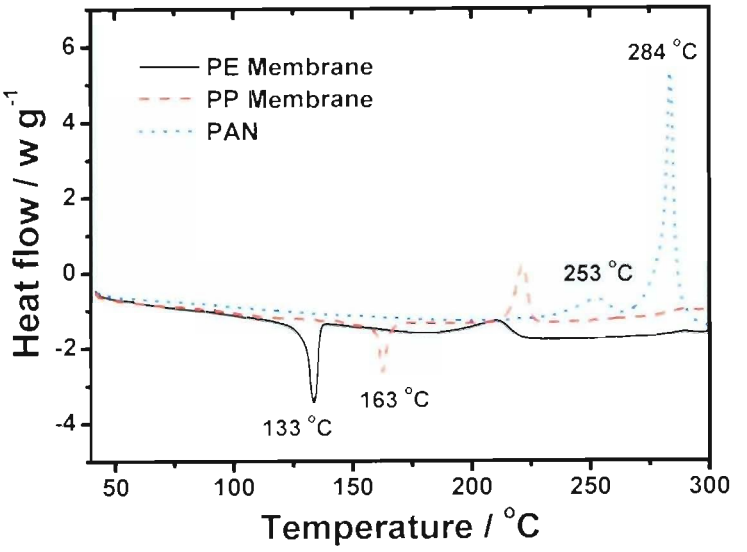

Figure 2.1.10 DSC thermograms of PE and PP based separators and electrospun PAN nano-fiber base nonwoven separator.

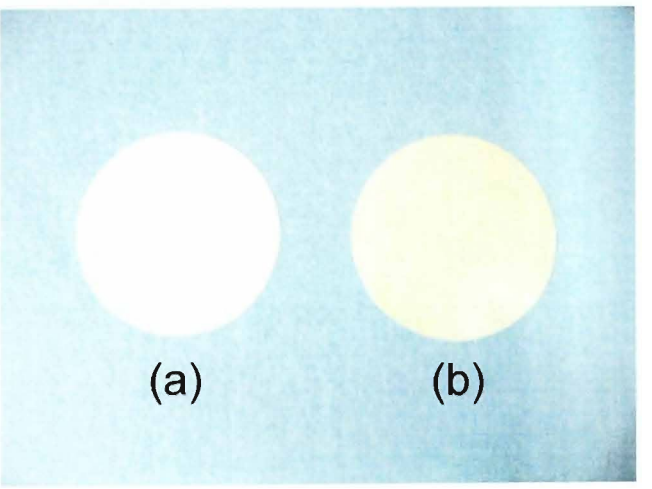

Figure 2.1.11 Photographs of the PAN nonwovens (a) before and (b) after hot oven test at 200 °C for 60 minutes.

To confirm thermal shrinkage of the PAN separator at high temperature, I have carried out thermal treatment for the separator at 200 °C for 1hr then observed changing of its shape. Fig. 2.1.11 (a) and (b) show shape of the PAN nonwovens before and after the hot oven test at 200 °C for 1h, respectively. The PAN nonwoven did not show any shrinkage at 200 °C, even though the color of the PAN nonwoven changed from white to light brown. Subsequently, hot oven tests using the CR-2032 coin type cell after charging up to 4.2 V were carried out for the PAN nonwoven, compared with the cell with the Celgard membrane. After the hot oven test at 120 °C for 1h, the shape of the separators was almost unchanged and vigorous voltage changes were not observed during the test. Next, the hot oven test was carried out at 150 °C. The variations of voltage profiles *vs.* time for the cells during the hot oven test are presented in the Fig. 2.1.12. Unfortunately, both of the cells showed sudden voltage drop after 10 (Celgard membrane) and 14 minutes (PAN nonwoven), respectively, from start of the test, probably corresponding to the short circuit. The short circuits could be caused by the shrinkage of the separators at high temperature of 150 °C in the electrolyte.

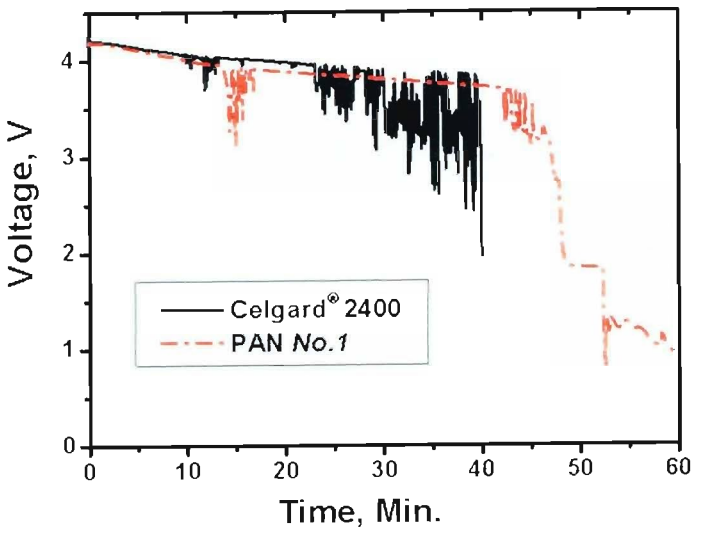

Figure 2.1.12 The voltage profiles for the cells with Celgard membrane and PAN *No.1* during the hot oven test at 150 °C.

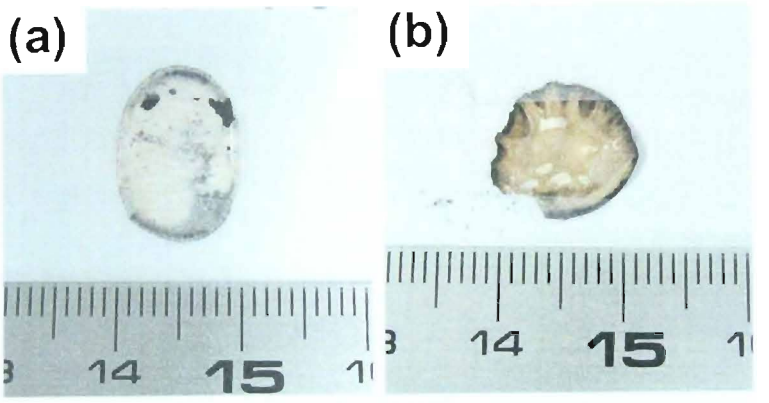

Figure 2.1.13 Photographs of the (a) Celgard membrane and the (b) PAN nonwoven after the hot oven test at 150 °C.

After the tests, we have observed macro and micro (only for the PAN *No.1*) morphological changes for the separators as presented in Fig. 2.1.13 and Fig. 2.1.14, respectively. Shrinkages were observed for both of the separators. The Celgard membrane showed uniaxial shrinkage of about 30 % along the machine direction (Fig. 2.1.13 (a)). The PAN nonwoven also showed isotropic shrinkage of about 26 % and some warping (Fig. 2.1.13 (b)). Figure 2.1.14 (a) - (c) show micro morphologies of the

PAN *No.1* before and after the hot oven test at 150 °C. The SEM photographs revealed that the fine PAN fibers became thicker by swelling and bonded each other, giving rise to thermal shrinkage of the separator, and also collapse of the porous structure in the nonwoven. Interestingly, a clear difference between cathode side and anode one was observed for the morphologies of the PAN fibers. The fibers which contacted with the cathode (Fig. 2.1.14 (b)) became crook, whereas the fibers which contacted with the anode (Fig. 2.1.14 (c)) kept their morphologies, though the observed diameters of the fibers for both the sides of PAN nonwoven were almost the same. The difference in morphological changes between the cathode side and the anode one would bring about the warping of the PAN nonwoven due to their different shrinkage ratio. The reason for the crook of the fibers could be attributed to oxidation of the fibers under the oxidative condition on the charged cathode at high temperature of 150 °C. This result indicates that the thermal stability of the PAN nonwoven membrane at the high temperature of 150 °C is not sufficient yet.

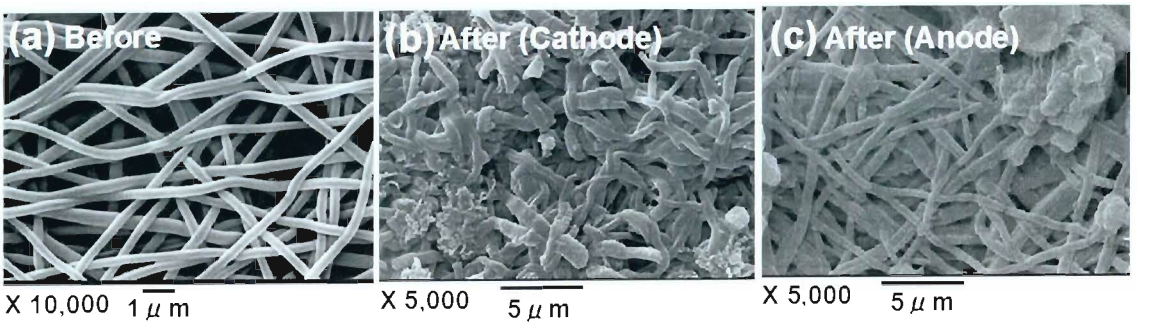

Figure 2.1.14 SEM photographs of the PAN nonwoven membrane before and after the hot oven test.

2.1.4 Conclusion

The micro-porous polyacrylonitrile (PAN) nonwoven have been manufactured by electrospinning technique. The PAN nonwovens exhibited similar pore size to the

conventional micro porous membrane with homogeneous pore size distribution. The PAN nonwovens with small mean pore sizes were successfully manufactured by using nano-fibers of 250 and 380 nm in diameter without remarkable decrease in its porosity. The separator was confirmed to be electrochemically stable in the voltage range 3 – 4.5 V by cyclic voltammetry study. The PAN nonwovens showed higher ionic conductivities than that of the Celgard membrane because of their high porosities. The cells with the PAN nonwovens showed better cycle lives at the 0.5 C-rate with smaller increase in the charge-transfer resistances than that with the Celgard membrane during charge-discharge test. Moreover, the cells with the PAN based separators exhibited superior rate capability to the conventional one due to smaller diffusion resistance of the separators during charge discharge process at high rate as confirmed by pulse discharging test. Therefore, the newly developed PAN based separators can be promising candidate for separators for the lithium ion battery, especially battery for high power application. The PAN nonwovens are thermally stable at 120 °C, but become unstable at 150 °C. In order to apply it as a separator for practical lithium-ion battery, the thermal stability of the nonwoven has to be improved.

Reference

[1] P. Azora and Z. Zhang, *Chem. Rev. (Washington, D.C.)*, **104** (2004) 4419.

[2] J. Saunier, F. Alloin, J. Y. Sanchez, and G. Caillon, *J. Power Sources*, **119-121** (2003) 451.

[3] Y. M. Lee, J. W. Kim, N. S. Choi, J. A. Lee, W. H. Seol, and J. K. Park, *J. Power Sources*, **139** (2005) 235.

[4] F.G.B. Ooms, E.M. Kelder, J. Schoonman, N. Gerrits, J. Smedinga, and G. Callis, *J. Power Sources,* **97-98** (2001) 598.

[5] C. Zhang, X. Yuan, L. Wu, Y. Han, and J. Sheng, *Eur. Polym. J.*, **41** (2005) 423.

[6] S. S. Zhang, *J. Power Sources*, **164** (2007) 351.

[7] K. M. Abraham, *Electrochim. Acta*, **38** (1993) 1233.

[8] K. K. Patel, J. M. Paulsen, and J. Desilvestro, *J. Power Sources,* **122** (2003) 144.

2.2 Development and Characterization of PVA based Nano-fiber Nonwoven Separator for lithium-ion battery

2.2.1 Introduction

Recently, a large scale lithium ion battery with high power and energy has been studied to expand current usage for portable appliances into electric vehicles, hybrid vehicles and robots. Although a separator is positively necessary to separate positive and negative electrodes, it is known that the presence of a separator cause the increase in internal resistance of a battery by a factor of 6-7 [1]. Thus, the power of the battery depends strongly on the properties of the separator. Polyolefin based conventional micro porous membrane separators, which are used as major separators for the lithium ion battery, have some disadvantages to be improved, such as low wettability [2,3] and lower porosity [4], which would restrict input and output power of the lithium ion battery.

The PVA is one of the attractive ingredients to fabricate porous films as separators for battery because of its insolubility in alkaline solution and non-aqueous solvents. Moreover, the polymer has several advantages such as relatively low price, easiness in fabrication on a commercial scale from aqueous solution, low health hazard to personnel and low pollution treat to the environment. The PVA films were studied as separators in various alkaline battery applications such as nickel oxide – zinc and silver oxide – zinc batteries [5,6], and it has been using practically as a separator in the battery system [1]. However, it is hard to find reports or papers corresponding to the PVA separators for the lithium ion battery with non-aqueous liquid electrolyte. Therefore, in this section, I have developed PVA nano-fiber based nonwoven membranes for high power lithium ion battery using the electrospinning technique and have investigated a potential of the nonwoven as a separator for the high power lithium ion battery. In this

chapter, I discussed the physical and electrochemical properties of the PVA nonwovens as well as battery performances of cells using them.

2.2.2 Experimental

I have prepared PVA nonwovens by using electrospun PVA nano-fibers. For spinning the nano-fibers, 15 wt. % of PVA solution was prepared by dissolving a PVA polymer in distilled water, and then ejected with a feeding rate of 1.0 ml hr^{-1} through a voltage applied (27 kV) nozzle to the grounded target plate. The distance between capillary and target plate was 9 cm. The thickness of the obtained fabric was controlled by a roll-pressing after drying process.

Scanning Electron Microscope (SEM) observation was carried out in order to observe the morphology of the PVA nonwovens before and after charge-discharge tests. The average pore sizes and pore size distributions of the PVA nonwovens were measured by using the Automated Perm Porometer (Porous Materials, Inc., USA).

Cyclic voltammetry study was conducted at a scanning rate of 1 mV sec^{-1} in the voltage range of 3 to 4.5 V vs. Li using a 2032 type coin cell. The test cell was composed of $LiCoO_2$ as a working electrode, 1M $LiPF_6$-EC/DEC (1:1 in volume) as an electrolyte and lithium foil as a counter electrode and reference.

Battery performances for cells assembled with the Celgard membranes (Celgard® 2400 and Celgard® 2730) and the PVA nonwovens were evaluated using the 2032 type coin cells. Details for preparing $LiCoO_2$ electrode are described in elsewhere. The coin type cell was composed of the $LiCoO_2$ as a cathode, lithium foil (Honjo metal, Japan) or graphite electrode (Hohsen, Japan) as an anode and 1M $LiPF_6$-EC/DEC (1:1 in volume)

as an electrolyte. The electrochemical cycling tests were carried out in the voltage range of 3.0 to 4.2 V at 30 °C.

2.2.3 Results and Discussion

In this study, I have prepared two PVA nano-fiber nonwoven separators having different thickness and porosity. Table 2.2.1 shows brief physical properties of the PVA nonwovens, compared with Celgard® 2730 (PE) and 2400 (PP) micro porous membranes. Hereinafter, I have referred the two PVA nonwovens as PVA #1 and PVA #2, respectively. The most noticeable differences between the PVA nonwovens and the Celgard membranes are their porosities and Gurley values. The nonwovens have higher porosities and lower Gurley values than the Celgard membranes. The porosities of the PVA #1 and #2 are 84 % and 75 %, respectively, which are more than two times that of the Celgard membranes.

Table 1. Physical properties of the separators

Properties	Celgard® 2730	Celgard® 2400	PVA #1	PVA #2
Composition	PE	PP	PVA	PVA
Thickness *(μm)*	20	25	26	39
Pore size *(μm)*	0.1 × 0.05	0.1 × 0.04	0.39	0.32
Porosity *(%)*	43	40	84	75
Gurley* *(s 100 cm^{-3})*	530	730	2.5	5.6
Density *(g cm^{-3})*	–	–	0.20	0.32

* *Measured value*

Moreover, the PVA nonwovens have lower Gurley values compared to the Celgard membranes by a factor of 100 – 200. The higher porosity can allow uptake more amount of electrolyte in the separator, which could provide higher ionic conductivity [3] and better cycle life to the lithium ion battery. Further, the Gurley value

of separator is closely related to the ionic resistivity of the separator, i.e., a separator with low Gurley value could afford low ionic resistivity to the battery [7]. Thus, it is expected that the cells assembled with the PVA nonwovens would show better battery performance than the cells using the Celgard membranes.

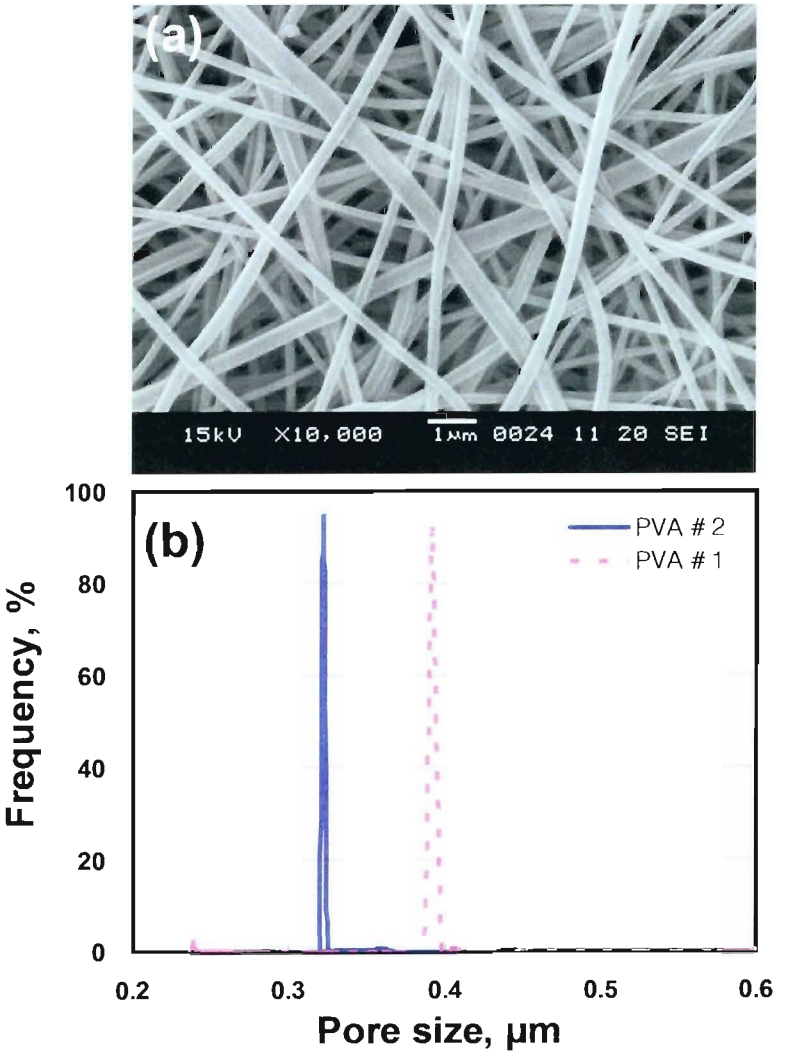

Figure 2.2.1 (a) Morphology of the electrospun PVA nano-fiber obtained by SEM observation and (b) pore size distributions of PVA nonwovens.

Generally requisite properties to a membrane separator for lithium ion battery are chemical stability, homogeneity of pore size distribution, small pore size and complex

pore structure, because a separator having large pore size and simple pore structure could not protect a cell from internal short circuit [8]. Moreover, inhomogeneous pore size would encourage the Li dendrite formation and poor cycle stability due to inhomogeneous current distribution. Therefore, it is very important to use nano-fibers with fine and homogeneous diameter for producing nonwoven separator. Fig. 2.2.1 (a) shows morphology of the PVA #1. The nonwoven membrane consists of finer fiber with homogeneous diameter of around 250 nm as shown in the Fig. 2.2.1 (a). Figure 2.2.1 (b) shows pores size distributions of the PVA nonwovens obtained by the bubble point method. The results exhibited that the PVA #1 and #2 have very narrow pore size distributions with mean pore sizes of 0.39 and 0.32 μm, respectively.

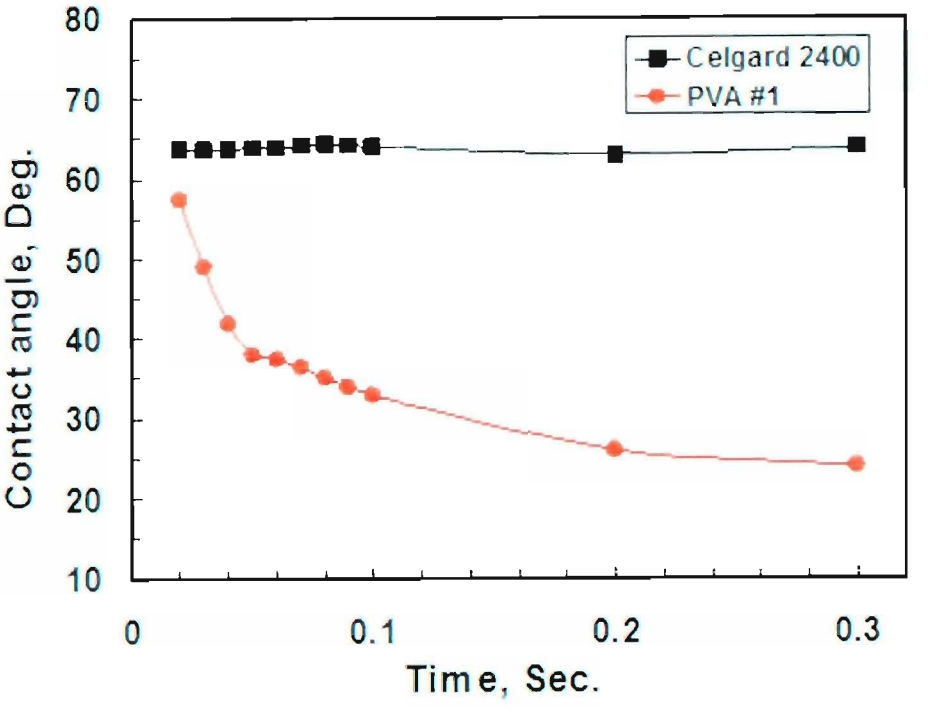

Figure 2.2.2 The time *vs.* contact angles between separators and electrolyte.

The wettabilities of the polyolefin membrane and the PVA nonwoven were evaluated by measuring contact angles between a liquid electrolyte and the separators.

The contact angles were monitored by using the DAT1100 (Fibro system ab, Sweden). As shown in Fig. 2.2.2, the contact angles of the polyolefin membrane and the PVA nonwoven were 49.6 ^{o} and 57.1 ^{o} for initial stage, respectively. As compare to the polyolefin membrane, the PVA nonwoven showed rapid decrease on the contact angle as shown in the Fig. 2.2.2. The result indicates that the PVA nonwoven has better wettability than the polyolefin one due to hydrophilicity of the PVA polymer.

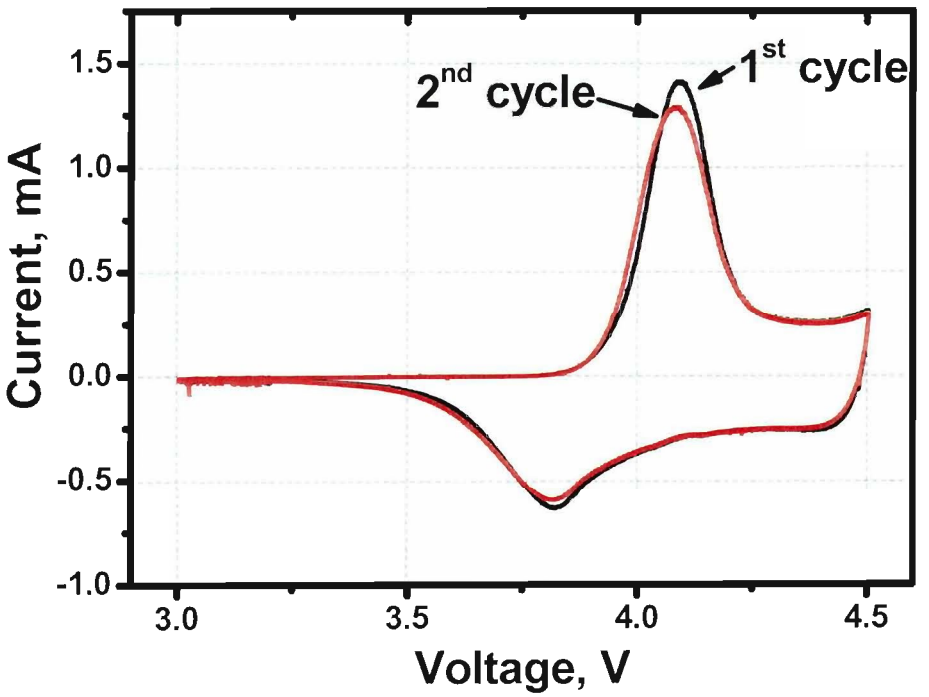

Figure 2.2.3 Cyclic voltammogram of the cell using PVA nonwoven separator.

An electrochemical stability of the PVA nonwoven was investigated by the cyclic voltammetry study. Figure 2.2.3 shows cyclic voltammogram for the coin type cell in the voltage range of 3 to 4.5 V vs. Li^{+}/Li. The coin type cell assembled with the PVA #1 showed well-defined redox peaks corresponding to the lithium extraction/insertion

from/into $LiCoO_2$ and any observable extra peak did not exist. The result indicates that the PVA nonwoven separator is stable in the voltage range of 3 to 4.5V vs. Li^+/Li. The voltage range is large enough to accept various cathode materials such as $LiCoO_2$, $LiMn_2O_4$, $Li[Co_{1/3}Mn_{1/3}Ni_{1/3}]O_2$ and $Li[Mn_{1/2}Ni_{1/2}]O_2$.

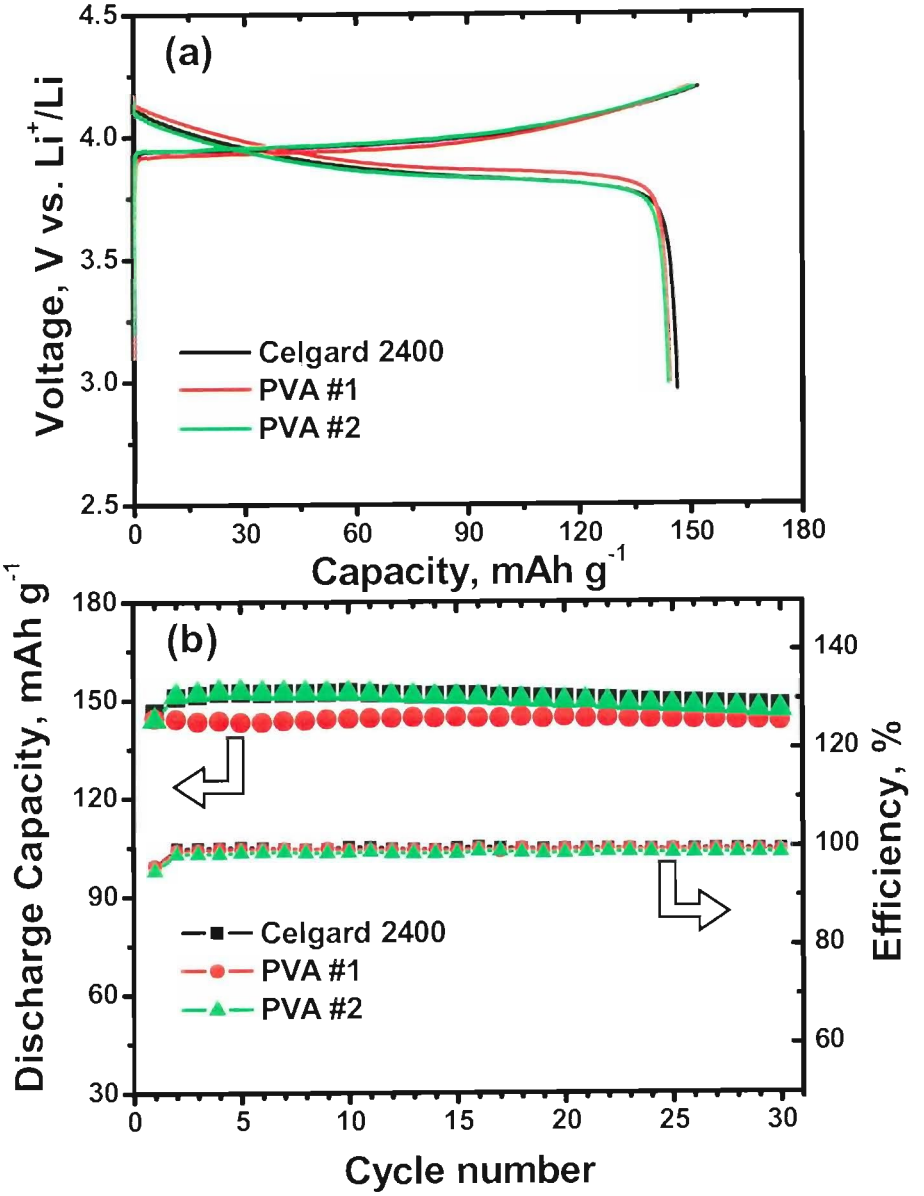

Figure 2.2.4 (a) Initial charge discharge curves of the cells using lithium foil as an anode and (b) discharge capacities and coulombic efficiencies of the test cells as a function of cycle number with a C-rate of 0.2.

Figure 2.2.4 (a) and (b) show initial charge-discharge curves and cycling performances for coin type cells using lithium foil as an anode in the voltage range of 3 to 4.2 V with a 0.2 C-rate based on the capacity of the $LiCoO_2$ electrode. As shown in the Fig. 2.2.4 (a), the test cells showed stable charge-discharge curves without any unstable voltage profile originated from the micro short circuit due to the formation of Li-dendrite and the cells exhibited stable cycling performance with high coulombic efficiency of about 100 %.

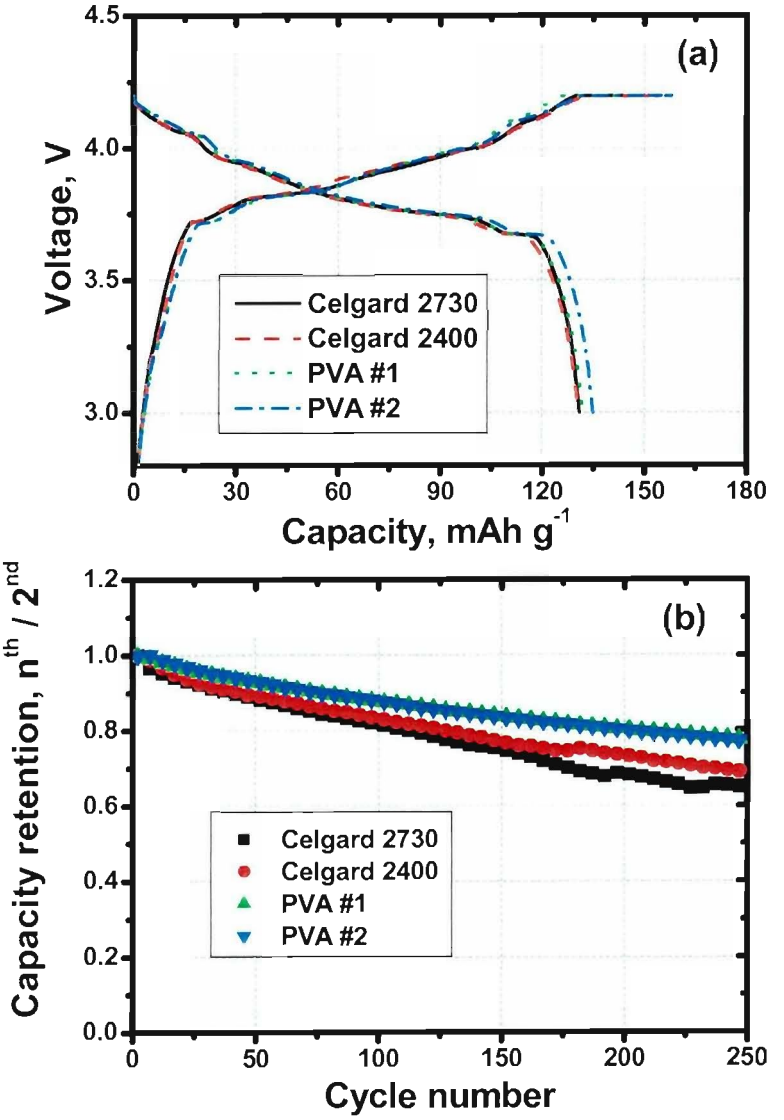

Figure 2.2.5 (a) Initial charge discharge curves of the cells using graphite as an anode and (b) discharge capacities of the test cells as a function of cycle number with a C-rate of 0.5.

Figure 2.2.5 (a) shows initial charge-discharge curves of cells using graphite as an anode. In the first cycle, the cells were charged up to 4.2 V under constant current with a 0.2 C-rate and then continuously charged at 4.2 V under constant voltage mode for 10 h. After that, the cells were discharged to 3.0 V under constant current with the 0.2 C-rate. In the following cycles, the cells were cycled in the voltage range of 3.0 – 4.2 V under constant current mode with a 0.5 C-rate. Figure 2.2.5 (b) shows capacity retention ratios of the cells over 250 cycles. After 250 cycles, the cells with the PVA #1 and PVA #2 showed capacity retention ratios of 77.3 % and 76.9 %, respectively, of which values are higher than those obtained for the cells using the Celgard membranes (64.6 % for the PE membrane and 68.7 % for the PP membrane). The long cycle lives of the cells with the PVA nonwovens can be ascribed to their higher porosity and wettability which could help retaining the liquid electrolyte between positive and negative electrodes during cycling.

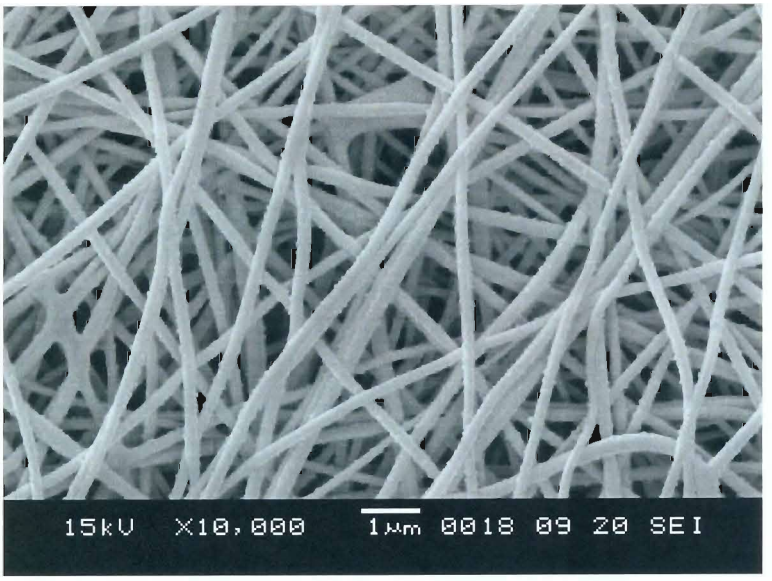

Figure 2.2.6 SEM photograph of the PVA #1 after 250th cycle.

Figure 2.2.6 shows morphology of the PVA #1 after cycling test for 250 cycles. As compare with the fresh PVA #1 (Fig. 2.2.1 (a)), the morphological change due to swell or gel with liquid electrolyte was not observed for the PVA nonwoven after long term cycling test.

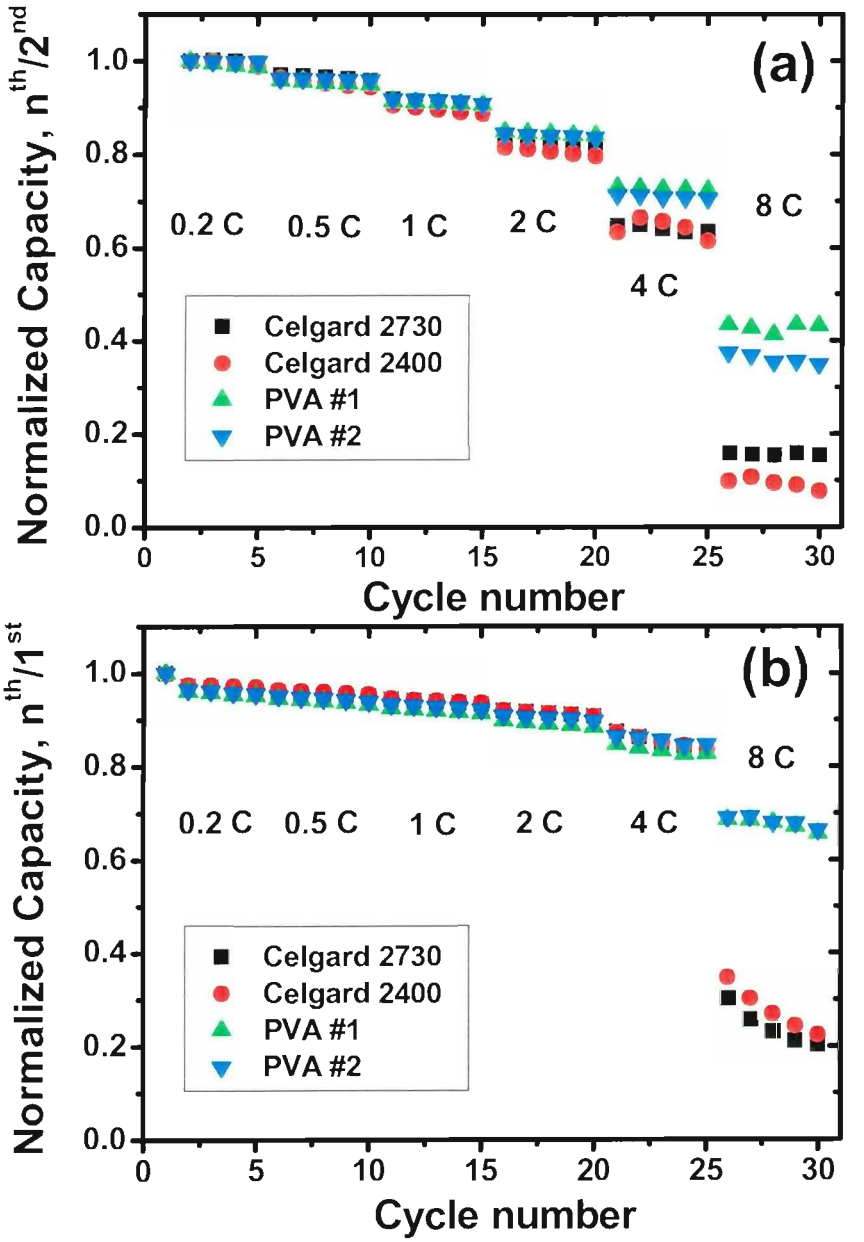

Figure 2.2.7 (a) Results of charge rate capability tests and (b) discharge rate capability tests for the cells with four kinds of separators.

Charge and discharge rate capability tests for cells using graphite anode were carried out. For the tests, we prepared 2 set of cells and carried out the tests separately. Figure 2.2.7 (a) and (b) show results of the charge and the discharge rate capability tests for the cells, respectively. For the charge rate capability tests, the test cells were charged up to 4.2 V with various C-rates of 0.2, 0.5, 1, 2, 4 and 8, and then discharged to 3.0 V with the 0.2 C-rate. For the discharge rate capability tests, the cells were charged up to 4.2 V with the 0.2 C-rate and then discharged to 3.0 V with various C-rates of 0.2, 0.5, 1, 2, 4 and 8. For the charge rate capability tests (Fig. 2.2.7 (a)), the cells showed similar capacity retentions up to the 2 C-rate. However, the difference of capacity retentions became clear above the 4 C-rate. At the 8 C-rate, the cells with the PVA #1 and #2 showed capacity retention ratios of about 40 %, whereas the cells using the Celgard membranes delivered capacity retention ratios of about 10 - 15 %. The same trend was observed for the discharge rate capability tests. The cells with PVA nonwovens showed better discharge rate capabilities than that of the Celgard membranes. The better charge and discharge rate capabilities of the cells with the PVA nonwovens could be attributed to high porosities, low Gurley values and high wettability of the PVA nonwovens.

Considering high power application of a battery, a higher instantaneous discharging capability is desired to the battery. In order to investigate the effect of separator on the instantaneous discharging characteristic of cells, a pulse-type discharging tests were carried out. Details for the experiment are described in elsewhere [9]. Fig. 2.2.8 (a) - (d) show the voltage responses upon the discharging for 1 minute at various C-rate. For discharging tests at low C-rates (below the 8 C), all the cells showed flat voltage profiles. However, different type of separators, i.e., the Celgard membranes and the PVA nonwovens, exhibited different voltage profiles for the discharging tests at

the high C-rates (above the 8 C). The cells using the Celgard membranes showed more

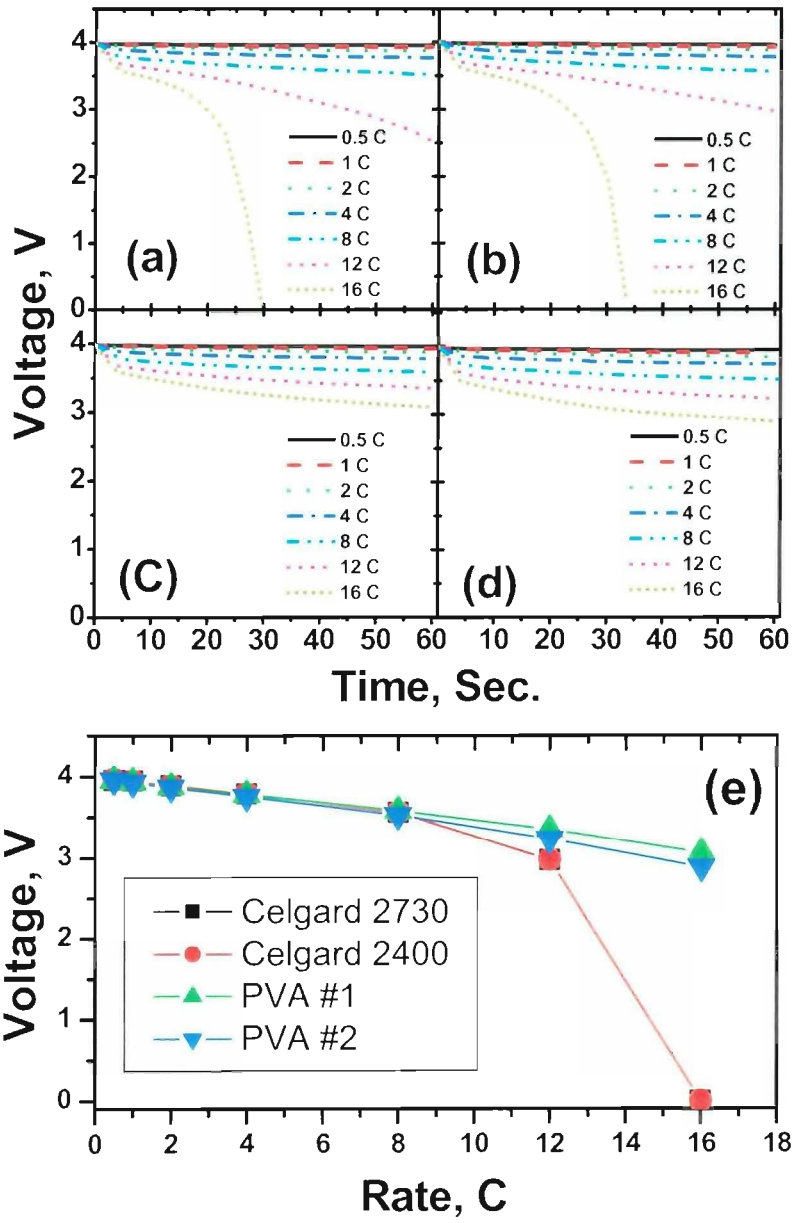

Figure 2.2.8 The voltage responses for the cells using (a) the Celgard PE membrane, (b) the Celgard PP membrane, (c) the PVA #1 and (d) the PVA #2 upon the pulse type discharging for 1 minute. (e) The relationship between the discharge rates and the voltages of the cells after discharging for 1 minute.

rapid voltage drops than those using the PVA nonwovens. The cell voltages after the discharging tests at each C-rate were summarized in Fig. 2.2.8 (e). All cells showed

similar trends on the decrease in cell voltages with increasing the C-rate up to 8, however, a clear difference on the cell volages was observed above the 12 C-rate. At the 16 C-rate, the voltages of the cells with the Celgard membranes dropped to 0 V vs. Li^+/Li, while the cells with the PVA nonwovens exhibited higher voltages of about 3 V vs. Li^+/Li. The results can be interpreted that the PVA nonwovens can provide higher maximum power to the lithium ion battery than that of the conventional micro porous membrane separators.

2.2.4 Conclusions

The PVA nonwoven separators were successfully developed by the electrospinning technique. The separator was electrochemically stable in the voltage range of 3 to 4.5 V vs. Li^+/Li on the CV measurement. In spite of high porosities and low Gurley values, any internal short circuit was not observed for the cells using the PVA nonwovens during cycling test. The cells using the PVA nonwovens showed better cycle stability and rate capability than the cells with the Celgard membranes. Moreover, the cells with the PVA nonwovens exhibited larger maximum power than the cells with the Celgard membranes. The remarkable improvement of the battery performance for the cells using the PVA nonwovens could be attributed to the higher porosity, better wettability and lower Gurley values of the PVA nonwovens than those of the Celgard membranes. Therefore, the PVA nonwoven could be promising candidate as a separator for the high power lithium ion battery.

References

[1] P. Azora, and Z. Zhang, *Chem. Rev.*, **104**, 4419 (2004).

[2] J. Saunier, F. Alloin, J. Y. Sanchez, and G. Caillon, *J. Power Sources*, **119-121**, 451 (2003).

[3] Y. M. Lee, J. W. Kim, N. S. Choi, J. A. Lee, W. H. Seol, and J. K. Park, *J. Power Sources*, **139**, 235 (2005).

[4] F.G.B. Ooms, E.M. Kelder, J. Schoonman, N. Gerrits, J. Smedinga, and G. Callis, *J. Power Sources,* **97-98**, 598 (2001).

[5] D. W. Sheibley, M. A. Manzo, and O. D. Gonzalez-Sanabria, *J. Electrochem. Soc.*, **130**, 255 (1983).

[6] L. C. Hsu and D. W. Sheibley, *J. Electrochem. Soc.*, **129**, 251 (1982).

[7] D. Takemura, S. Aihara, K. Hamano, M. Kise, T. Nishimura, H. Urushibata, and H. Yoshiyasu, *J. Power Sources*, **146**, 779 (2005).

[8] K. M. Abraham, *Electrochim. Acta*, **38**, 1233 (1993).

[9] M. Yao, K. Okuno, T. Iwaki, M. Kato, S. Tanase, K. Emura, and T. Sakai, *J. Power Sources*, **173**, 545 (2007).

Chapter 3

Silica-Composite Nonwoven Separators for Lithium-Ion Battery : Development and Characterization

3.1 Introduction

The market shares of the lithium ion battery for civilian applications, such as notebook computer, cellular phone and camcorder, have been increased year by year. Recently, the battery is highlighted as power sources for hybrid electric vehicles (HEVs), electric vehicles (EVs), power tools and robots. The applications require high energy density as well as high power density of battery, which results in upsizing of the battery. However, the upsizing claims more safety concerns.

Up to now, polyolefin micro porous membranes have been used for the lithium ion battery as separators due to their suitable properties, such as chemical stability, thickness and mechanical strength. However, the polyolefin membrane separators have several drawbacks as follows;

i) Low thermal stability :

The polyolefin micro porous membranes show large thermal shrinkage around its melting or softening temperature. For example, the PE membrane shows shrinkage of about 10 % when it was exposed at 120 ^{o}C for only 10 minutes [1]. It could lead to a thermal runaway of the battery caused by short circuit.

ii) An insufficiency of high rate performance :

Generally, the membranes have low porosity of about 40 % [2] and low wettability in polar electrolyte [3,4]. The low porosity and wettability lead to a lowering of the high rate performance of battery.

Application of nonwoven separators is a very effective way to enhance the high rate capability of battery with relation to the high porosity of the nonwoven separator. However, because of large pore size and inhomogeneous pore size distribution, nonwovens generally suffer from internal short circuit by growing of lithium dendrites during charge-discharge process. In order to reduce pore size and obtain homogeneous

pore size distribution, finer fibers are necessary as we have reported previously. Another way to reduce the pore size is filling fine ceramic particles into the large pore. In addition, according to previously reported work, ceramic composite or ceramic separator could increase in wettability [1] and thermal stability of the separator [5-7]. However, the ceramic separator suffers from inflexibility. Since the ceramic composite separators were produced by slip coating of ceramic particles with few micro meters in diameter, the separators showed large mean pore sizes and wide pore size distributions, compared to a conventional micro porous membrane separator.

In order to reduce mean pore size of a ceramic-composite nonwoven separator, I have applied nano size silica powders for fabricating ceramic-composite nonwoven separators. Moreover, I have applied an air-laid method in order to fabricate silica-composite nonwovne separator with homogeneous distribution of silica powders. In this chapter, I will discuss thermal stability and battery performance of the nonwoven separators.

3.2 Experimental

A fine polyethylene-polypropylene sheath-core composite fibers, which have 2 μm in mean diameter and about 1 mm in length, and nano size silica powders on the market were used for preparing the silica-composite nonwoven separators. The fibers consist of 50 wt. % of PE (sheath) and 50 wt. % of PP (core). Prior to form silica-composite nonwoven web, we washed the fibers using ethanol and distilled water in order to remove residual oily impurity on it. The silica powders contain small amount of impurities, such as Al_2O_3 (< 0.01 %), Fe_2O_3 (< 0.001 %), TiO_2 (< 0.01 %) and HCl (< 0.005 %). The fibers and the silica powder were mixed homogeneously at various weight ratios, and then webs containing the powder were formed by an air-laid method.

The webs were heat-bonded in a hot oven. Thicknesses of the webs were controlled by roll-press.

The morphologies of the silica-free and silica-composite nonwoven separators were observed by scanning electron microscope. The pore size distributions of the silica-composite nonwoven separators and the Celgard® 2400 were measured by a mercury porosimeter (Auto Pore IV 9510, Shimazu, Japan).

For the electrochemical characterization, cathode slurry was prepared as follow; the lithium cobalt oxide (Nippon Chemical industrial Co. Ltd., Japan), ketjen black and polyvinylidene (90: 5: 5 in wt. %) were blended in *N*-methylpyrrolidinon. The blended slurry was coated on an aluminum foil. The electrode sheet was roll-pressed and then punched out as disks from the sheet. The $LiCoO_2$ cathode and graphite anode (Hohsen Co. Ltd.) were dried at 140 °C for 6 h. under vacuum state. The 2032 coin type cell was composed of the dried electrodes and 1M $LiPF_6$-EC/DEC (1:1 in volume) as an electrolyte. The battery performances, such as cycle life and rate capability were investigated in the voltage range of 3.0 to 4.2 V at 30 °C.

The ionic conductivity of the electrolyte with and without separators were measured by an ac impedance spectroscopy using HS cell (Hohsen, Japan). The cells formed by sandwiching the electrolyte or electrolyte soaked separator between two stainless steel electrodes. AC impedance measurements were carried out using Solatron SI 1280B frequency response analyzer over the frequency range 20 kHz to 1 Hz with 10 mV of the ac amplitude.

3.3 Results and Discussion

Figure 3.1 shows initial charge-discharge curves for coin type cells assembled using silica-free nonwoven and polyolefin micro porous membrane separator (Celgard®

2400). Hereinafter a SFN and a SCN refer to a silica-free nonwoven and a silica-composite nonwoven, respectively. The cell with the Celgard membrane showed stable voltage profile at the first cycle with a coulombic efficiency of 86.3 %. The initial irreversible capacity loss of 13.7 % can be attributed to a formation of solid electrolyte interface (SEI) on the graphite anode [8]. On the contrary, the cell assembled with the SFN showed unstable voltage profile in the voltage range of 4.0 to 4.2 V at the first charge process, resulting low coulombic efficiency of 41.1 % despite of similar discharge capacity to the cell with the Celgard membrane. The reason for the unstable voltage profile could be attributed to micro short by formation of dendritic Li due to a sparse structure (See Fig. 3.2 (a)) of the silica-free nonwoven separator.

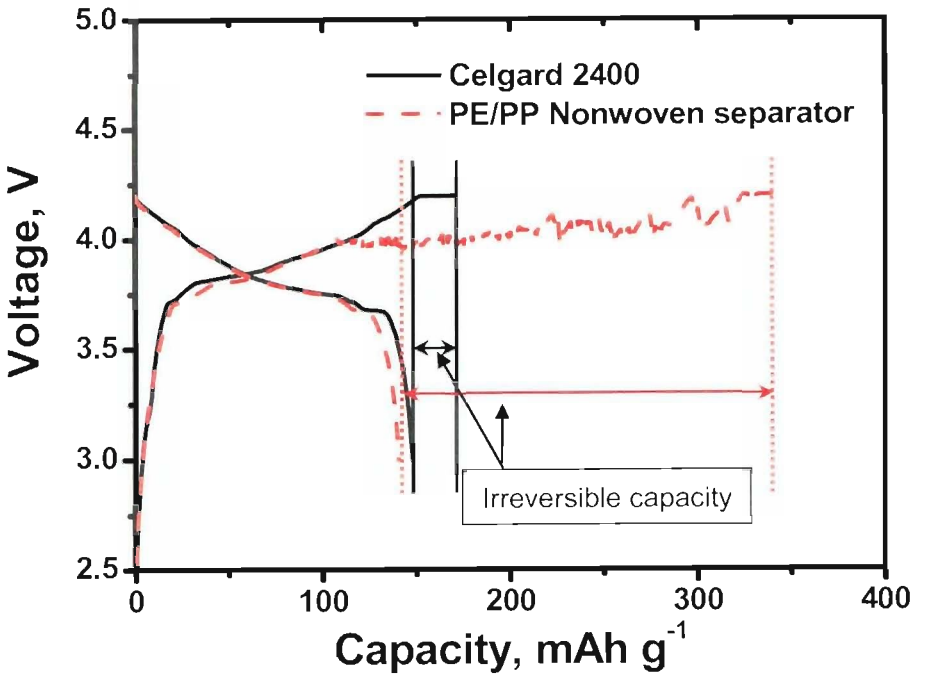

Figure 3.1 Initial charge-discharge curves for the cells with the Celgard membrane and the silica-free nonwoven.

In order to prevent micro short by growing of lithium dendrite, small pore size and complex pore structure are necessary [9]. The pore size and complexity of pore structure

could be estimated indirectly by Gurley value of separator, i.e., high Gurley value indicates more complex pore structure and/or small pore size of separator. The necessary Gurley value for the SCN in order to suppress micro short of battery was investigated. The Gurley values of the SCNs were controlled in the range of 6 to 452 s 100 cm^{-3} by controlling thickness, mass of polymers and weight ratio of silica powder. The physical properties of the SFN and the SCNs were summarized in the Table 1. The properties of the Celgard membrane were also given in the Table 1 as a reference.

Figure 3.2 (a) shows morphology of the SFN and Fig. 3.2 (b) and (c) show surface and cross section of the SCN *No.3*, respectively. As shown in the Fig. 3.2 (a), the SFN showed highly porous structure and large pore size. The large pores of the SFN disappeared by filling of the silica powder as shown in the Fig. 3.2 (b). It was also confirmed that the silica particles are homogeneously distributed overall the nonwoven matrix as shown in the Fig. 3.2 (c).

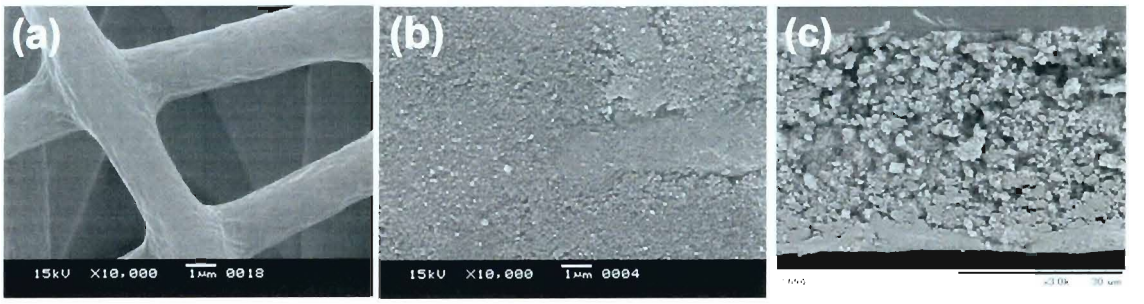

Figure 3.2 SEM photographs of (a) the silica-free nonwoven. (b) and (c) are surface and cross section of the silica-composite nonwoven (SCN *No.3* in the Table 3.1), respectively.

Figure 3.3 shows pore size distributions of the SCN *No.2*, *No.3* and *No.4*, compared with the Celgard membrane. The pore size distribution of the SCN *No.2* ranges about 10 nm to 2 μm with mean pose size of 130 nm. The ranges of the pore size

distribution for the SCNs became narrow and shifted to smaller pore size region with increasing the Gurley values of the SCNs. The mean pore sizes of the SCN *No.3* and *No.4* were 98 and 63 nm, respectively. The large pore of the SFN was reduced to the similar mean pore size of the Celgard one (55 nm) by filling of nano-size silica powder. However, the SCN *No.4* showed wide pore size distribution, compared with the Celgard membrane, as shown in the Fig. 3.3.

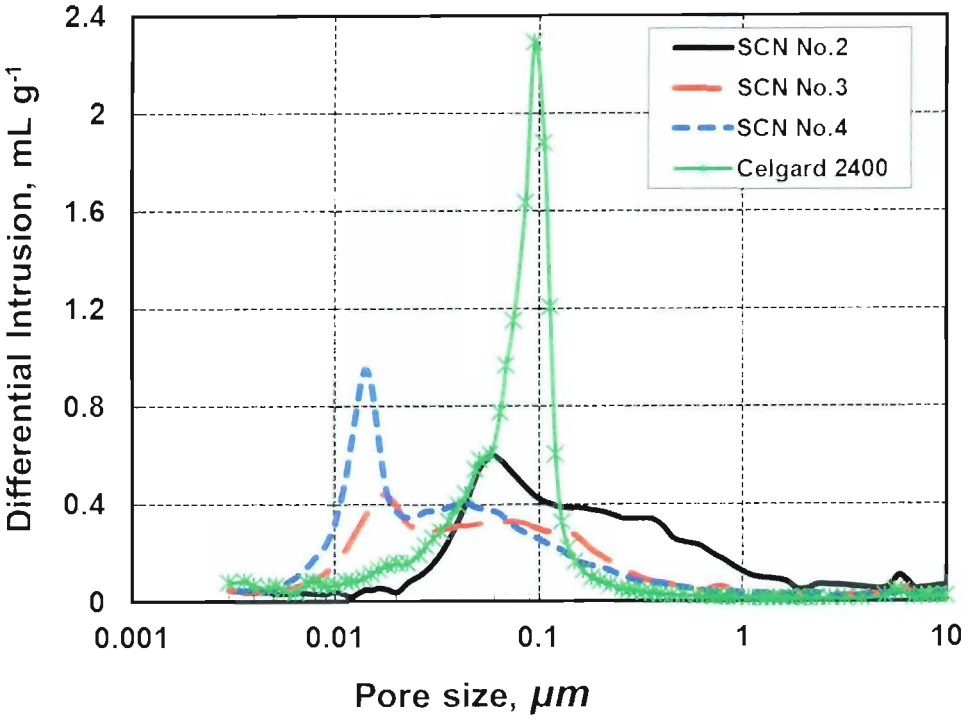

Figure 3.3. Pore size distributions of the silica-composite nonwovens and the Celgard membrane.

In order to wet easily in a non-aqueous liquid electrolyte and retain the electrolyte effectively during charge-discharge test, a separator should have high wettability [1]. The wettabilities of the Celgard membrane, the SFN and the SCN were investigated by monitoring variation of contact angles between the liquid electrolyte and the separators using DAT1100 (Fibro system ab, Sweden). Fig 3.4 shows the

Table 3.1. Physical properties of separators.

Properties	Celgard®2400	SFN	SCN *No.1*	SCN *No.2*	SCN *No.3*	SCN *No.4*	SCN *No.5*
Composition	Polypropylene	PE/PP	PE/PP – SiO_2	PE/PP – SiO_2	PE/PP – SiO_2	PE/PP – SiO_2	PE/PP – SiO_2
Weight of Separator (g/m^2)	14.3	15	24	21	21	18	26
Ratio of Powder (Wt. %)	–	–	50	27	30	39	42
Thickness (μm)	25	35	32	33	31	28	44
Density (g/cm^3)	0.57	0.43	0.75	0.64	0.67	0.64	0.59
Porosity (%)	37	56	46	45	43	49	54
Gurley (s /100 cm^3)	730	< 1	6	48	222	377	452

variation of the contact angles *vs.* time. The Celgard membrane showed initial contact angle of about 63 ° and showed almost constant values for 0.3 sec. The SFN showed similar initial contact angle to the Celgard membrane, but its contact angle reduced more rapidly compared to the Celgard membrane probably due to the sparse surface structure of the SFN. The SCN showed smaller initial contact angle of about 47 °, compared to the Celgard membrane and the SFN. The SCN showed similar trend in the variation of the contact angles to the SFN depending on time. The contact angles of the polyolefin micro porous membrane, the SFN and the SCN were 63.8 °, 34.2 ° and 23.6 °, respectively, after 0.3 sec from the initial contact. The result indicates that the wettability of nonwoven was improved by compounding with silica powder.

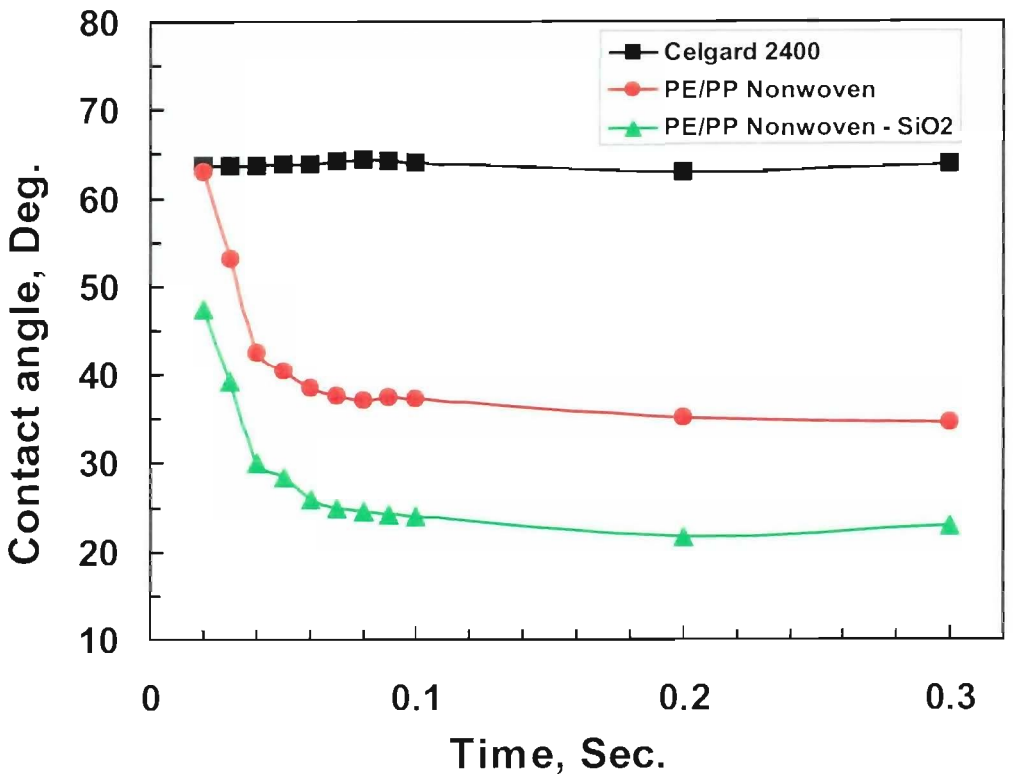

Figure 3.4 The variations of contact angels between the separators and liquid electrolyte (1M $LiPF_6$-EC/DEC (1:1 in vol.)).

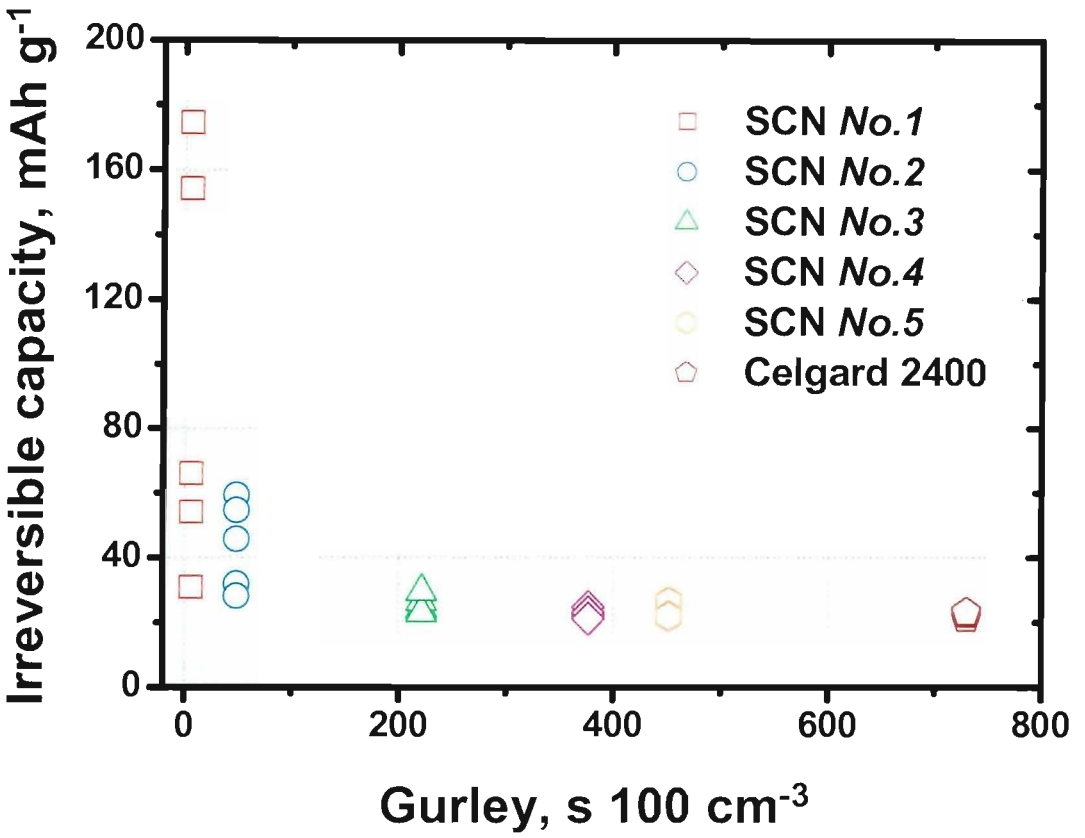

Figure 3.5 Relationship between initial irreversible capacities of the cells with separators *vs.* the Gurley values of the separators.

The existence of the micro short and the irreversible capacities for the cells assembled with the Celgard membrane and the SCNs were monitored using 5 coin cells for each separator. Fig. 3.5 clearly shows a relationship between the Gurley values of the SCNs and obtained irreversible capacities for the cells with the SCNs. The 5 cells assembled using the SCN *No.1*, which possess Gurley value of 6 s 100 cm^{-3}, showed existence of micro short and their irreversible capacities were widely distributed in the range of 31.0 to 174.7 mAh g^{-1}. The distribution of the irreversible capacities became narrow with increase in the Gurley value up to 48 s 100 cm^{-3}, though the 5 cells assembled using the SCN *No.2* showed the unstable voltage profiles in charge process. The micro short (unstable voltage profile) was not observed for the cells with the SCN

No.3 – No.5 which have higher the Gurley value than 200 s 100 cm^{-3}. Moreover, the irreversible capacities for the cells were almost the same to that of the cells with the Celgard membrane. The stable charge-discharge performance for the SCN *No.3 – No.5* could be attributed to their high Gurely values corresponding to small mean pore size and relatively narrow pore size distribution. This result indicates that the Gurley value of the SCN should be higher than 200 s 100 cm^{-3} in order to prevent the micro short of battery effectively during charge-discharge process.

Cycle lives for cells with the Celgard membrane and the SCN *No.3 – No.5* were investigated. At the first cycle, the cells were charged up to 4.2 V under constant current–constant voltage mode with a 0.2 C-rate, and then discharged to 3.0 V under constant current mode. All of the cells showed similar coulombic efficiencies of about 86 % and any unstable voltage profile was not observed. Following charge-discharge tests were carried out under constant current mode with the C-rate of 0.5. Fig. 3.6 (a) and (b) show charge-discharge curves and capacity retention ratios for the test cells, respectively. As shown in the Fig. 3.6 (b), the cells with the SCNs showed stable cycling performances through the charge-discharge test and slightly higher capacity retention ratios than that of the Celgard one at 250^{th} cycle. The obtained capacity retention ratios at the 250^{th} cycle for the cells with the Celgard membrane, the SCN *No.3*, *-No.4* and *-No.5* were 71.6 %, 76.4 %, 76.3 % and 79.8 %, respectively. The better cycle lives of the cells with the SCNs could be attributed to their higher porosities and better wettabilities than that of the Celgard one.

As discussed above, the high Gurley value is necessary for the SCN in order to obtain stable cycling performance. On the other hand, since increasing the Gurley value leads increase in an internal resistance of a cell, the high Gurley value decreases the high rate performance of the battery [5,10]. The MacMullin number, N_M, of separator

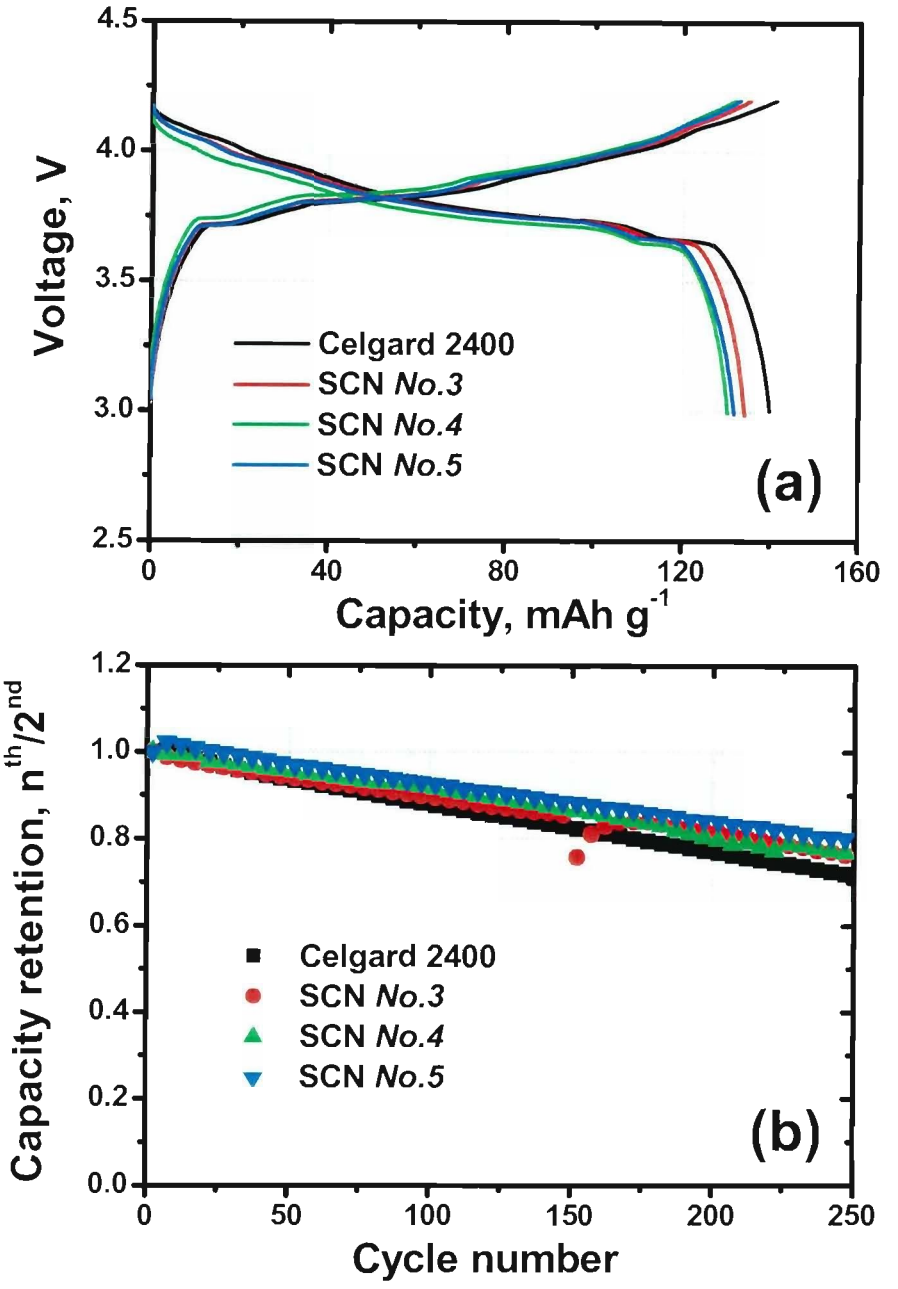

Figure 3.6 (a) Charge-discharge curves and (b) capacity retention ratios as a function of cycle number of cells at the C-rate of 0.5.

could be used as an indicator to evaluate the high rate performance of the separator [9,11]. For example, a separator with lower N_M value shows higher rate performace than that of higher N_M value one. The N_M value can be calculated by follow equation [10]:

$$N_M = \frac{\sigma_0}{\sigma_{eff}} \quad (1)$$

where σ_0 and σ_{eff}, are the conductivity of liquid electrolyte and the conductivity of electrolyte with separator, respectively. The obtained N_M values of the Celgard membrane, the SFN and the SCN *No.3 – No.5* were presented in Table 3.2. The SFN showed the lowest N_M value of 5.6 and the number was increased up to about 10 with increasing the Gurley value of the SCNs. The N_M values of the SCNs were lower than that of the Celgard one. Thus, the SCNs seem to show better high rate performances than the Celgard membrane.

Table 3.2 The values of porosity, conductivity (σ_{eff}) and MacMullin number (N_M) obtained from conductivity measurement of separators.

Separator	Porosity, %	Conductivity	N_M
Celgard® 2400	37	0.8 mS cm^{-1}	12.3
SFN	54	1.7 mS cm^{-1}	5.6
SCN *No.3*	45	1.0 mS cm^{-1}	9.9
SCN *No.4*	55	0.9 mS cm^{-1}	10.3
SCN *No.5*	49	0.9 mS cm^{-1}	10.4

σ_0 = 9.64 mS cm^{-1} at 30 °C

In order to apply batteries to HEVs system, the batteries have to possess high instantaneous discharging performance for rapid acceleration [12]. The instantaneous discharge characteristics for the cell assembled with the Celgard membrane and the SCNs were investigated by a pulse-type discharging tests for 30 seconds with various

C-rates. Figure 3.7 shows the obtained voltages after discharging for 30 seconds at each C-rate. The test cells showed linear voltage drop with increase in C-rate up to the 12 C and a clear difference on the voltages for the test cells was not observed. At the 16 C-rate, 27 mA cm^{-2}, the difference on the retained voltages became clear. The voltage for the cell using the Celgard membrane dropped to 1.9 V *vs.* Li/Li^+, whereas the cells with the SCNs exhibited higher voltages (around 2.9 V *vs.* Li/Li^+) than that of the Celgard membrane. Consequently, the SCNs could deliver higher maximum power than that of the Celgard one. The instantaneous discharge characteristics of the cells at the 16 C-rate were coincident with the trend on the $N_{1/}$ values of the separators tested in this work.

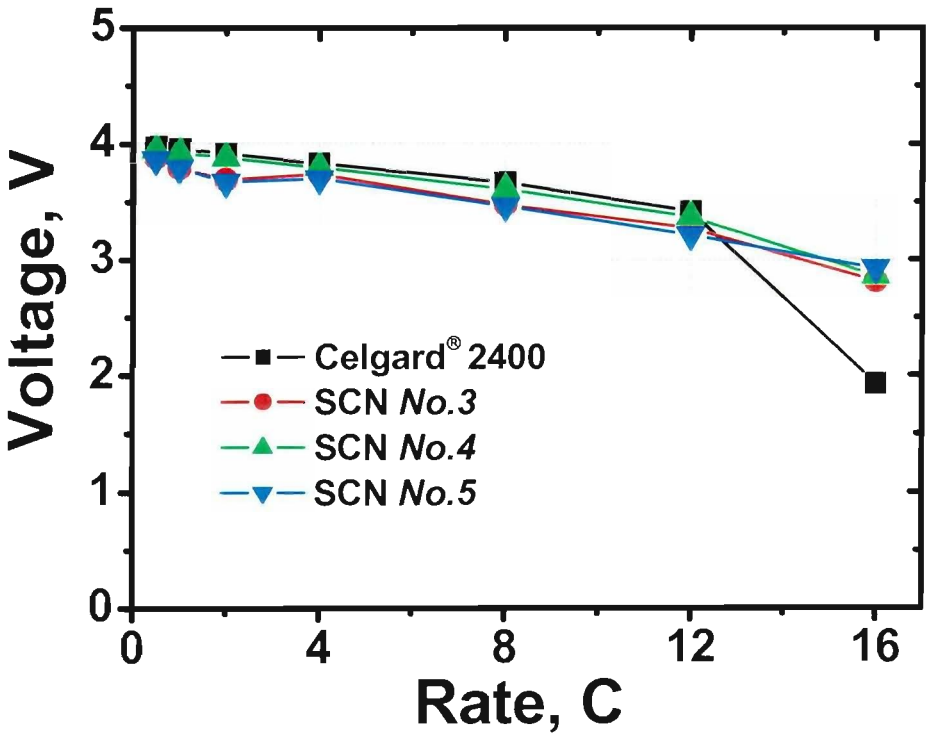

Figure 3.7 Relationship between the C-rates and the cell voltages after discharging for 30 seconds.

In order to investigate thermal stabilities of separators, hot oven test was conducted for the Celgard membrane and the SCN *No.3* at 160 °C for 20 min. The

Celgard membrane showed thermal shrinkage of about 37 % along the machine direction as shown in Fig. 3.8 (a). The Celgard membrane was prepared by stretching a polyolefin film along to the machine direction. The separator showed shrinkage along to the machine direction before meltdown at around its melting temperature. On the contrary, a nonwoven web was formed by deposition and thermal bonding of thin fiber, together with the nano-size silica powder. Therefore, the nonwoven show negligible shrinkage around its melting temperature, compared to the Celgard membrane. The SCN *No.3* showed only about 3 % of shrinkage after the hot oven test (Fig. 3.8 (b)).

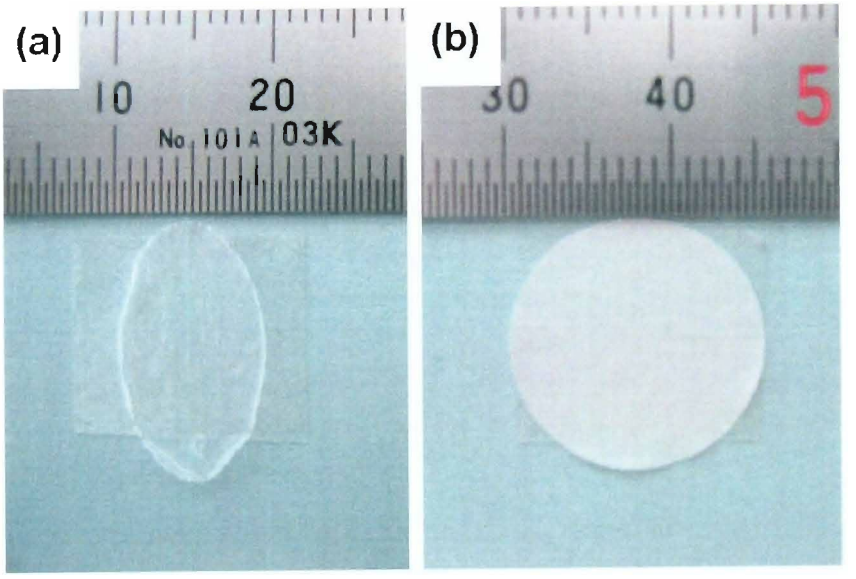

Figure 3.8 Photographs of the (a) Celgard membrane and (b) the SCN *No.3* after hot oven test at 160 °C for 20 minutes.

Besides, thermally stable silica powder, which occupies space inside of a nonwoven, could separate positive and negative electrodes even if the polyolefin nonwoven matrix melt down at a high temperature. Subsequently, we carried out the hot oven tests for charged cells with the Celgard and the SCNs at 150 °C for 1h. For the experiment, firstly we charged the cells up to 4.2 V, and then kept the cells inside the hot oven. After

that, we monitored variation of the cell voltages. The variation of the cells voltages depending on time were given in the Fig. 3.9. The cell with the Celgard membrane showed sudden voltage drop after 10 minute from the start of the test probably due to short circuit. The short circuit may be caused by shrinkage of the Celgard membrane. On the other hand, the cells with the SCNs showed gentle voltage drops during the hot oven test and any sudden voltage changes were not observed. The results indicate that the SCNs are thermally stable at high temperature of 150 °C in the liquid electrolyte.

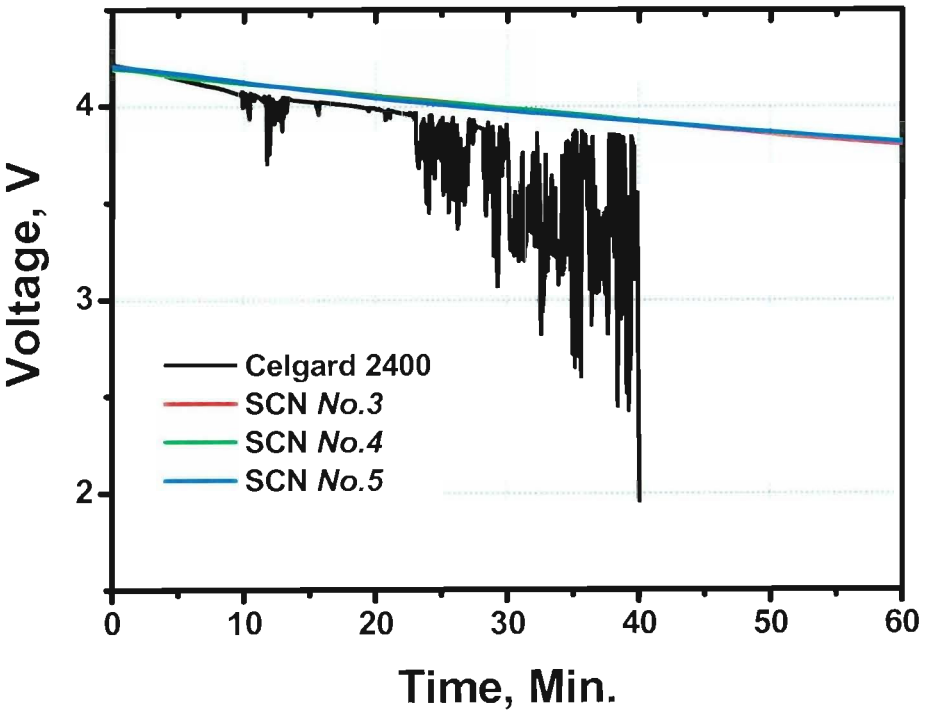

Figure 3.9 The voltage profiles for the cells with the Celgard membrane and the SCNs during the hot oven test at 150 °C for 1h.

3.4 Conclusion

The silica-composite nonwovens comprising polyolefin nonwoven as a support and nano-size silica powder as filler for the lithium ion battery have been successfully developed. The silica-composite nonwoven showed better wettability than the

polyolefin based membrane and nonwoven. The Gurley value of the silica-composite nonwoven has to be higher than 200 in order to suppress micro short of battery. The cells with the silica-composite nonwovens showed better cycle lives than that with the Celgard membrane over 250 cycles at the C-rate of 0.5. The pulse-type discharging test revealed that the silica-composite nonwovens could deliver higher maximum power than that of the Celgard membrane. The silica-composite nonwovens showed thermal shrinkage of about 3 % at 160 °C under air atmosphere and thermally stable at 150 °C in the liquid electrolyte. Therefore, we believe that the silica-composite nonwovens can increase the high power performance and thermal stability of the lithium ion battery.

References

[1]. S. S. Zhang, *J. Power Sources*, **164**, 351 (2007).

[2]. F.G.B. Ooms, E.M. Kelder, J. Schoonman, N. Gerrits, J. Smedinga, G. Callis, *J. Power Sources,* **97-98**, 598 (2001).

[3]. J. Saunier, F. Alloin, J. Y. Sanchez, G. Caillon, *J. Power Sources*, **119-121**, 451 (2003).

[4]. Y. M. Lee, J. W. Kim, N. S. Choi, J. A. Lee, W. H. Seol, J. K. Park, *J. Power Sources*, **139**, 235 (2005).

[5]. D. Takemura, S. Aihara, K. Hamano, M. Kise, T. Nishimura, H. Urushibata, H. Yoshiyasu, *J. Power Sources*, **146**, 779 (2005).

[6]. S. Augustin, V. D. Hennige, G. Hörpel, C. Hying, P. Haug, A. Perner, M. Pompetzki, T. Wöhrle, C. Wurm, D. Ilic, Meet. Abstr.-Electrochem. Soc., **502**, 84 (2006).

[7]. S. Augustin, V. Hennige, G. Hoerpel, C. Hying, M. Saito, Meet. Abstr.-Electrochem. Soc., **502**, 89 (2006).

[8]. R. Fong, U. V. Sacken, and J. R. Dahn, *J. Electrochem. Soc.*, **137**, 2009 (1990).

[9]. K. M. Abraham, *Electrochim. Acta*, **38**, 1233 (1993).

[10]. P. Azora, Z. Zhang, *Chem. Rev.*, **104**, 4419 (2004).

[11]. K. K. Patel, J. M. Paulsen, and J. Desilvestro, *J. Power Sources,* **122** (2003) 144.

[12]. Japan Automobile Research Institute Standards Committee, Cycle life test procedure of sealed nickel–metal hydride batteries for hybrid electric vehicles, JEVS D 716, Japan Automobile Research Institute, Tokyo, 2004.

Chapter 4

Composite Nonwoven Separator for Lithium-ion Battery : Development and Characterization

4.1 Introduction

The market shares of the lithium-ion battery for the civilian applications, such as notebook computer, cellular phone, digital camera and camcorder, have been increased year by year. In addition, a large scale lithium ion battery has been studied intensively to expand its current usage, power sources for portable electric devices, into industrial usage, such as power sources for plug in electric vehicles (PEVs), hybrid vehicles (HEVs), power tools and robots. The industrial application demands more energy and power density from the battery as well as safety concerns [1-3].

A nonwoven fabric is very attractive material to satisfy the demands, because it has high porosity [4] and can readily composite with other materials such as ceramic powder [5-7] and polymer electrolyte [8-12]. The former can enhance power density of the battery and the latter can provide extra function such as high thermal stability to the battery. As a matter of fact, we had developed two types of nonwoven separators with close thickness and pore size to a conventional micro porous membrane separator [7,13-14]. The one is a nano-fiber nonwoven separator. Cells with the separator showed outstanding rate capabilities and stable cycling performances. However, it suffers from low tensile strength and thermal stability above 150 °C in an electrolyte. The other is a ceramic composite nonwoven separator. Cells with the separator could provide stable battery performances and better thermal stabilities than a cell with a conventional micro porous membrane separator. But, it also has some drawbacks for instance dropping out of ceramic particles and low air permeability due to the large amount of ceramic powder inside of the separator. In order to increase the air permeability of the separator, the amount of the ceramic powder has to be reduced, but it leads large pore size and inhomogeneous pore size distribution resulting internal short circuit during charge-discharge process. Therefore, it is necessary to remove these drawbacks of the

nonwoven separators to apply them for practical use.

In order to remove the shortcomings of the formerly developed separators, I have developed a new type composite nonwoven separator by combining nano-fiber nonwoven and ceramic containing nonwoven the ceramic containing polyolefin nonwoven part could provide high tensile strength and thermal stability to the separator and nano-fiber nonwoven part prevents dropping out of the ceramic powder as well as furnishing small pore-size and narrow pore-size distributions to the separator. Therefore, in this chapter, I would like to discuss physical and electrochemical properties of the composite nonwoven separator.

4.2 Experimental

4.2.1 Fabrication of the composite nonwoven separator

A polyolefin nonwoven for filling ceramic powder was fabricated by a two-step wet laid method. An aqueous suspension was prepared by dispersing polyethylene (PE) – polypropylene (PP) sheath core composite fibers, which consists of 50 wt. % of PE sheath part and 50 wt. % of PP core part, with fineness of 0.8 dtex (10 μm in diameter) and length of 5 mm in distilled water, and then it was laid down on a screen web to form a fiber web. The fiber web was heat bonded by using a hot roll press at 135 °C. After that, another aqueous suspension was prepared by using fine PP fibers with fineness of 0.02 dtex (2 μm in diameter) and 2 mm in length, and then it was laid down on the previously prepared nonwoven, and then the web was heat bonded again by the hot roll press at 135 °C.

A PAN nano-fiber nonwoven was prepared by an electrospinning technique. The spinning conditions of the PAN nano-fiber nonwoven were described in the previous report [13].

Prior to combine the base nonwoven with the PAN nano-fiber nonwoven, we filled silica or alumina powder with mean particle size of 0.2 μm by spraying the powder on the one side of the base nonwoven. And then, the PAN nano-fiber nonwoven and the ceramic charged nonwoven were combined through the hot roll press at 135 °C. A scheme for the combining process was given in the Fig. 4.1.

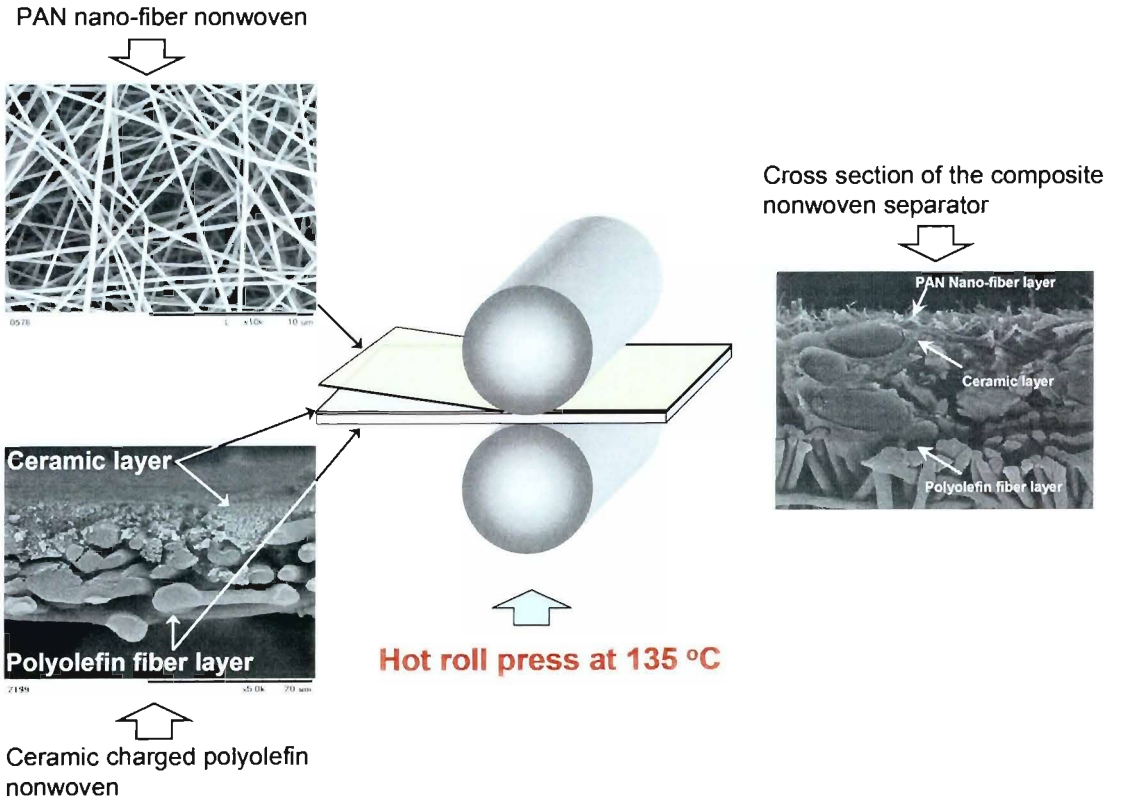

Figure 4.1 Schematic depiction of combining process.

4.2.2 Physical and electrochemical characterizations.

The morphologies of the composite nonwoven separator were observed by scanning electron microscope (Miniscope TM-1000, Hitachi, Japan). The mean pore size and pore size distributions of the composite nonwoven separators and the base nonwoven were measured by bubble point method using Automated Perm Porometer

(Porous Materials, Inc., USA). The Gurley values of the separators were measured in accordance with Japanese industrial standard JIS P8177 using Gurley type densometer (Yasuda Co., Japan). The tensile strengths of the separators were measured at strain rate of 5×10^{-2} s^{-1} using UCT-100 (Orientec Co., Japan). The samples were cut into 200 mm × 50 mm (length and width) and then carefully mounted with a gauge length of 100 mm.

Battery tests such as cycle life and rate capability were carried out in the voltage range of 3.0 to 4.2 V at 20 °C using 2032 coin type cell consisting of $LiCoO_2$ electrode as a cathode, graphite electrode purchased from Hohsen Co. Ltd as an anode and 1M $LiPF_6$-EC/DEC (1:1 in volume) (Kishida Cehmical Co., Ltd) as an electrolyte. The reversible capacities of the both electrodes were about 1.7 mAh cm^{-2} and the anode to the cathode capacity ratio of fabricated cells was about 1.15. The cathode for the coin type cells were fabricated as follow; the lithium cobalt oxide (Nippon Chemical industrial Co. Ltd., Japan), ketjen black and polyvinylidenefluoride (90: 5: 5 in wt. %) were blended in *N*-methyl-2-pyrrolidinon. The blended slurry was coated on an aluminum foil, and then dried at 120 °C. The cathode sheet was roll-pressed and then punched out as disks from the sheet with 12 mm in diameter. The electrodes, cathode and anode, and separators were dried at 140 °C for 6 h and 90 °C for 1 day under vacuum state, respectively. The cells were assembled in a glove box under Ar atmosphere.

4.3 Results and discussion

Small pore-size and narrow pore-size distribution are generally requisite properties to a separator for the lithium ion battery. Because wide pore-size distribution leads inhomogeneous current distribution resulting poor cycle life of battery and

dendritic growth of lithium. In previous work [7], I had tried to control pore-size and pore-size distribution of a nonwoven by filling of ceramic powder. Since the pore-size and the pore-size distribution can be controlled by volume of the ceramic powder, large amount of the ceramic powder (more than 30 wt. % to total weight of separator) has to be inside of the separator in order to obtain small pore-size and narrow pore-size distribution. Accordingly, it is inevitable increasing Gurley value of the separator. As a result, we found that the Gurley value of the separator has to be more than 200 s 100 cm^{-3} to obtain stable battery performance. However, since the pore-size and the pore-size distribution of the composite nonwoven separator are controlled by not only quantity of the ceramic powder but also PAN nono-fiber nonwoven, the separator does not need large volume of the ceramic powder. Consequently, it is possible to manufacture a separator having small pore-size and narrow pore-size distribution without considerable loss on the air permeability. Fig. 4.2 shows pore-size distributions of the base nonwoven, the composite nonwoven separators containing silica and alumina powder measured by the bubble point method. Hereinafter, we refer the silica charged composite nonwoven separator as CNS No.1 and the alumina charged nonwoven separator as CNS No.2. The base nonwoven fabric showed mean pore-size of about 10 μm and wide pore-size distribution. The large mean pore-size of the nonwoven fabric reduced and its pore-size distribution became narrow by charging the ceramic powders and combining with PAN nano-fiber nonwoven fabric. The CNS No.1 and No.2 shows mean pore-size of 0.86 μm and 0.79 μm, respectively. The brief physical properties of the CNS No.1, No.2 and the Celgard membrane were summarized in the Table 4.1.

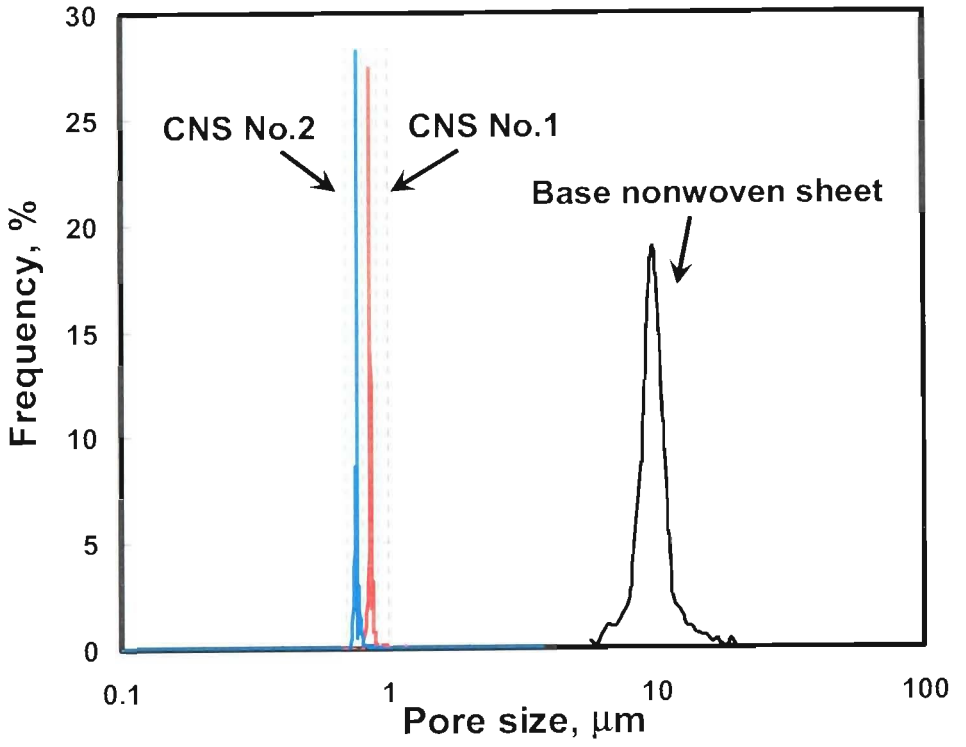

Figure 4.2 Pore size distributions of the base nonwoven sheet, the CNS No.1 and No.2.

Table 4.1 Physical properties of separators

Properties		Unit	CNS No.1	CNS No.2	Celgard® 2400
Composition		–	Polyolefin, PAN, SiO_2	Polyolefin, PAN, Al_2O_3	Polypropylene
Weight of Separator		g m^{-2}	20	19	14.3
Weight ratio of	Ceramic	%	15	11	–
	PAN		12	13	–
Thickness		μm	34	33	25
Mean pore size		μm	0.86	0.79	<0.1
Porosity		%	46	50	40
The Gurley value		s 100cm^{-3}	1.3	1.2	730

Figure 4.3 (a) – (c) show surface of the PAN nano-fiber nonwoven layer, polyolefin nonwoven layer and cross section of the CNS No.1, respectively. The ceramic powder was sandwiched by the PAN nano-fiber nonwoven and the polyolefin nonwoven layer, and the ceramic particles were not observed on the surface of the CNS as shown in the Fig. 4.3. In order to confirm dropping out of the powder from the

separator, we roughly crumpled the separator by hand and then measured weight loss of the separator. Despite of binder free, negligible weight loss (less than 1 %) was observed from the separator after the crumpling. This result indicates that the structure of the separator is very suitable for preventing drop out of the ceramic powder from the separator.

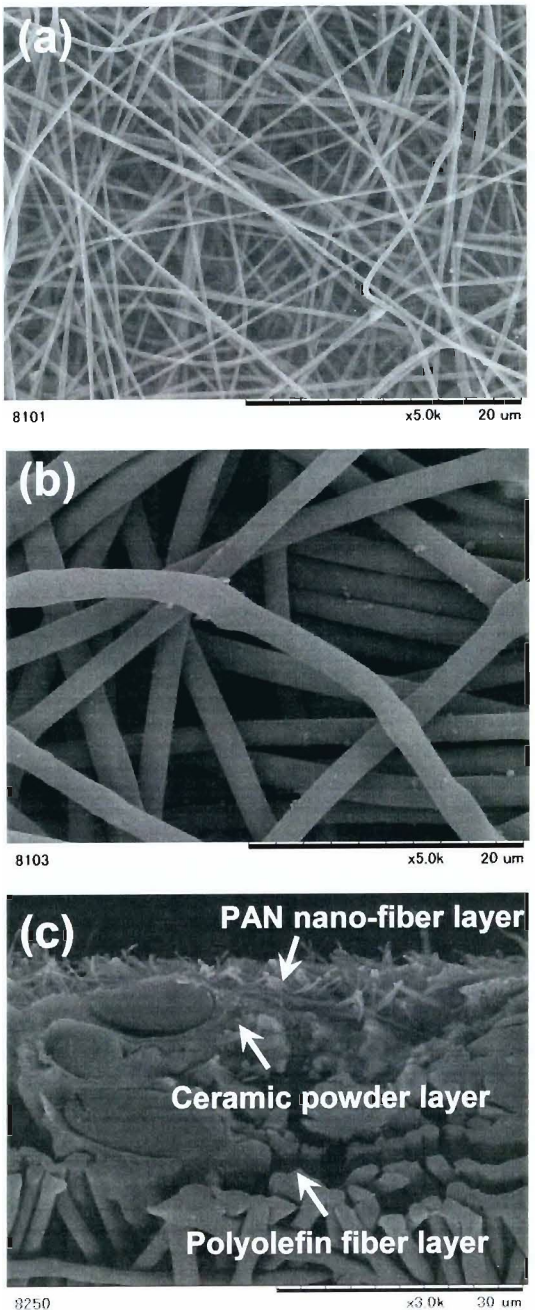

Figure 4.3 SEM photographs for the CNS No.1; (a) PAN nano-fiber nonwoven side, (b) polyolefin nonwoven side and (c) cross section of the separator.

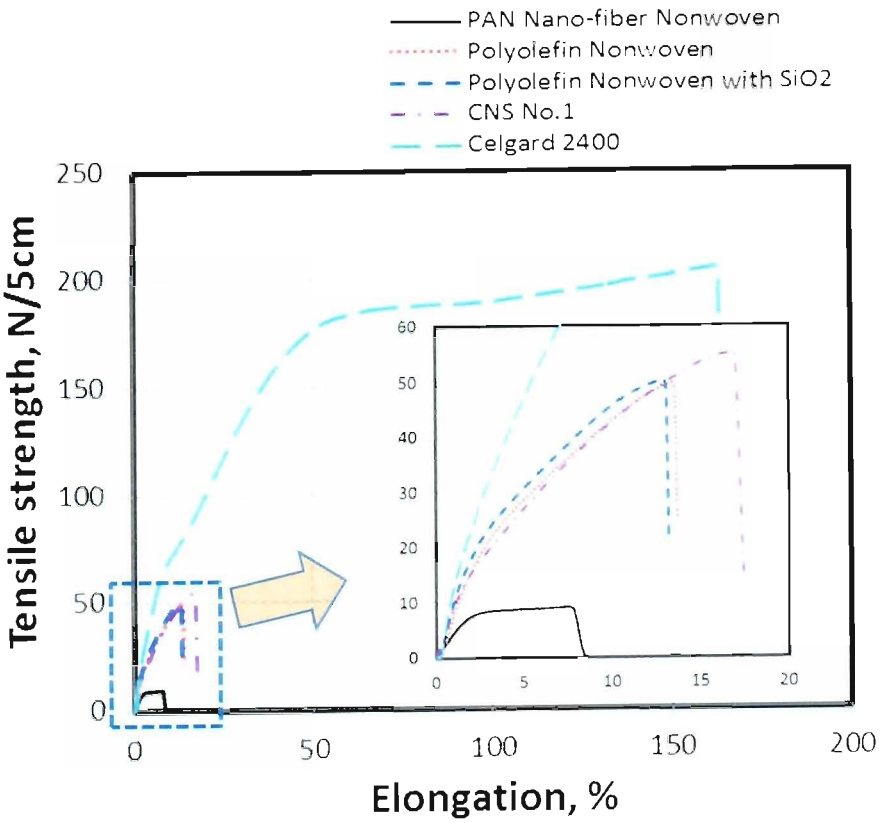

Figure 4.4 Stress-strain curves for the Celgard® 2400, the PAN nano-fiber nonwoven and the CNS No.1.

Table 4.2 The tensile properties of the separators

Elongation	Unit	PAN nonwoven	PO nonwoven	PO nonwoven with SiO_2	CNS No.1	Celgard® 2400
2%		7.6	15.6	18.1	15.5	23.3
5%	N	8.8	28.4	30.6	26.9	46.5
10%	$5cm^{-1}$	—	42.9	45.6	42.8	70.8
Break down		9.2	49.6	50.2	55.2	205.4

Figure 4.4 shows tensile strength–elongation curves of the two separators, the Celgard 2400 membrane and the CNS No.1, and components of the CNS No.1 such as a PAN nano-fiber nonwoven, a PO nonwoven and a PO nonwoven with SiO_2. The obtained properties were summarized in the Table 4.2. The PAN nano-fiber nonwoven showed the lowest tensile strength of 7.6 and 8.8 N 5 cm^{-1} at 2 and 5 % elongation and showed 9.2 N 5 cm^{-1} as a maximum tensile strength. As compare to the PAN nano-fiber

nonwoven, the PO nonwoven and the PO nonwoven with SiO_2 showed higher tensile strength as shown in the Fig. 4.4 and the Table 4.2. The difference in the tensile strength between the PAN nano-fiber nonwoven and the PO nonwovens (with and without SiO_2) can be attributed to their composition. The PAN one consists of only PAN nano-fiber, thus it does not has any binder inside of it. On the contrary, the PO nonwovens contain thermally bondable fibers (polyolefin sheath core composite fiber, 0.8 dtex). The PO nonwovens showed similar tensile strength irrespective of existence of SiO_2 as shown in the Fig. 4.4 because the SiO_2 did not contain any binder for stick them on the PO nonwoven. The CNS No.1 prepared by combination of the PAN nano-fiber nonwoven and the PO nonwoven with SiO_2 showed similar tensile strength to the PO nonwovens up to 10 % elongation, but its maximum tensile strength is about 5 % higher than the PO ones. The measured maximum tensile strength of the CNS No.1 is 55.2 N $5cm^{-1}$. These results well indicate that the tensile strength of nonwoven separator can be increased by combination of strong PO nonwoven and nano-fiber nonwoven. Although the CNS No.1 has low tensile strength comparing to the Celgard membrane, I believe that the separator can stand for deformation during winding process.

Battery performances for cells with the Celgard membrane, the CNS No.1 and No.2 were investigated. At the first cycle, the cells were charged up to 4.2 V under constant current–constant voltage mode, and then discharged to 3.0 V under constant current mode. The initial ten charge-discharge cycles were tested with a 0.2 C-rate. Following charge-discharge tests were carried out with a 0.5 C-rate. Fig. 4.5 (a) and (b) show charge-discharge curves at the 0.2 C-rate and capacity retention ratios as a function of cycle number of the test cells, respectively. All of the cells showed similar coulombic efficiencies of about 90 % at the first cycle. Any unstable voltage profiles were not observed for the cells with the CNSs as shown in the Fig. 4.5 (a) despite of

their low Gurley values. The stable voltage profiles would be ascribed to the small pore-size and narrow pore-size distribution of them. The cells with the CNS No.1 and No.2 showed stable cycling performances through the charge-discharge tests with capacity retention ratios of 86.0 and 88.5 % covering 200 cycles, respectively.

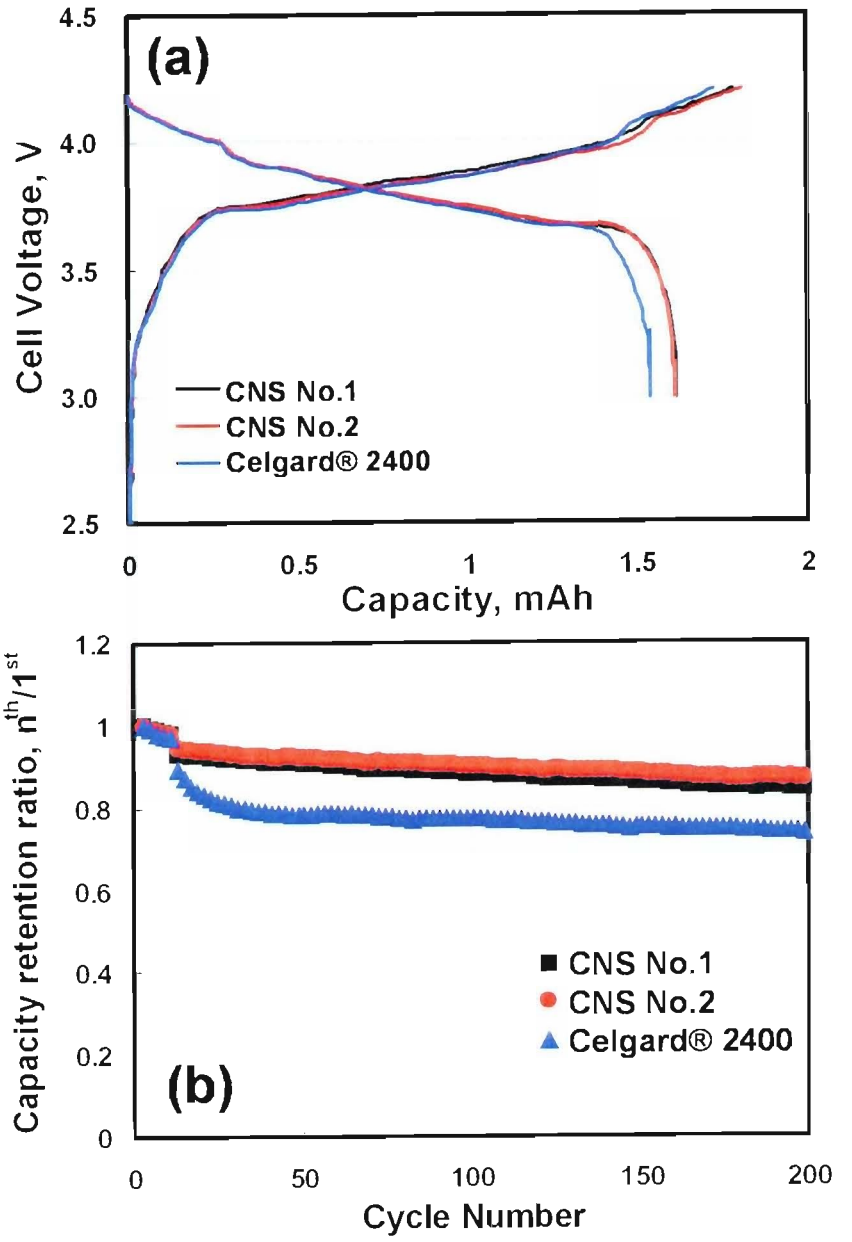

Figure 4.5 (a) Initial charge-discharge curves for the cells with the Celgard® 2400, the CNS No.1 and No.2. (b) Discharge capacities vs. cycle mumbers of the test cells.

Figure 4.6 shows rate capabilities of cells with the separators. The rate capabilities of the cells were investigated as follow; the test cells were charged up to 4.2 V at the 0.2 C-rate, and then discharged to 3.0 V at the C-rates of 0.2, 0.5, 1, 2, 4 and 8 C. The obtained discharge capacity of the cell with the Celgard membrane was gradually decreased with increase in the C-rate up to the 2 C-rate, and then abruptly decreased with increasing the C-rate up to 8 C-rate. The capacity retention ratios at the 4 and 8 C-rate were 42 and 11 %, respectively. The cells with the CNSs showed better rate capabilities than the cells with the Celgard one. The obtained discharge capacities of the cells with the CNSs at 2, 4, and 8 C-rate were about 90, 70 and 27 % of the initial discharge capacities. The better rate capabilities of the cells with the CNSs can be ascribed to their high porosities and low Gurley values than that of the Celgard one.

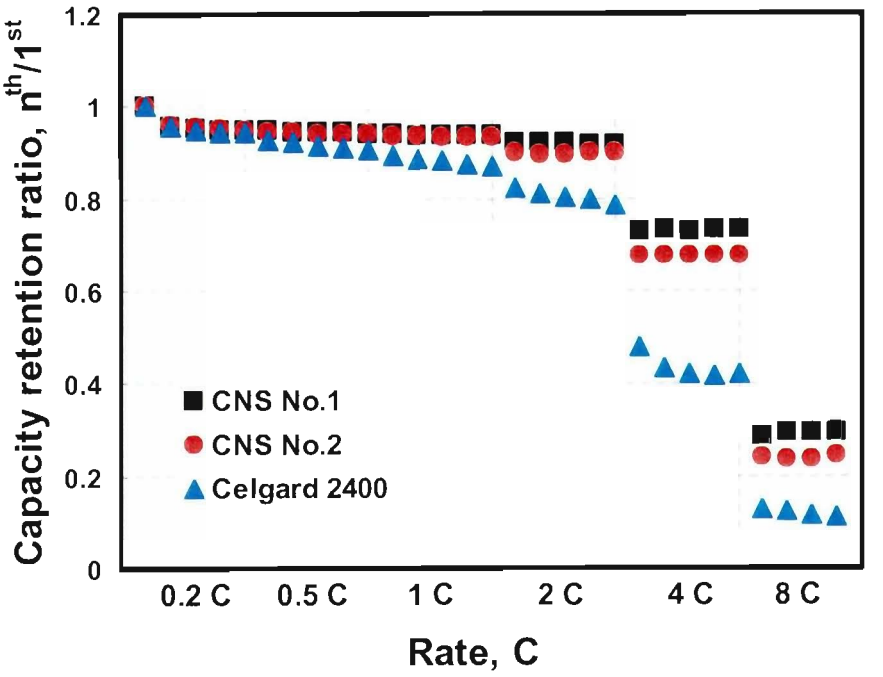

Figure 4.6 Results of rate capability tests for the cells with the Celgard® 2400, the CNS No.1 and No.2.

In order to investigate thermal stabilities of separators, a hot oven test was conducted for a polyolefin membrane and the CNS No.1 at 150°C for 10 min under air atmosphere. The results were presented in the Fig. 4.7. After the hot oven test, the polyolefin membrane showed thermal shrinkage of about 20 % in diameter (36 % in area). On the contrary, The CNS No.1 showed only about 4 % of thermal shrinkage in diameter (8% in area).

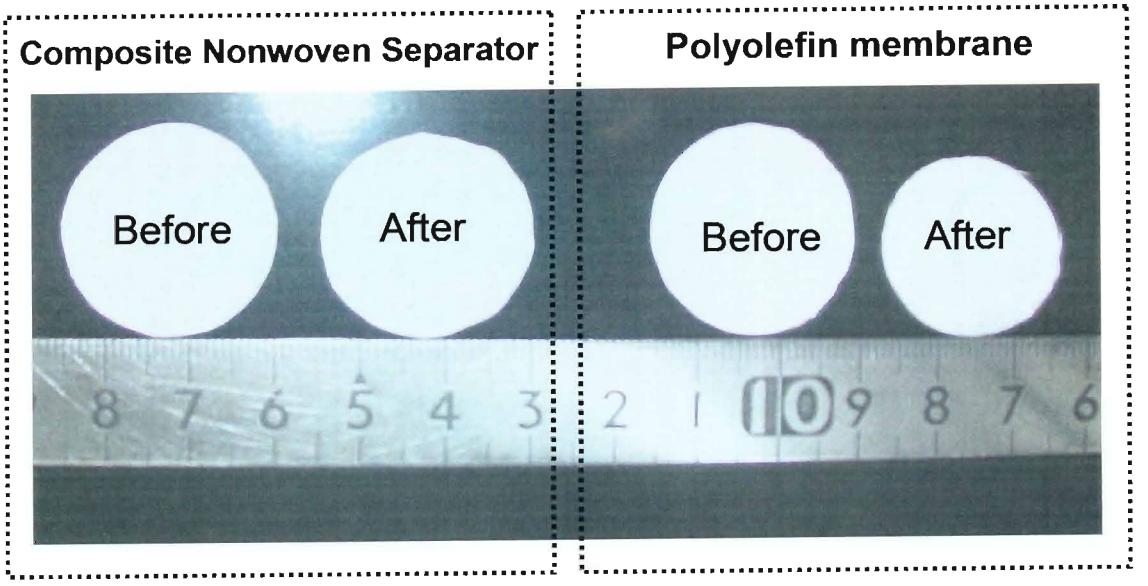

Figure 4.7 Photographs of the CNS No.1 and a conventional micro porous membrane before and after hot oven test at 150 °C for 10 minutes.

Subsequently, hot oven tests using CR-2032 coin type cells, which were charged up to 4.2 V, with the Celgard membrane, the PAN nano-fiber nonwoven separator and the CNS No.1 were carried out by exposing the cells at 150 °C for 1h. During the hot oven test, variations for open circuit voltage of the cells were monitored. Results of the hot oven tests were given in the Fig. 4.8. The cells with the Celgard and the PAN nano-fiber nonwoven separator showed sudden voltage drop after 10 and 14 minutes from the start of the test, respectively, probably due to the internal short circuit by shrinking of the

separators. On the other hand, the cell with the CNS No.1 showed gentle voltage drop and any sudden voltage change was not observed during the hot oven test. The results indicate that the CNS is thermally stable at high temperature of 150 °C in the liquid electrolyte.

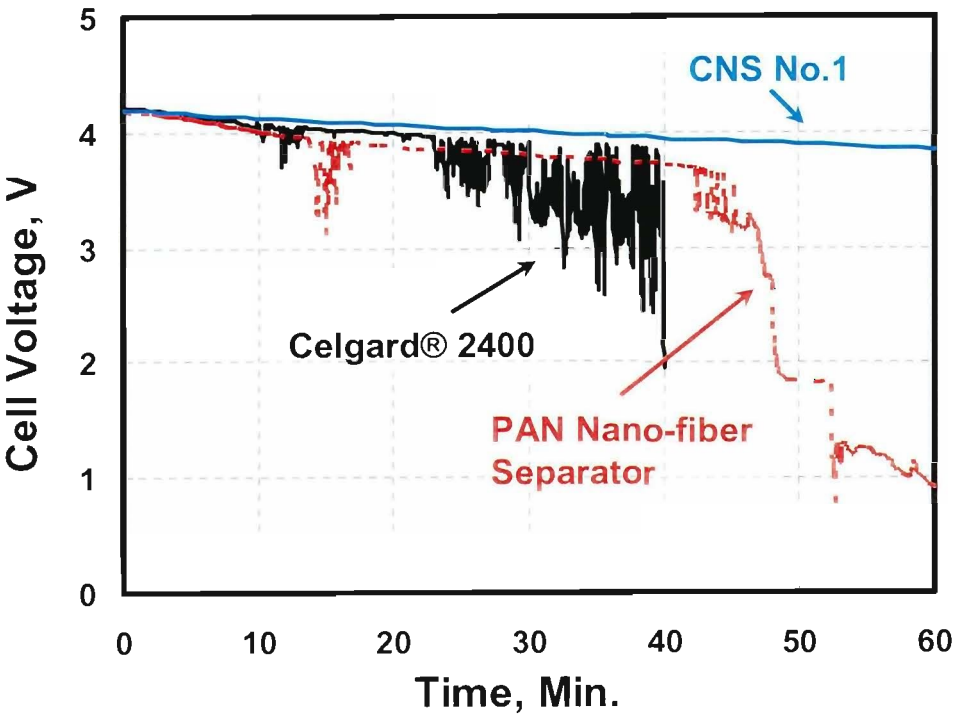

Figure 4.8 The open circuit voltage profiles for the cells with the Celgard® 2400, the PAN nano-fiber nonwoven and the CNS No.1 during the hot oven test at 150 °C for 1 hour.

4.4 Conclusions

In order to enhance physical and electrochemical properties of the nonwoven separators, we have tried to develop a new type composite nonwoven separator by combining ceramic containing polyolefin nonwoven and PAN nano-fiber nonwoven. By combining the two nonwovens, we could successfully develop a separator having small pore-size and narrow pore-size distribution as well as high air permeability. The

combination of PAN and polyolefin nonwoven separators retained the ceramic powder better in the composite nonwoven separator. Unstable voltage profile caused by internal short circuit was not observed during charge-discharge tests for cells with the CNSs and the cells showed stable cycling performance with high capacity retentions of about 88 % covering 200 cycles. The cells with the CNSs showed better rate capabilities than that with the Celgard membrane by help of their high air permeability and porosity. The CNSs showed thermal shrinkage of about 4 % at 150°C under air atmosphere, and a cell with the separator did not showed any internal short circuit caused by thermal shrinkage of separator even though it was exposed at 150°C for 1 hour. Therefore, the newly developed composite nonwoven separator can be a promising candidate for separators of the lithium-ion battery.

References

[1] M. S. Whittingham, *Chem. Rev.*, **104** (2004) 4271.

[2] M. S. Wu and P. C. J. Chiang, *Electrochim. Acta*, **52** (2007) 3719.

[3] Y. B. He, Q. Liu, Z. Y. Tang, Y. H. Chen, and Q. S. Song, *Electrochim. Acta*, **52** (2007) 3534.

[4] P. Kritzer, and J. A. Cook, *Electrochem., Soc.*, **154** (2007) A481.

[5] S. Augustin, V. D. Hennige, G. Hörpel, C. Hying, P. Haug, A. Perner, M. Pompetzki, T. Wöhrle, C. Wurm, D. Ilic, *Meet. Abstr.-Electrochem. Soc.*, **502** (2006) 84.

[6] S. Augustin, V. Hennige, G. Hoerpel, C. Hying, M. Saito, *Meet. Abstr.-Electrochem. Soc.*, **502** (2006) 89.

[7] T. -H. Cho, M. Tanaka, H. Onishi, Y. Kondo, T. Nakamura, H. Yamazaki, S. Tanase, and T. Sakai, *Electrochem. Soc.*, **155** (2008) A699.

[8] S. -S. Choi, Y. S. Lee, C. W. Joo, S. G. Lee, J. K. Park, and K. -S. Han, *Electrochim. Acta*, **50** (2004) 339.

[9] Y. M. Lee, J. -W. Kim, N. -S. Choi, J. A. Lee, W. -H. Seol, and J. -K. Park, *J. Power Sources*, **139** (2005) 235.

[10] K. Gao, X. Hu, C. Dai, and T. Yi, *Mater. Sci. Eng. B*, **131** (2006) 100.

[11] P. Kritzer, *J. Power Sources*, **161** (2006) 1335.

[12] D. Bansal, B. Meyer, and M. Salomon, *J. Power Sources*, **178** (2008) 848.

[13] T. -H. Cho, T. Sakai, S. Tanase, K. Kimura, Y. Kondo, T. Tarao, and M. Tanaka, *Electrochem. Solid-state Lett.*, **10** (2007) A159.

[14] T. -H. Cho, M. Tanaka, H. Onishi, Y. Kondo, T. Nakamura, H. Yamazaki S. Tanase, and T. Sakai, *J. Power Sources,* **181** (2008) 155.

Chapter 5

General Conclusion

General Conclusion

Separator is a kind of porous materials placed between positive and negative electrodes. Its function is to keep the electrodes apart to prevent electrical short circuits and at the same time allow rapid transport of ion. The property of separator is one of the main factors affecting the battery performance and safety of batteries. The micro porous polyolefin membranes (PP, PE and laminates of PP and PE) are the most widely used Li-ion battery separators. But the heat resistant properties of polyolefin are not enough, in addition, its low porosity and low wettability in non-aqueous electrolyte limits its use in large scale high power batteries. In order to increase safety and battery performance such as power density and cycle life, I have proposed several kinds of novel nonwoven separators. My research work can be summarized as following:

1. The micro-porous polyacrylonitrile (PAN) nonwoven have been developed by an electrospinning technique. The PAN nonwovens exhibited similar pore size to the conventional micro porous membrane with homogeneous pore size distribution. The separator was confirmed to be electrochemically stable in the voltage range 3 – 4.5 V by cyclic voltammetry study. The PAN nonwovens showed higher ionic conductivities than that of the Celgard membrane because of their high porosities. The cells with the PAN nonwovens showed better cycle lives at the 0.5 C-rate with smaller increase in the charge-transfer resistances than that with the Celgard membrane during charge-discharge test. Moreover, the cells with the PAN based separators exhibited superior rate capability to the conventional one due to smaller diffusion resistance of the separators during charge discharge process. Therefore, the newly developed PAN based separators can be promising candidate for separators for the lithium ion battery, especially battery for high power application. But, its low thermal stability prevents it from

practical application. In order to apply it as a separator for practical lithium-ion battery, the thermal stability of the nonwoven has to be improved.

2. The PVA nonwoven separators were successfully developed by the electrospinning technique. The separator was electrochemically stable in the voltage range of 3 to 4.5 V vs. Li^+/Li on the CV measurement. In spite of high porosities and low Gurley values, any internal short circuit was not observed for the cells using the PVA nonwovens during cycling test. The cells using the PVA nonwovens showed better cycle stability and rate capability than the cells with the Celgard membranes. Moreover, the cells with the PVA nonwovens exhibited larger maximum power than the cells with the Celgard membranes. The remarkable improvement of the battery performance for the cells using the PVA nonwovens could be attributed to the higher porosity, better wettability and lower Gurley values of the PVA nonwovens than those of the Celgard membranes. Therefore, the PVA nonwoven could be promising candidate as a separator for the high power lithium ion battery.
3. The silica-composite nonwovens comprising polyolefin nonwoven as a support and nano-size silica powder as filler for the lithium ion battery have been successfully developed. The silica-composite nonwoven showed better wettability than the polyolefin based membrane and nonwoven. The Gurley value of the silica-composite nonwoven has to be higher than 200 s 100 ml^{-1} in order to suppress micro short of battery. The cells with the silica-composite nonwovens showed better cycle lives than that with the Celgard membrane over 250 cycles at the C-rate of 0.5. The pulse-type discharging test revealed that the silica-composite nonwovens could deliver higher maximum power than that of the Celgard membrane. The silica-composite nonwovens showed thermal

shrinkage of about 3 % at 160 °C under air atmosphere and thermally stable at 150 °C in the liquid electrolyte. Therefore, I believe that the silica-composite nonwovens can increase the high power performance and thermal stability of the lithium ion battery.

4. New type composite nonwoven separators were developed by combining ceramic containing polyolefin nonwoven and PAN nano-fiber nonwoven. The separators have small pore-size and narrow pore-size distribution as well as high air permeability. The combination of PAN and polyolefin nonwoven separators retained the ceramic powder better in the composite nonwoven separator. Unstable voltage profile caused by internal short circuit was not observed during charge-discharge tests for cells with the composite nonwoven separators and the cells showed stable cycling performance with high capacity retentions of about 88 % covering 200 cycles. The cells with the separators showed better rate capabilities than that with the Celgard membrane by help of their high air permeability and porosity. The separators showed thermal shrinkage of about 4 % at 150°C under air atmosphere, and a cell with the separator did not showed any internal short circuit caused by thermal shrinkage of separator even though it was exposed at 150°C for 1 hour. Therefore, the newly developed composite nonwoven separator can be a promising candidate for separators of the lithium-ion battery.

PUBLICATIONS

1. **Electrochemical Performance of Polyvinyl Alcohol Nano-fiber based Nonwoven Separator for Lithium ion Battery**

   Masanao Tanaka, Tae-Hyung Cho, Tatsuo Nakamura, Takashi Tarao, Masaaki Kawabe, and Tetsuo Sakai

   Seni gakkaishi, Acceped (in print)

2. ***Electrochemical Performances of Polyacrylonitrile Nano-fiber based Nonwoven Separator for Lithium ion Battery***

   Masanao Tanaka, Tae-Hyung Cho, Tatsuo Nakamura, Takashi Tarao, Masaaki-Kawabe, and Tetsuo Sakai

   Electrochemistry, **78(12)**, 982-987 (2010)

3. **Composite nonwoven separator for lithium-ion battery: Development and characterization**

   Tae-Hyung Cho, **Masanao Tanaka**, Hiroshi Ohnishi, Yuka Kondo, Miyata Yoshikazu, Tatsuo Nakamura, Tetsuo Sakai

   Journal of Power Sources, **195**, 4272-4277 (2010)

4. **Battery performances and thermal stability of polyacrylonitrile nano-fiber-based nonwoven separators for Li-ion battery**

   Tae-Hyung Cho, **Masanao Tanaka**, Hiroshi Onishi, Yuka Kondo, Tatsuo Nakamura, Hiroaki Yamazaki, Shigeo Tanase, Tetsuo Sakai

   Journal of Power Sources, **181**, 155-160 (2008)

5. **Silica-Composite Nonwoven Separators for Lithium-Ion Battery: Development and Characterization**

   Tae-Hyung Cho, **Masanao Tanaka**, Hiroshi Onishi, Yuka Kondo, Tatsuo

Nakamura, Hiroaki Yamazaki, Shigeo Tanase, and Tetsuo Sakai

J. Electrochem. Soc., **155(9)**, A699-A703 (2008)

6. **Electrochemical Performances of Polyacrylonitrile Nanofiber-Based Nonwoven Separator for Lithium-Ion Battery**

T. H. Cho, T. Sakai, S. Tanase, K. Kimura, Y. Kondo, T. Tarao, and **M. Tanaka**

Electrochem. Solid-State Lett., **10**(7), A159-A162 (2007)

ACADEMIC ACTIVITIES

1. **Characterization of Lithium ion Battery with Polyvinylalcohol (PVA) nano-fiber Nonwoven Separator**

   T. H. Cho, H. Ohnishi, A. Takezaki, Y. Miyata, T. Nakamura, **M. Tanaka**, and T. Sakai

   The 50th Battery Symposium in Japan, Kyoto, Nov. 30-Dec. 2, 2009.

2. **High Temperature property of Li-ion battery using Nano-fiber Nonwoven Separator**

   T. H. Cho, H. Ohnishi, Y. Kondo, Y. Miyata, T. Nakamura, **M. Tanaka**, H. Yamazaki and T. Sakai

   The 49th Battery Symposium in Japan, Osaka, November 5-7, 2008.

3. **Electrochemical Performance of Li-ion battery using Ceramic Composite Nonwoven Fabric as a Separator**

   T. H. Cho, T. Sakai, S. Tanase, K. Kimura, Y. Kondo, H. Onishi, T. Nakamura, **M. Tanaka**, and H. Yamazaki

   The 48th Battery Symposium in Japan, Fukuoka, November 13-15, 2007.

4. **Development of PVA Nano-fiber Nonwoven Separator and Its battery performances**

   T. H. Cho, T. Sakai, and S. Tanase K. Kimura, Y. Kondo, H. Onishi, T. Nakamura, **M. Tanaka**, H. Yamazaki

   The 74th Fall Meeting of Electrochemical Society of Japan, Tokyo, Japan, September 19-20, 2007.

5. **Electrochemical Performance of Li-ion battery using Nano-fiber Non-woven Fabric as a Separator**

   T. H. Cho, T. Sakai, S. Tanase K. Kimura, Y. Kondo, T. Tarao, and **M. Tanaka**

   The 47th Battery Symposium in Japan, Tokyo, November 20-22, 2006.

6. **Development and Characterization of Polyacrylonitrile nano fiber Nonwoven Separator for a High power Li-ion Battery**

   K. Kimura, Y. Kondo, T. Tarao, **M. Tanaka**, T. H. Cho, T. Sakai, and S. Tanase

   The 211th Meeting of the Electrochemical Society, Chicago, Illinois, May 6-10, 2007.

7. **High Power Lithium Ion Battery Employing Novel Nano-fiber Non-woven Separator**

Tae-hyung Cho, Tetsuo Sakai, Shigeo Tanase, Koji Kimura, Yuka Kondo, Takashi Tarao, and **Masanao Tanaka**

The 73rd Fall Meeting of Electrochemical Society of Japan, Kyoto, Japan, September 14-15, 2006.

8. **Development of Novel Nano-fiber Non-woven Separator for Li-ion battery**

Koji Kimura, Yuka Kondo, Takashi Tarao, **Masanao Tanaka**, Tae-hyung Cho, Tetsuo Sakai, and Shigeo Tanase

The 73rd Fall Meeting of Electrochemical Society of Japan, Kyoto, Japan, September 14-15, 2006.

Acknowledgement

The present thesis is a collection of the author's studies that have been carried out at Japan Vilene Corporation, Kobe University and The National Institute of Advanced Industrial Science and Technology (AIST).

The author would like to gratefully thank Professor Tetsuo Sakai for fruitful supervision and solicitous care. Without his patient instruction, this work could not be fulfilled.

The author wishes to thank Professor Minoru Mizuhata and Professor Qiang Xu for their kind reviewing and valuable comments.

The author sincerely acknowledges valuable discussion and unselfish help of Dr. Tae-Hyung Cho belongs to Central Research Laboratory of Japan Vilene Corporation during three years.

I gratefully appreciate Japan Vilene Corporation for giving me the opportunity for this study and their helpful support.

I wish to thank my wife Chieko and our children Yusuke and Emi for their continuous encouragement and thoughtful support.

Masanao TANAKA

January, 2012